EVALUATION OF ASPHALT LAYER INTERFACE RESISTANCE TO BOND DEGRADATION THROUGH REPEATED LOAD

By

JEREMY ALEXIS MAGRUDER WAISOME

A DISSERTATION PRESENTED TO THE GRADUATE SCHOOL
OF THE UNIVERSITY OF FLORIDA IN PARTIAL FULFILLMENT
OF THE REQUIREMENTS FOR THE DEGREE OF
DOCTOR OF PHILOSOPHY

UNIVERSITY OF FLORIDA

2017

To God be the glory forever and ever. Amen.

ACKNOWLEDGMENTS

I would like to thank my parents who inspired me to reach further and higher regardless of the obstacles in my way. They kept me grounded in my faith in Jesus Christ, and reminded me of life's greater purpose. To my brother who made me laugh, even when I did not want to, I appreciate you. I would also like to thank my husband who always believed in me, and sacrificed his time and energy to ensure I would succeed. Thank you also to my mentor, Dr. Jonathan F. K. Earle, for his encouragement since high school. Thank you to my friends who encouraged me. Thank you from the depths of my soul. For anyone who has ever had a childhood dream and was told it could not be done and persisted in spite of adversity, this is for you.

TABLE OF CONTENTS

page

LIST OF TABLES

LIST OF FIGURES

Abstract of Dissertation Presented to the Graduate School
of the University of Florida in Partial Fulfillment of the
Requirements for the Degree of Doctor of Philosophy

EVALUATION OF ASPHALT LAYER INTERFACE RESISTANCE TO BOND DEGRADATION THROUGH REPEATED LOAD

By

Jeremy Alexis Magruder Waisome

December 2017

Chair: Reynaldo Roque
Cochair: Mang Tia
Major: Civil Engineering

One of the most prevalent forms of pavement distress is top-down cracking. There is incomplete understanding of how this type of near-surface cracking occurs. Recent attention to the importance of pavement interface bond suggests that loss of bond may be a primary contributor to this problem. The vast majority of previous research focused on evaluating near-surface cracking through bond strength tests, which predominately relates to debonding of the uppermost surface layers. However, research suggested the potential for a different mechanism of debonding that relates to repeated shear along an interface located lower in the pavement system.

The primary objective of this study was to identify a method to compare relative performance of various interface conditions with the results of an existing bond strength device. Using the newly proposed method, this research evaluated the effect of interface conditions on a pavement system’s ability to retain bond when subjected to repeated application of shear stress. An existing interface shear strength test device developed by the Louisiana State University was significantly modified to allow for repeated load testing. A testing scheme called the repeated shear test (RST) method

and data collection and interpretation methods were developed to properly analyze the results.

Three tack coats were evaluated including a trackless tack coat, a conventional tack coat and a polymer modified asphalt emulsion (PMAE). As a reference, no tack at the interface was also considered. Two application rates of the conventional tack coat were investigated to evaluate the importance of application rate. An elastic layer analysis indicated the location of critical stress states within the pavement system that could lead to debonding at more structural interfaces.

Strength test data indicated trackless tack, no tack, and low application rate of the conventional tack perform similarly, reaching on average 126.5, 126.6 and 126.4 psi, respectively. The results of the shear strength tests were consistent with the literature suggesting that brittle systems perform best. However, when these materials were tested using the RST method, trackless tack and no tack specimens were among the worst performers.

Using an energy analysis, the results of the two test methods were compared. Generally, the rankings provided by each analysis were reversed, with exception to the conventional tack coats. Overall the results support the hypothesis of this study, which is that monotonic testing does not capture the resistance to loss of bond over time. This type of repeated shear testing is needed to identify the best material for use at interfaces located deeper in the pavement system. The results show that non-brittle systems may perform best in the conditions found in these critical locations, deeper in the pavement system.

CHAPTER 1
INTRODUCTION

1.1 Background

Top-down cracking has been reported as a mode of pavement distress since the late 1990s. Initial understanding of this mechanism of cracking originated as an observation of surface cracking in the late 1980s (Dauzats and Rampal, 1987), and has been increasingly studied in a concerted effort to reduce its occurrence. Top-down cracking manifests itself as near-surface, longitudinal cracks along the wheel path. Numerous reports of this mechanism of failure exist from across the United States (US) and other countries. In the past, the Florida Department of Transportation (FDOT) reported that top-down cracking was the primary distress mode for 90% of the roads scheduled for resurfacing (Myers and Roque, 2002). Even today, the state of Florida considers top-down cracking as the most common cause of pavement rehabilitation.

Recent attention to the importance of interface bond suggests that loss of bond may be a primary contributor to near-surface cracking. Researchers have focused on assessing interface bond primarily by way of bond strength testing. These tests focus on evaluating the bond between the uppermost layer of pavement and the pavement beneath. At these surface level interfaces, shear stresses induced by braking are considered the most critical.

At the surface, vehicle braking can ultimately lead to slippage, sliding and delamination. Slippage is characterized by a crescent shaped crack along the wheel path as shown in Figure 1-1. Delamination occurs when sections of the overlay are completely separated from the structure below. These failure modes are often caused

by a single load excursion to failure that monotonic bond strength tests may capture well.

Figure 1-1. Surface failure due to poor interface bond in asphalt pavements. Source: West, R. C., J. Zhang, and J. Moore. Evaluation of Bond Strength between Pavement Layers. *National Center for Asphalt Technology*, 2005, pp. 1-58.

Recent field observations revealed that near-surface longitudinal cracking is present when there is poor bond between the pavement layers. The debonding identified was found at structural interfaces located deeper in the pavement system, and was connected to the failure at the surface by vertical cracks (Willis and Timm, 2007). Identifying which of these failures at the surface or structural level manifest itself first is nearly impossible. However, there is the potential for this type of debonding to contribute to the aforementioned surface failures, by introducing discontinuities within the pavement structure.

Previous research efforts have not considered interfaces located deeper in the pavement structure, where the shear stresses are possibly lower than values measured by bond strength tests. It is necessary to determine whether or not a high shear stress

value, such as those resulting from monotonic bond strength tests, is representative of the failure loads that cause debonding in these deeper pavement interface locations. In these areas, potentially low levels of vertical confinement and the repeated application of lower magnitude shear stresses might contribute to accelerated failure at the interface by breaking down the bond between pavement layers over time. As a result, a new testing methodology is necessary to study this type of mechanism. This research addresses this potential pavement distress mechanism for interface bond breakdown.

1.2 Hypothesis

Monotonic bond strength tests are unable to capture interface bond resistance to breakdown caused by the repetitive application of lower magnitude shear stresses in areas of low confinement. As a result, performance of the materials used at the interface is improperly assessed when based primarily on the outcomes of bond strength testing.

1.3 Objectives

The primary objective of this study was to determine whether the results from monotonic bond strength tests provide an accurate reflection of interfacial bond resistance to breakdown under repeated load. Detailed objectives to identify and evaluate interface bond breakdown are summarized in the following statements:

- Determine the stress states (magnitude and extent) at critical locations where pavement interfaces are typically located
- Develop a test that can allow for repeated application of shear stress to assess the relative performance of interface bond conditions using stress states identified in the previous objective
- Evaluate the effects of tack coat type and application rate on the resistance to interface bond breakdown

- Compare the relative performance of each interface condition resulting from monotonic and repeated shear stress tests

1.4 Scope

In order to develop testing protocols for the Repeated Shear Test (RST), one Superpave dense-graded mixture was selected. A conventional asphalt binder, PG-67-22, was used for the mixture in addition to a commonly utilized Georgia granite gradation.

Four types of interface bonding conditions were examined: a polymer modified asphalt emulsion (PMAE) developed by Road Science; a conventional SS-1, created by Ergon Asphalt & Emulsions, Inc.; a widely used trackless tack, NTSS-1HM, produced by Blacklidge Emulsions; and no tack (i.e., no tack coat was applied). For PMAE and trackless tack, one application rate was examined, as recommended by FDOT specification. For the conventional tack material, two application rates were selected (low and high) based on previous research.

A modified version of the Louisiana Interlayer Shear Strength Test was chosen to evaluate interface bond strength and resistance to bond breakdown. The device was chosen due to its extensive use in the National Cooperative Highway Research Program (NCHRP) Report 712, Optimization of Tack Coat for HMA Placement, which provides a baseline of measurements that were initially used to evaluate the accuracy of the bond strength test results.

It is important to note that surface conditions, i.e., milled vs. compacted, clean vs. dirty, wet vs. dry, can influence interface bond. Only clean, dry, laboratory compacted surfaces were evaluated in this work. All tests were conducted at room temperature, which was measured and recorded.

1.5 Research Approach

This research primarily focused on the comparison of results of various interface bond types and application rates (described in section 1.4) from an existing interface bond strength test method to those obtained from a newly developed method designed to evaluate the resistance of interface bond breakdown. The overall approach taken to meet the objectives of this study includes:

- Literature review: investigate existing and potential mechanisms of near-surface cracking, evaluate factors that impact the performance of the asphalt pavement interface, and identify existing test methods/devices for evaluating both shear strength and interface bond breakdown. Choose an appropriate device that can accommodate both strength and repeated load testing, or identify the characteristics of one for modification to do both testing modes.

- Stress-state analysis: utilize an elastic layer analysis program to determine the critical locations and stress states in areas where structural interfaces can occur within asphalt pavement.

- Shear strength testing: evaluate the effect of application rate and tack coat on interface bond and compare the results to those found in existing literature for quality control purposes. Determine whether or not additional adjustments to the device are necessary for testing.

- Repeated shear test method development: develop or modify an existing strength test to allow for repeated application of shear stress at the interface. This includes determination of the appropriate (1) loading mode (load-controlled vs. deformation-controlled), (2) loading procedure which includes the magnitude, duration and load-shape, and (3) device configuration. Determine an appropriate associated data interpretation method for evaluating the effect of repeated shear stress on interfacial bond. This requires not only assuring reasonable testing and data interpretation time, but also the adequate frequency of data acquisition. It will also include the modification of the device to eliminate any errors that affect the results of the chosen test method. This iterative process is indicated in Figure 1-2.

- Repeated shear testing: evaluate the various interface bond types and application rates using the method determined from the previous step.

- Data analysis: rank the results of each test to compare relative results. Evaluate the effect of application rate and tack coat on interface bond.

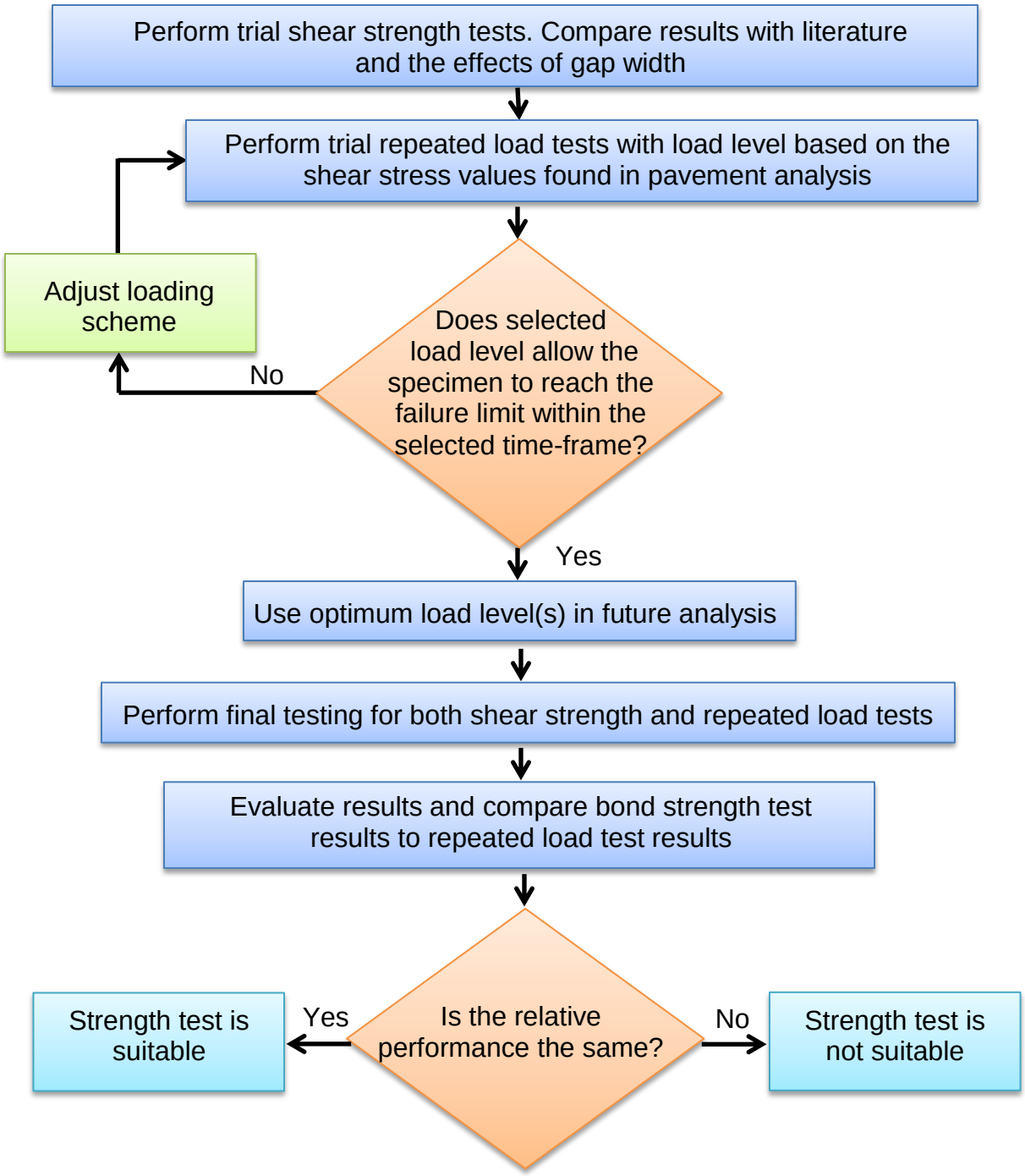

Figure 1-2. Research approach flow chart.

CHAPTER 2
LITERATURE REVIEW

2.1 Background

Roadways are layered systems designed to work as a monolithic structure to carry traffic loads. The uppermost portion of this system is typically composed of layers of asphalt concrete (AC). Where two adjacent AC layers meet is referred to as an interface. Interfaces are inherent components of our pavement systems, created during both new construction and pavement rehabilitation.

Without proper bond between adjacent pavement layers, the magnitude and location of the critical responses (stress and strain) varies from a fully bonded system (Willis and Timm, 2007). A number of factors influence the quality of the bond between pavement layers including tack coat type, application rate, temperature, surface conditions, moisture, pavement structure, construction methods and more. This makes predicting the performance and longevity of the pavement structure challenging. However, previous research indicates that ensuring proper bond at these potential discontinuities is paramount to good pavement performance.

Tack coats are applied to the underlying pavement surface (new or milled) prior to the placement of a new layer of hot mix asphalt (HMA) to enhance interface bond and improve the structural performance of pavements. This material helps to fully integrate the adjacent layers into one system. In current practice, tack coats are often virgin asphalt binder, or an asphalt emulsion (emulsified asphalt). According to a recent worldwide study, the most widely used method to bond adjacent pavement layers is by applying emulsified asphalt tack coat (Mohammad et al., 2012). Emulsified asphalt is asphalt binder suspended in water by way of an emulsifying agent, like soap. When

combined, the asphalt binder disperses into small droplets within the water. After being applied to the pavement surface, the emulsion breaks, leaving behind an asphalt binder residue.

Tack coats are applied in a thin layer by a sprayer attached to a distributor vehicle. In the US, tack coat application rates are determined by state Departments of Transportation (DOTs) based on characteristics of the existing pavement surface. Application rates are often described by the percent of asphalt binder residue required to remain on the surface. Tack coats can be applied at higher rates to allow the material to infiltrate the void systems of the adjacent pavement layers. However, applying tack coats at higher rates can lead to construction issues like tracking or bleeding. According to Mohammad et al. 2012, it is best to apply tack coat on a dry, clean pavement surface, to achieve optimal bond. Contractors may also choose not to use a bonding agent, which is often done in new construction if it is not required by the state.

Researchers have used several methods to evaluate pavement interface bond. Torque tests, pull off tests, shear strength tests, direct tension tests, etc. are all methods used in previous research (Mohammad et al. 2012; Tran et al. 2012). Most researchers use a unique device specifically designed to apply one of the aforementioned loading schemes to assess bond strength.

A review of methods used for the evaluation of pavement interface bond in both field and laboratory studies is presented in the following sections. Though many test devices and loading methods exist in the literature, the focus of this review was on interface bond strength and fatigue testing. Emphasis was placed on identifying

potential factors that cause premature bond failure, including material properties, application rates, construction conditions and environmental conditions.

2.2 Interface Bond Testing

The evaluation of pavement interface bond is typically conducted using bond strength testing devices. These tests are typically designed to assess whether adequate shear strength is present to resist stresses induced by traffic loading. The principal technique used in these tests involves the application of a single load excursion applied at a designated rate until the specimen fails. However, each device is unique in construction and the loading technique employed. While most bond tests use a single load excursion of shear stress, there are several variations between tests including specimen size and geometry, loading rate, and more.

In addition to shear bond tests, pull-off tests and torsional shear tests are utilized to assess interface bond. Researchers believe that a variety of failure mechanisms, including tension, torsion and/or shear modes occur due to traffic loading.

2.2.1 Interface Bond Strength Tests

Uzan et al. (1978) conducted one of the first reported studies to better understand pavement interface bond. This study used a shear test to assess the bond strength variations due to temperature, tack coat application rate, vertical pressures and asphalt binder types. Laboratory compacted specimens were tested at 25.0 °C, and 55.0 °C (77.0 °F and 131.0 °F) in constant deformation at 2.5 mm/min (0.1 in/min). The apparatus used measured deformation from deflectometers. The study concluded that optimum tack coat rates are influenced by both the binder and the testing temperature. It also showed that decreasing temperature and increasing vertical pressure enhanced interface bond strength.

In 1997, Hachiya and Sato evaluated the bond strength of surface courses typically used at airports, to address debonding caused by the horizontal force of aircrafts as they brake and turn on the pavement. Through the computer analysis program BISAR, stresses were calculated at the interface between the wearing and binder courses. Results of the BISAR analysis indicated that failure of the surface course is a result of horizontal shear stress and insufficient adhesion at the pavement interface. The authors suggest increased thickness of the wearing course and increased bond strength help to reduce the shear stress at the interface from BISAR results.

Laboratory tension and flexure tests were conducted to obtain the bond strength for dense-graded asphalt concrete specimens cut from laboratory roller-compacted specimens with and without tack coat. Tack coats included cationic asphalt emulsions, which were developed to counteract the impact of dirt on the surface. Three of the four developed emulsions included rubber. In addition to determining bond strength at the interface for the various tack materials, tack coat application rate, curing time, low and high temperature, surface preparation (clean or with sand), and lift thickness were also evaluated by way of shear and tensile strength tests. Findings suggested the introduction of a thick lift as the surface course or the utilization of tack coat to increase bond strength by improving adhesion. Bond strength was found to be similar for both emulsion types at higher temperatures, while at low temperatures, the rubber-modified asphalt emulsions provided more strength at the interface than cationic asphalt emulsions. In addition, the importance of adequate curing time and the implications it has on bond strength was emphasized.

In 2001, Romanoschi and Metcalf sought to characterize asphalt concrete interfaces, particularly those at the surface layer. The research consisted of two major components: the development of a constitutive model from direct shear testing data, and the development of a shear fatigue test, which will be discussed in section 2.2.2. Specimens with asphalt-to-asphalt interfaces cored from the Louisiana Pavement Research Facility site were tested using a direct shear test at a constant normal load. Some specimens had 0.1 l/m^2 (0.32 gal/yd^2) of tack coat, while others had no tack coat. A schematic of the device used for testing is shown in Figure 2-1.

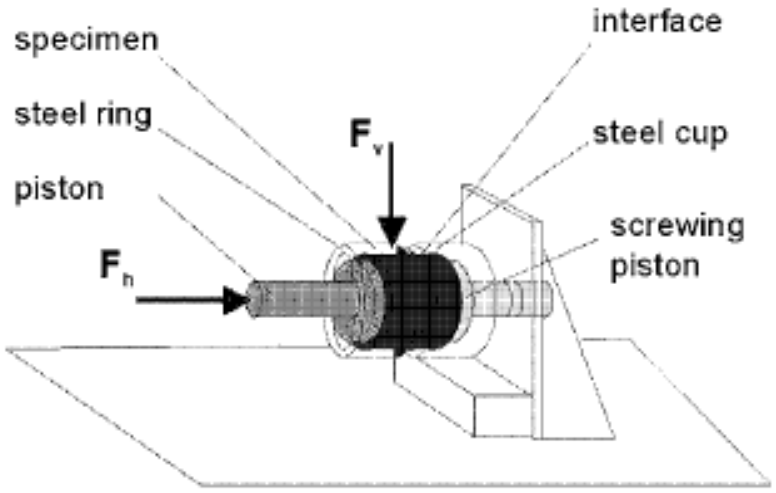

Figure 2-1. Direct shear test with normal load schematic. Source: Romanoschi, S. A., and J. B. Metcalf. Characterization of Asphalt Concrete Layer Interfaces. *Transportation Research Record: Journal of the Transportation Research Board*, No. 1778, 2001, pp. 132-139.

A constant displacement rate of 0.2 mm/s (0.008 in/s) was used until 12.0 mm (0.472 in) of total shear displacement was achieved. Normal stress levels varied from 138.0, 276.0, 414.0 and 522.0 kPa (20.0, 40.0, 60.0 and 80.0 psi, respectively). The gap width over the interface of the specimen was 5.0 mm (0.197 in), which according to the authors, allowed shear force to be applied to the interface and not across the asphalt concrete mixture. Testing was conducted at 15.0 °C, 25.0 °C and 35.0 °C (59.0

°F, 77.0 °F and 95.0 °F). Five cores were tested for each combination of the variables indicated. Using this test configuration, all specimens failed along the plane of the interface, regardless of the variables involved in testing. Linear variable differential transducer (LVDT) sensors measured the displacement at the interface. Shear and normal force and displacement were measured and controlled by an MTS Systems Corporation (MTS) loading frame device.

Using a typical shear stress-displacement curve, three distinguishable sections of the curve were characterized for the derivation of the interface constitutive model. The curve was described by an initial linear shear section, a post-failure section and ultimately a friction section. Parameters for the post-failure section were not computed, and specimens were considered to be completely separated after failure. Thus, the model proposed was a two-stage model where in the first stage the shear stress is smaller than the shear strength of the interface, and once the interface fails the second stage begins. An important finding was that shear stress and displacement were proportional until the shear stress equaled the shear strength, causing the interface to fail. The authors also suggested that testing be conducted at several temperatures to identify temperature dependency of parameters used in interface modeling.

Sholar et al. (2004) investigated the effects of moisture, application rate and the interaction of aggregate at the interface using a direct shear bond test (Figure 2-2) and procedure they developed. The device was a modified version of the Iowa Department of Transportation shearing device for Portland cement concrete. The device had a 0.125 inch gap width and was designed to house 4.0 inch diameter cylindrical specimens. Specimens were cored from three Florida Department of Transportation (FDOT) field

projects with rates of tack coat application varying from no tack to 0.362 l/m^2. (0.08 gal/yd^2).

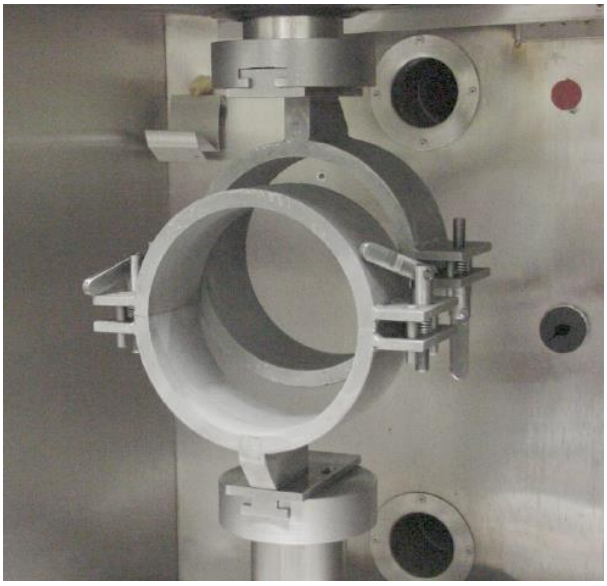

Figure 2-2. FDOT shearing apparatus. Source: Sholar, G. A., G. C. Page, J. A. Musselman, P. B. Upshaw, and H. L. Moseley. Preliminary Investigation of a Test Method to Evaluate Bond Strength of Bituminous Tack Coats. *Journal of the Association of Asphalt Paving Technologists*, Vol. 73, 2004.

Results indicated that the presence of water on the surface prior to tack coat application can significantly decrease interface bond strength. This finding substantiated that tack coats should be applied to dry surfaces, and at times when there is no potential for rain. Aggregate gradation of the mixtures was also found to directly impact the magnitude of the shear strength at the interface. Coarse gradations produced higher shear strengths than fine gradations. In addition, a milled surface at the interface produced the highest shear strengths of the specimens tested.

In 2005, Canestrari and Santagata utilized the Ancona shear testing research analysis (ASTRA) device (Figure 2-3a) to analyze the effect of temperature and normal stress on the interface. ASTRA shear tests were conducted at a constant displacement rate of 2.5 mm/min (0.10 in/min) on 9.2 mm (0.36 in) thick specimens. Specimens either

received no tack coat or a conventional cationic emulsion with 60.0% bitumen. The specimens with tack coat were coated with 0.5 kg/m^2 (0.11 gal/yd^2) of emulsion. Various combinations of normal stress at 1.27, 3.00 or 4.73 kg/cm^2 (18.1, 42.7, 67.3 psi) and testing temperature at +20.0 °C, +12.5 °C, +5.0 °C, -2.5 °C or -10 °C (+68.0 °F, +54.5 °F, +41.0 °F, -36.5 °F or -50.0 °F) were evaluated and for each combination, both treated (with tack coat) and untreated (without tack coat) interfaces were tested. The results indicate that as the test temperature was decreased, shear resistance increased. This was expected as the stiffness of the material increased with temperature, regardless of whether or not tack coat was applied at the interface. In addition, the authors suggest that the effectiveness of the tack coat on specimens increases with temperature. Another finding was that the increase of normal stress causes an increase of the maximum shear stress, regardless of whether or not tack coat is applied for all evaluated test temperatures.

An additional study conducted by Canestrari et al. (2005) focused on evaluating various interface behaviors. Two test methods were used including the ASTRA device in Figure 2-3a, as well as the layer-parallel direct shear (LPDS) tester Figure 2-3b which was developed by the Swiss Federal Laboratories for Material Testing and Research. Three interface treatments were utilized including a polymer modified cationic emulsion, a conventional cationic emulsion and no tack. The specimens with tack coat were coated with 300.0 g/m^2 (0.0948 gal/yd^2) of residual binder. Specimens were cored from double-layered, laboratory compacted slabs produced with two types of dense graded mixtures. The loading rates for each test were 2.5 mm/min (0.1 in/min) and 50.8 mm/min (2.0 in/min) for the ASTRA and LPDS respectively.

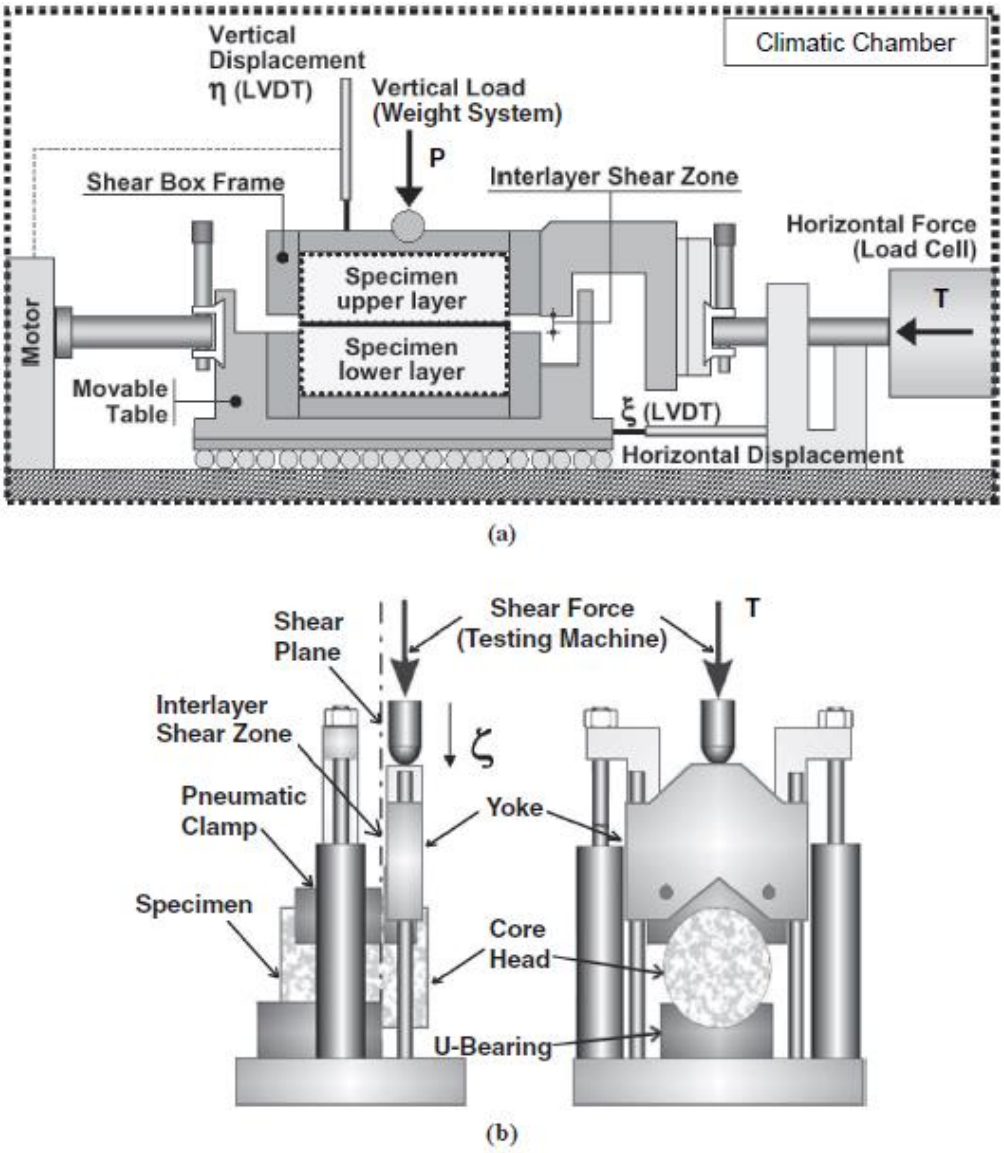

Figure 2-3. Schematics of the a) ASTRA test device and b) LPDS test device. Source: Canestrari, F., G. Ferrotti, M. Partl, and E. Santagata. Advanced Testing and Characterization of Interlayer Shear Resistance. *Transportation Research Record: Journal of the Transportation Research Board*, No. 1929, 2005, pp. 69-78.

The peak shear stress for the ASTRA device was previously determined to be an idealized linear superposition of stress contributions from the residual friction, inner cohesion, dilatancy, and tack coat adhesion. Peak shear values from specimens tested using the ASTRA device were compared to peak shear stress from the LPDS device (which is computed from a shear force versus relative displacement diagram). The tests

resulted in similar and comparable rankings of the shear resistance for the various interface conditions. Results showed that modified emulsions provided greater interlayer shear stress resistance for each applied normal stress at 20.0 °C (68.0 °F). It also showed that when temperatures reach 40.0 °C (104.0 °F), mixture characteristics played a more dominate role in peak shear stress than the presence of or type of tack coat.

Also in 2005, a study was performed by West et al. at the National Center for Asphalt Technologies (NCAT) to develop a test that measured the bond strength between pavement layers. This study included both a laboratory and field phase that evaluated a variety of tack coats and application rates for use by the Alabama Department of Transportation (ALDOT). The authors chose to develop a simple shear device (Figure 2-4) that is comparable to devices used by other researchers. Specimens were tested at 50.0 °F, 77.0 °F, and 140.0 °F (10.0 °C, 25.0 °C, and 60.0 °C) at a loading rate of 50.8 mm/min (2.0 in/min).

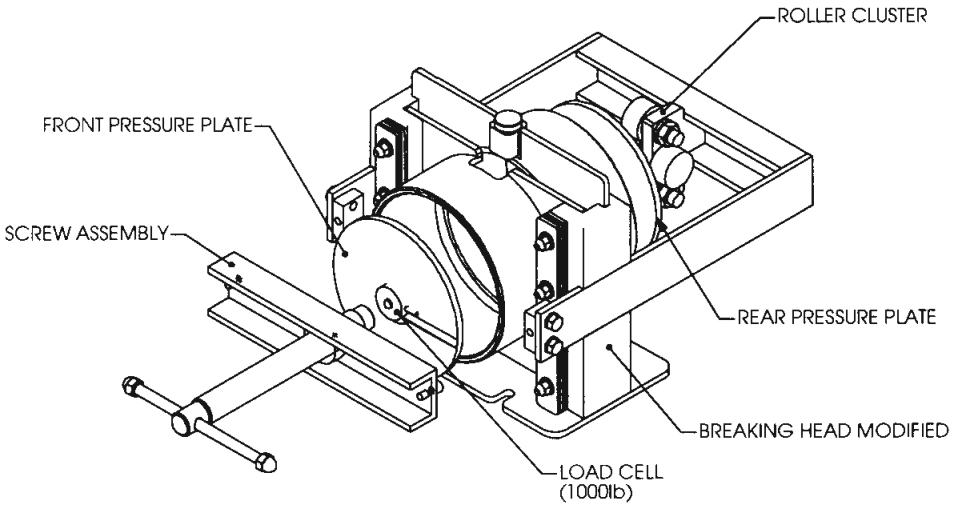

Figure 2-4. Schematic of the NCAT Bond Strength device. Source: West, R. C., J. Zhang, and J. Moore. Evaluation of Bond Strength between Pavement Layers. *National Center for Asphalt Technology*, 2005, pp. 1-58.

In 2012 the most comprehensive study on the influence of tack coat on pavement was conducted by the National Cooperative Highway Research Program (Mohammad et al., 2012). A total of 432 specimens were evaluated in this study. Project 9-40 involved identifying the best asphalt binder material and method of tack coat application, application rates, equipment and procedures used in the asphalt industry. From this study, recommendations for revision were made to the American Association of State Highway and Transportation Officials (AASHTO) to improve existing tack coat related practices. The work consisted of two phases in which Phase I involved a literature review of current standard practices, and Phase II involved laboratory testing and field experiments.

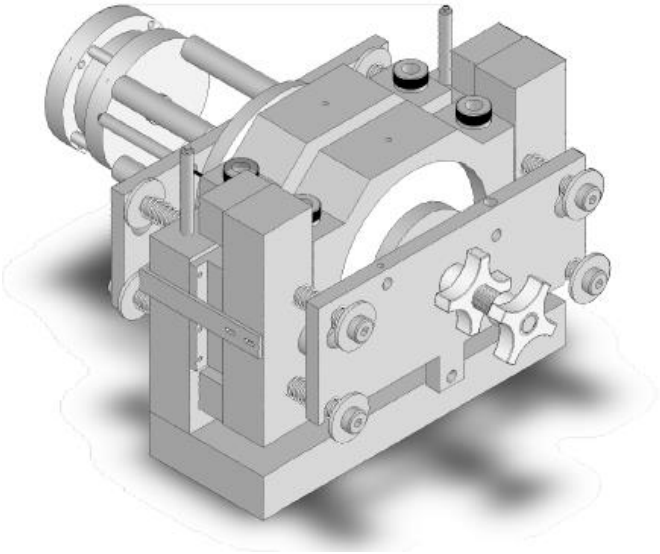

Figure 2-5. Schematic of the LISST device. Source: Mohammad, L. N., M. A. Elseifi, A. Bae, N. B. Patel, J. Button, and J. A. Scherocman. Optimization of Tack Coat for HMA Placement. *National Cooperative Highway Research Program*, Vol. 712, 2012.

Phase II was separated into two distinct studies. One focused on the characterization of the quality of tack coat using the Louisiana Tack Coat Quality Tester (LTCQT). The second involved the development of a new test method to evaluate bond

strength called the Louisiana Interface Shear Strength Test (LISST). This device was comparable to the Superpave Shear Tester, but easy to use, portable, and reasonable in cost and could be adopted for universal testing machines. Both laboratory prepared specimens (used to develop the device) and field cores were produced for this project. Field cores were obtained from projects across the US in a variety of climates and under varied traffic conditions were evaluated with this device, while researchers at the Louisiana Transportation Research Center (LTRC) Pavement Research Facility constructed full-scale pavements for analysis.

The primary focus was to evaluate the effects of a number of variables on the bonding characteristics of the interface including: Trackless, CRS-1 and SS-1h tack coats; 0.031, 0.062 and 0.155 gal/yd^2 applications rates; old, new and milled HMA, and Portland cement concrete (PCC) pavement surfaces; and swept, not swept, wet and dry pavement surface conditions. Issues with coring specimens without tack coat prevented this condition from being analyzed. A confinement condition was also evaluated at 20 psi. Testing was conducted at 25° C with three replicates of each specimen. Using a preliminary analysis, a loading rate of 0.1 in/min was chosen to simulate the rate of loading at the interface that would be encountered in the field.

Results were presented in terms of the interface shear stress (ISS) which is computed as follows in Equation 2-1:

$$ISS = P_{ULT} / A \qquad (2\text{-}1)$$

Where,

ISS=Interface Shear Strength (ksi);

P_{ULT}=Ultimate load applied to the specimen (lb); and

A=Cross-sectional area of the specimen (in^2)

Statistical analysis indicated that test results had less than a 10% coefficient of variation. At the highest application rate (0.155 gal/yd^2), all tack coats tested in this study exhibited the highest strength. For the SS-1 and Trackless tack coats, strength increased as application rate increased. Yet for the CRS-1 tack coat, the results remained stable at and above the 0.062 gal/yd^2 rate. Results were consistent with or without confinement, but dusty and dry conditions made the effect of confinement more distinctive. Full mixtures (no interface) were also analyzed and shown to be the best performers in the LISST evaluation with an ISS of 105 psi. Trackless specimens proved to be the best overall performer in comparison, reaching 60% of ISS of the full mixture.

In terms of evaluating clean and dusty surfaces, 13 of the 24 cases studied indicated a significant effect on the ISS values with dusty conditions displaying higher ISS values. However, there was no significant effect on the ISS response of the tested materials between wet and dry conditions. Milled HMA surfaces gave the highest ISS values, followed by grooved PCC surfaces. In most cases, old HMA surfaces provided higher ISS values than new HMA surfaces. Additionally, the findings from the surface type analysis were more pronounced with low application rates than higher ones. The authors suspect that microstructure contributes to the surface texture/roughness which is less pronounced with the application of tack coat.

Using the results from a finite element analysis, a minimum ISS of 40 psi at 25° C was determined to be acceptable for performance. A clean and dry surface was recommended as well to avoid any negative effects on the bonding at the interface due

to the presence of water. Ultimately the authors provided recommendations for residual application rates to use with various surface types as presented in Table 2-1.

Table 2-1. Recommended residual application rates of tack coat.

Surface Type	Residual Application Rate (gal/yd^2)
New Asphalt	0.035
Old Asphalt	0.055
Milled Asphalt	0.055
Portland Cement Concrete	0.045

These findings indicate that the LISST was successful at distinguishing between the conditions at the interface.

2.2.2 Interface Bond Fatigue Tests

Romanoschi and Metcalf were some of the first to document the use of fatigue testing of the AC layer interface. The primary focus of their work was to evaluate a constitutive model that relates an interface reaction modulus, *K*, which is the slope of the shear-stress displacement curve; shear strength *S*max; and the friction coefficient μ (Romanoschi and Metcalf, 2001) using the results from strength testing. In addition they developed a shear fatigue test to determine pavement fatigue resistance to obtain a parameter for validation of their constitutive model.

As shown in Figure 2-6, the longitudinal axis of the specimen was held at an angle of 25.5 degrees from vertical so the shear stress at the interface would be half of the normal stress. This was to simulate interface conditions beneath the wearing course directly under a wheel load. Thus, results could be used to provide relative comparisons between bond strength and fatigue resistance as they were found for an interface in a

similar location. Four vertical loads were applied in the form of a haversine load using at a frequency of 5.0 Hz.

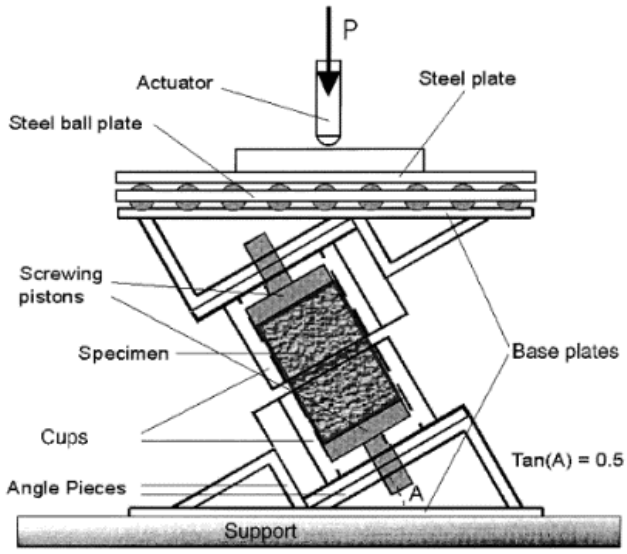

Figure 2-6. Schematic of shear fatigue test. Source: Romanoschi, S. A., and J. B. Metcalf. Characterization of Asphalt Concrete Layer Interfaces. *Transportation Research Record: Journal of the Transportation Research Board,* No. 1778, 2001, pp. 132-139.

Testing ended when permanent shear deformation (PSD) reached 6.0 mm (0.24 in) at the interface or when a number of cycles of PSD of 6.0 mm (0.24 in) could be extrapolated from the data. Ultimately their findings indicated that the increase in permanent shear deformation with the number of load deformations is linear and the rate of increase is higher for higher stresses. They also showed that all parameters used for the constitutive model were temperature dependent.

In 2006, Diakhaté et al. used the principles from a shear fatigue testing device called the Modified Compact Shearing (MCS) test developed by the Groupe d'Etudes des Matériaux Hétérogènes (GEMH) - Génie Civil et Durabilité (GCD) laboratory at the University of Limoges, France to investigate shear fatigue on tack coats. The device developed by Diakhate et al., shown in Figure 2-7, requires a three layer specimen

bonded specimen but can also work without tack coat. The device operated by subjecting the specimens to displacement in a repetitive manner. The two outside layers remain fixed, while the displacement is applied to the center layer, resulting in cyclic shear loading at each interface. Resistors measured the response at the interface to determine failure. Tests were run at a constant frequency of 1 Hz and at a constant temperature of 5.0 °C, which according to the authors, results in bituminous material moduli equivalent to similar tests run at 10 Hz and 15.0 °C. Compacting to 93.0%, materials typically utilized in France pavements were used according to French design specification.

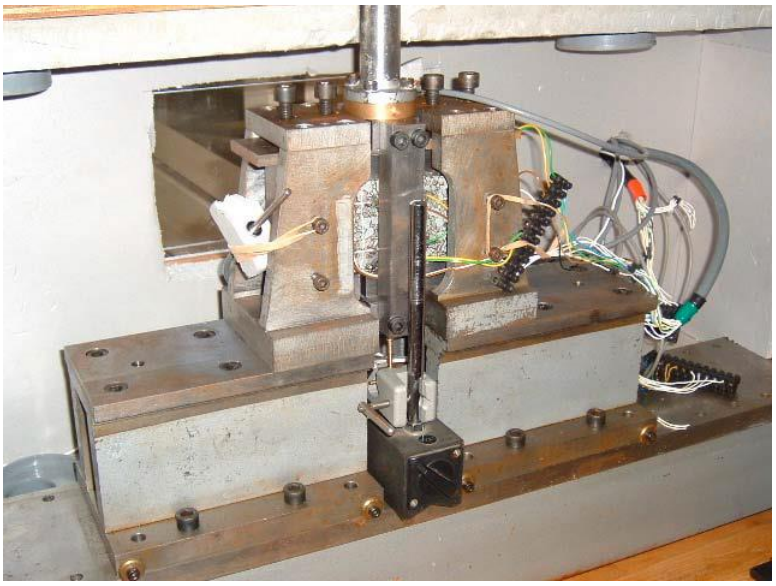

Figure 2-7. Specimen in the MCS device. Source: Diakhaté, M., A. Phelipot, A. Millien, and C. Petit. Shear Fatigue Behavior of Tack Coats in Pavements. *Road Materials and Pavement Design,* Vol. 7, No. 2, 2006, pp. 201-222.

Results indicated that there are two stages to interface failure resulting from this shear fatigue test. The first involves progressive failure, where the force amplitude decreases in a linear fashion. The second stage, however, involves more rapid failure, which the authors believe is the result of a loss of shear stiffness in the tack coat

material and aggregate interlock becoming the prevailing factor of the response. This study also included the use of direct shear testing for comparison purposes. It is believed that fatigue testing can be an asset to evaluating the durability of various interfaces. The authors suggest that further evaluation of fatigue testing is necessary to determine more interface parameters that can be assessed to ultimately improve modeling of the asphalt concrete interface.

In 2008, Diakhaté et al. showed the relationship between monotonic and cyclical testing of pavement interfaces. The correlation was developed to allow contractors to determine fatigue responses of tack coats from strength testing, reducing testing time. The relationship could be used to help contractors and pavement designers expeditiously predict pavement life.

Modeling efforts towards evaluating longitudinal top-down cracking were developed by Petit et al. using data from their previous work (Diakhaté et al., 2008). This research focused on introducing new failure modes, related to the repeated application of shear stress on thin surface layers into pavement design. The results indicated the necessity for evaluating interface fatigue in the pavement design process for pavements with thin surface layers to ensure the proper selection of tack coat and application rate. Results also suggested that this is research is of particular importance for curved roads, where horizontal loading is often more critical.

In 2011, Diakhaté et al. further investigated shear fatigue behavior using the Double Shear Test (DST) (Figure 2-8) to perform both an experimental and numerical study of interface fatigue behavior to enhance life cycle assessments of asphalt pavement. Specimen production for the test was very involved, and included several

steps from double-layered (one thick, one thin) slab compaction, applying tack coat, sawing the specimen and gluing steel plates onto the specimen to secure it to the loading frame. The frequency used for each test was 10 Hz, and specimens were tested at 10.0 °C and 20.0 °C.

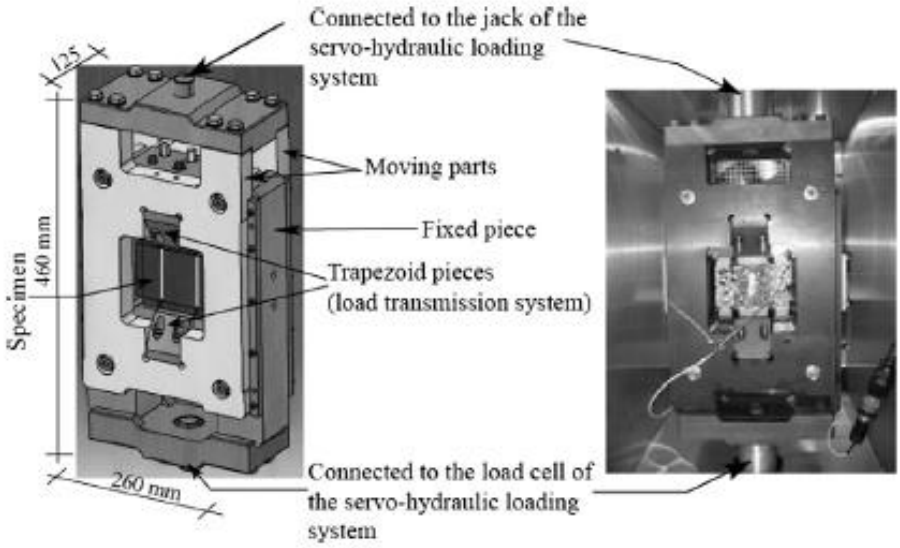

Figure 2-8. Schematic (left) and photograph (right) of the DST device. Source: Diakhaté, M., A. Millien, C. Petit, A. Phelipot-Mardelé, and B. Pouteau. Experimental Investigation of Tack Coat Fatigue Performance: Towards an Improved Lifetime Assessment of Pavement Structure Interfaces. *Construction and Building Materials*, Vol. 25, No. 2, 2011, pp. 1123-1133.

Results of this force-controlled test were presented as a plot of normalized shear stiffness modulus versus loading cycles. There were two observed stages within the resulting trend curve. Stage one shows an initial slow decrease in stiffness modulus was determined to result from the development of micro-cracks. The second stage was characterized by a rapid decrease in the stiffness modulus, which the authors believed macro-cracks propagated quickly at the interface. This finding directly supports previous findings by the author in 2008, as discussed earlier in this section.

A new apparatus developed at the Sapienza University in Rome, called the Sapienza Inclined Shear Test Machine (SISTM) (Figure 2-9), was utilized for dynamic shear testing (Tozzo et al., 2014). The test involved using both normal and shear stress to evaluate pavement interfaces. Using the CIRCLY software program, various stress levels were determined for evaluation of the uppermost pavement interface (wearing course) that would represent actual stress levels found in real pavements at the edge of the wheel path. Double layer specimens were constructed and the most common application rate of 0.4 kg/m^2 (0.088 gal/yd^2) residual binder was used to improve adhesion.

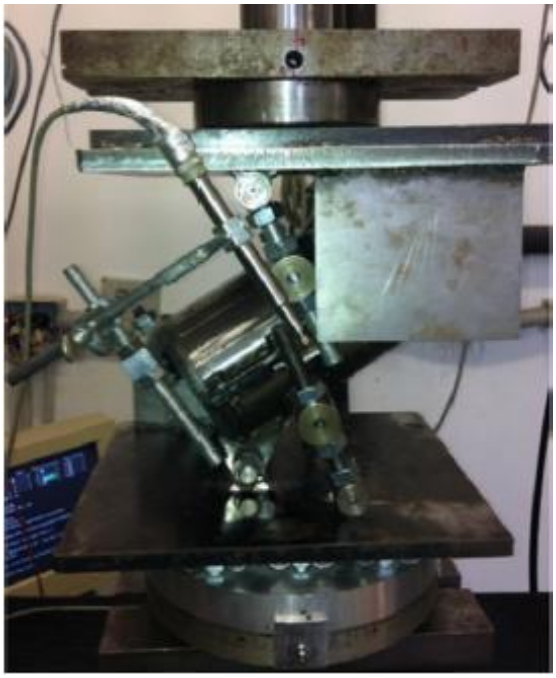

Figure 2-9. Image of the SISTM device. Source: Tozzo, C., A. D'Andrea, D. Cozzani, and A. Meo. Fatigue Investigation of the Interface Shear Performance in Asphalt Pavement. *Modern Applied Science*, Vol. 8, No. 2, 2014, pp. 1-11.

Using results from the CIRCLY analysis, a triangular load was selected for testing. Several normal and shear stress values were analyzed. Lower load states were selected to directly correlate with values determined from the CIRCLY analysis, while

higher loading states were incorporated to reduce testing time and potentially be used to estimate tack coat responses. Testing was conducted on double layer cylindrical specimens at 20.0 ± 0.5 °C. Loading times were held constant at 0.1 sec, but total cycle time varied from 0.2, 0.5 and 1.0 seconds to evaluate the effect of relaxation time (0.1 sec, 0.4 sec or 0.9 sec, respectively). The device was set to a 60 degree incline in the longitudinal direction of the specimen. This was done so that the normal and shear stress response measured would relate to 30.0 mm (1.299 in) from the edge of a tire wheel load. Using this set up, a fatigue law was developed to relate load level to the number of cycles to failure of a specimen. Results indicated that further analysis was required to capture the ratio between shear stress and normal stress for more accurate predictions.

The Sapienza Direct Shear Testing Machine (SDSTM) was developed next, to allow for the application of both shear and normal stress to a double layered cylindrical specimen. This guillotine style test involved one stationary and one dynamic side of the test device. This testing configuration has been used frequently to evaluate several pavement responses. Normal stress was applied using a pneumatic actuator. Interface displacement was captured from an LVDT. Shown in Figure 2-10, this novelty of this device was that fatigue response could be captured under dynamic loading conditions. A rapid setting cutback emulsion was used as a tack coat, and was applied at 0.46 kg/m^2 (0.101 gal/yd^2) residual binder. Testing was conducted at 21.5 ± 1.0 °C. A haversine shear load was applied until failure of the specimens. The load was applied in 0.1 sec for each specimen, but the relaxation time (rest period) varied from either 0.1 sec or 0.9 sec. Though preliminary results indicated that the shorter rest period would

be sufficient for viscoelastic recovery in low shear stress levels, for higher shear stress values, the longer period of 0.9 sec was preferred.

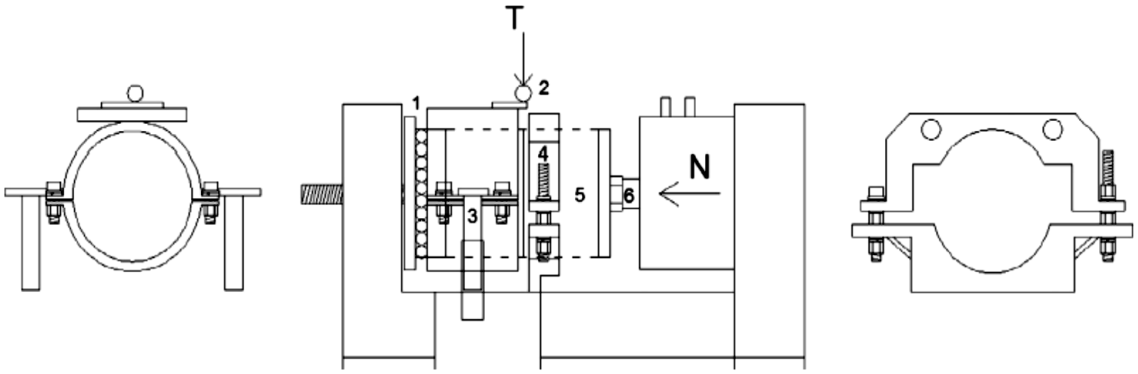

Figure 2-10. Schematic of the SDSTM. Source: Tozzo, C., N. Fiore, and A. D'Andrea. Dynamic Shear Tests for the Evaluation of the Effect of the Normal Load on the Interface Fatigue Resistance. *Construction and Building Materials*, Vol. 61, 2014, pp. 200-205.

According to the authors, displacement data indicated that there were three distinct periods during the progression of the test. The first stage involved aggregate interlocking, leading to a quick increase in displacement. The second stage involved a constant, and slow growth stage as sliding continues with an almost constant trend and ending with a slight inflection. The final stage showed a steep incline in displacement, indicating failure propagation. Ultimately, a 50% reduction in shear stiffness and the number of cycles to failure were used to categorize responses of the specimens. The authors also developed an interface regression law to relate shear stress, normal stress and number of cycles to failure. Monotonic testing results were compared in an attempt to show a correlation between the two tests, but it was not found in this study.

2.3 Summary

The importance of incorporating cyclical loading into the design process is clearly indicated through the efforts of the research described in section 2.2.2. This could have

a significant impact on the pavement design process. Better prediction of pavement life could be obtained through the introduction of a practical new method of analysis. It is important to note that there are many existing bond strength tests currently in practice, as indicated above. However, cyclical tests often take long periods to complete, and can require new equipment. Though more recent efforts have gone towards modifying existing bond strength testing devices to allow for fatigue testing, providing more functionality from a singular device.

Though several tests to evaluate interface bond exist, there is no consensus on which type of test provides the best prediction of pavement performance. Despite the fact that bond strength tests are a commonly accepted method of evaluation, they primarily focus on the uppermost layers of the pavement system. As a result, most bond strength tests evaluate the potential for slippage (high temperature) and/or delamination (low temperature). However, the literature suggests that there may be an additional mechanism of failure that is deeper within the pavement system which has not yet been fully evaluated.

It is common knowledge that the loading experienced by pavement is not the result of a single loading incident. Therefore, bond strength tests, which use monotonic loading modes, may not provide the best representation of what actually occurs in the field. Further, evaluating the quality of the bond at pavement layer interface is paramount to fully predicting pavement life. Therefore a proper evaluation of the materials used for bond should be incorporated into research evaluation, which to date has not been a major component fatigue or cyclical testing research efforts. Poor bond leads to an increase in the magnitude of critical strain and a change in its location.

Properly predicting pavement response at these inherent discontinuities (interfaces) during the pavement design process can enhance roadway performance.

CHAPTER 3
STRESS ANALYSIS

3.1 Identification of Critical Stress States

Based on the existing literature, the need for a test method that captures the resistance to breakdown response of the bond at the pavement interface became apparent. As previously discussed, field observations of trenched sections of pavement structures indicated near-surface cracking along the wheel path occurs in areas of deeper interface debonding (Willis and Timm, 2007). Identifying the location and magnitude of the critical stresses that promote this type of debonding was therefore necessary for the development of a new test method.

Traditional bond strength tests have been used to evaluate interfaces located 0.5 to 1.5 inches beneath the pavement surface. This is a typical thickness of a surface course. At these depths in the pavement system, bond strength is considered to be the driving factor for predicting pavement distress. However, there is a lack of knowledge about what occurs at interfaces deeper in the pavement system. As a result, a parametric study was conducted using an elastic layer analysis program to locate critical stress states at a number of depths within the pavement system.

3.2 Elastic Layer Analysis

It is common to utilize computer modeling to provide relative predictions of pavement performance. These models are often coupled with laboratory testing to provide input data to improve prediction accuracy. There are numerous modeling techniques that exist to predict pavement response. The KENPAVE program was selected to provide a linear elastic analysis of the pavement structures considered in

this research. Within the KENPAVE program is KENLAYER, a tool specifically developed for the evaluation of flexible pavement systems.

3.2.1 KENLAYER Data Analysis

KENLAYER was used to identify potentially critical stress states in typical flexible pavement systems. The following hypotheses were made:

- Pavements with higher stiffness ratios between the asphalt concrete (AC) layer and the base layer produce higher shear and confining stresses
- There are critical locations in the pavement system where interfaces can be located at which shear stresses are high and confining stresses are low

In order to evaluate these hypotheses, the following objectives were employed:

- Model various stiffness ratios to determine how temperature affects shear and confining stresses felt by the pavement system
- Identify critical locations in the pavement system where shear stresses are highest and confining stresses are lowest

Data analysis focused on identifying the locations of critical stress states within the pavement system. These critical locations were defined by having a high shear stress, combined with low levels of confinement. In these areas, it is suspected that the onset of debonding in the pavement is most likely to occur. The pavement layer was assumed to be fully bonded during this analysis.

A typical asphalt pavement section was analyzed to replicate systems that are traditionally found in the field. Figure 3-1 provides a characteristic cross-section of a flexible pavement, as it would be modeled using KENLAYER. It consists of a surface layer (friction course), an asphalt concrete layer (binder course), a base layer (base course) and the subgrade. In order to identify critical stress states, the surface (friction) and binder courses were considered fully bonded.

Initial analysis was conducted on an 8.0 inch binder course with a 12.0 inch base. The 8.0 inch structure, which is often found on interstate pavements and major highways, relates to pavement systems with relatively long service life. Further analysis was conducted on a 4.0 inch binder course layer and 12.0 inch base course as indicated in Table 3-1, which is more commonly found in the field. The evaluation of the 4.0 inch pavement structure generally represents a thin asphalt layer.

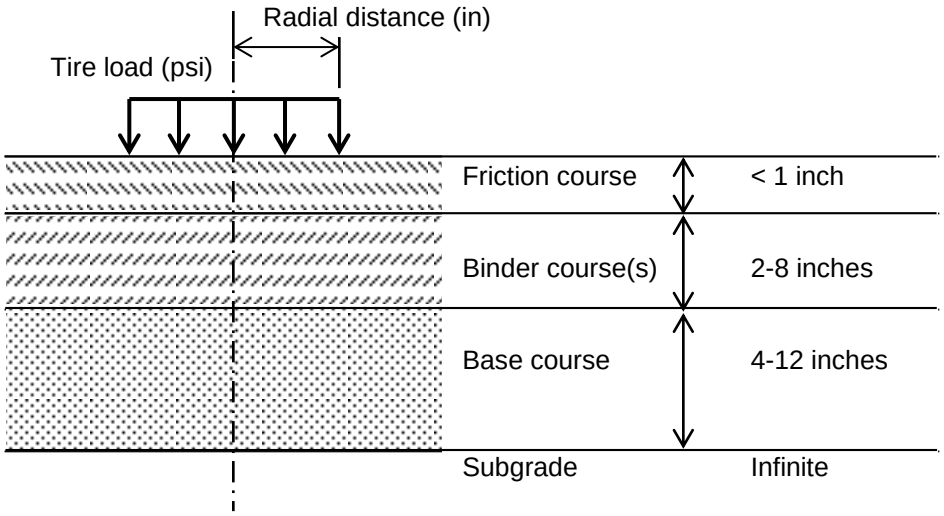

Figure 3-1. Typical cross section of a conventional flexible pavement

A circular loading condition was chosen to represent a single wheel. An 18.0-kip single-axle load with uniform tire pressure of 100.0 psi was used for evaluation. The tire was defined to have a 5.35 inch contact radius, which is typical for a single tire (Hwang, 2000). Appropriate elastic moduli (stiffness) were selected based on typical pavement temperatures. The values selected of both the AC and the base layers are also typical values seen in pavement analysis. However, AC layer elastic moduli varied from representing conditions on a hot summer's day (200000.0 psi) to a late fall/early spring evening (1200000.0 psi).

Table 3-1. Layer thickness and material properties.

Stiffness ratio	Pavement layer	Thickness (in)	Elastic modulus (psi)	Poisson's ratio
SR=5	Asphalt concrete	4.0	200000.0	0.35
	Base	12.0	40000.0	0.40
	Subgrade	Infinite	15000.0	0.45
SR=8	Asphalt concrete	4.0	200000.0	0.35
	Base	12.0	25000.0	0.40
	Subgrade	Infinite	15000.0	0.45
SR=20	Asphalt concrete	4.0	800000.0	0.35
	Base	12.0	40000.0	0.40
	Subgrade	Infinite	15000.0	0.45
SR=32	Asphalt concrete	4.0	800000.0	0.35
	Base	12.0	25000.0	0.40
	Subgrade	Infinite	15000.0	0.45
SR=Grad	Asphalt concrete	0.5	1200000.0	0.35
	Asphalt concrete	0.5	1100000.0	0.35
	Asphalt concrete	1.0	950000.0	0.35
	Asphalt concrete	1.0	780000.0	0.35
	Asphalt concrete	1.0	640000.0	0.35
	Base	12.0	40000.0	0.40
	Subgrade	Infinite	15000.0	0.45

AC layers are often idealized to possess a uniform stiffness throughout the cross-section of the pavement for evaluation. However, in the field, temperature change causes variations in stiffness throughout the structure of the pavement. Comparatively, high temperature (low stiffness) is associated with the viscous response where rutting is the primary form of pavement distress, while low temperatures (high stiffness) are associated with a brittle response, where cracking is the major form of pavement distress. Asphalt concrete exhibits viscoelastic properties due to the presence of asphalt binder, consequently, evaluating how the pavement responds to temperature is important. Thus, a stiffness gradient was used to evaluate the effect of temperature on the pavement response.

Based on previous research, the stiffness gradient selected was chosen to evaluate the “sharpest temperature gradient near-surface” (Myers, 2000). This can be caused by rapid cooling of the pavement due rains, age-hardening or temperature differentials due to climate. The addition of the gradient allowed for the evaluation of the effect of field oxidative aging. Since the AC layers analyzed in this study were 4.0 inch layers, only the top 4.0 inches of the stiffness gradient from Myers et al. were used as indicated in Table 3-1.

The stiffness ratio (SR) is the relationship between the stiffness of the asphalt concrete (AC) layer to the stiffness of the base layer described below in Equation 3-1.

$$\textit{Stiffness ratio (SR)} = E_{asphalt} / E_{base} \qquad (3\text{-}1)$$

Where,

$E_{asphalt}$=Elastic modulus of the asphalt layer (psi); and

E_{base}=Elastic modulus of the base layer (psi).

Each stiffness ratio is denoted above in Table 3-1, along with the structural and material properties chosen for evaluation. Also noted in Table 3-1 are the structural and material properties associated with the pavement, which were held constant. Figure 3-2 provides a summary of the pavement structures, and various characteristics evaluated. Pavements are labeled according to either SR or gradient.

As previously discussed, a broad range of AC elastic moduli were included in the analysis. Figure 3-2 summarizes each pavement structure and its corresponding characteristics, which are labeled according to its stiffness ratio or gradient.

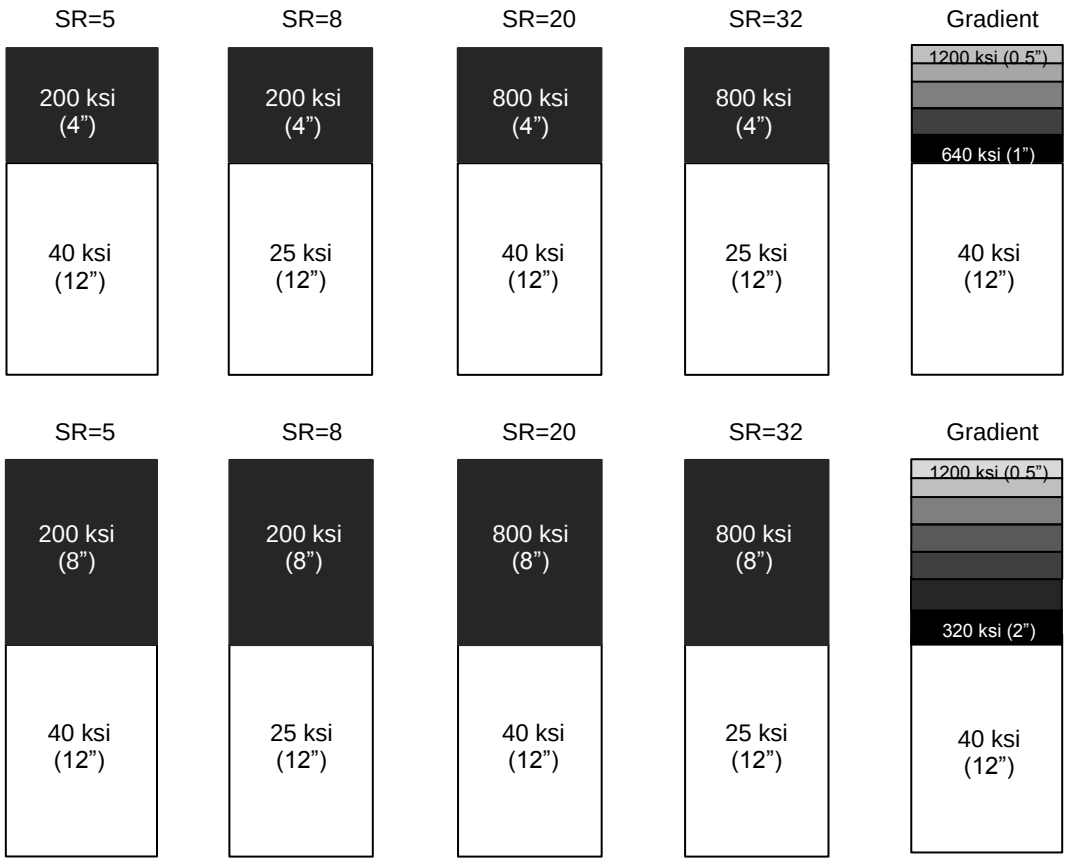

Figure 3-2. Structural characteristics of evaluated pavement sections (layer thickness in parenthesis)

3.2.2 Critical Zone for the Onset of Debonding

The results of the analysis indicate areas within the pavement structure where high shear stress is observed over a broad range of depths around the center of the AC layer. Figures 3-3 and 3-4 show the stress distribution results of the 4.0 inch pavement structures. From Figure 3-3, high shear stress is observed from 1.0 to 3.0 inches, with the maximum value occurring slightly above approximately 2.0 inches in depth. This depth in the pavement agrees with previous research field observations (Muench and Moomaw, 2008; Roque et al., 2011). In addition, as SR increases, shear stress also increases. This is expected, as shear stress is a function of bending, which increases with SR. The maximum shear stress occurred for SR-32, with the gradient having the second highest shear stress response.

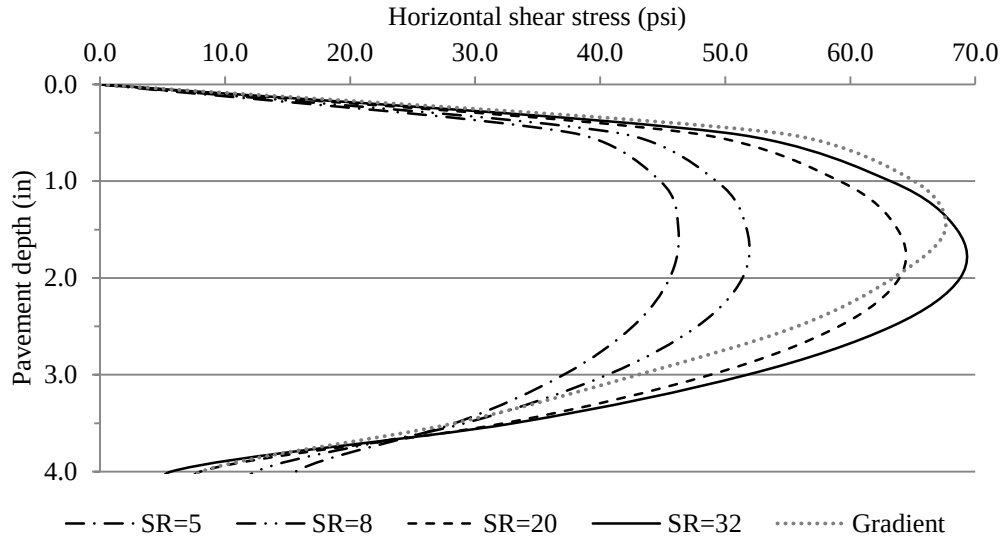

Figure 3-3. Horizontal shear stress through the depth of the 4.0 inch AC layer cases.

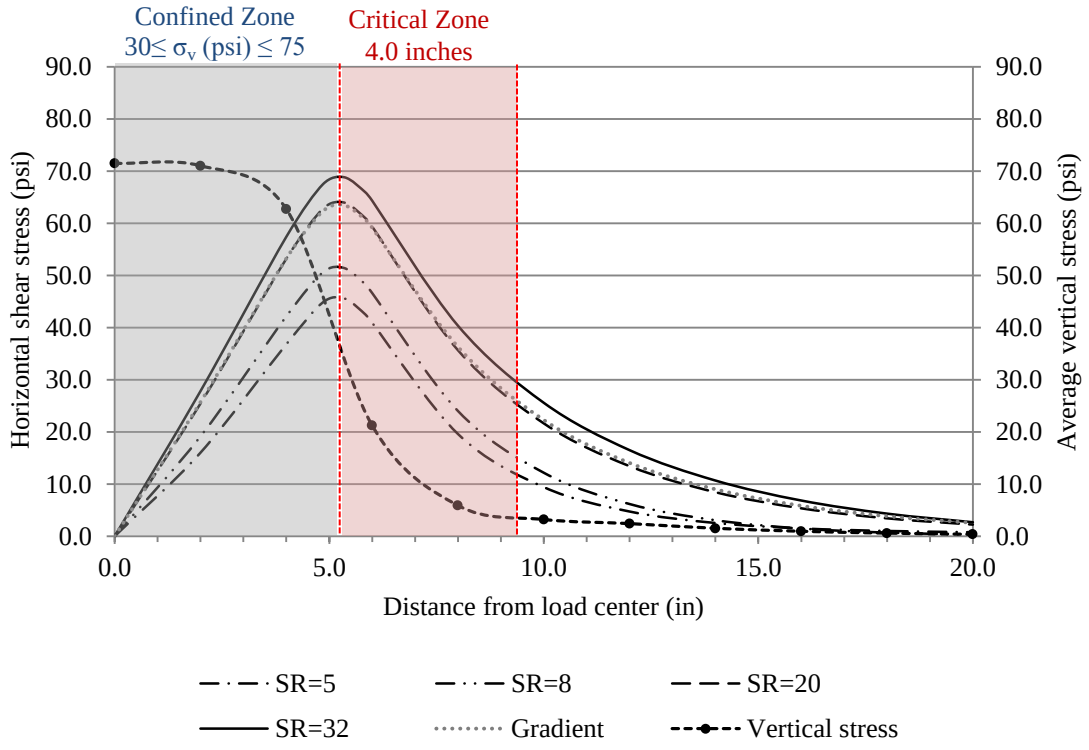

Figure 3-4. Horizontal shear stress and average vertical stress for the 4.0 inch AC layer cases at a depth of 2.0 inches.

Figure 3-4 shows the horizontal shear stress distribution at a depth of 2.0 inches in the AC layer. This figure indicates that the maximum shear stress for each case

occurred under the edge of the tire. The area of confinement (denoted as the “confined zone”) is located directly under the tire, where normal stress reaches nearly 75.0 psi. Once outside of the edge of the tire and the confined zone, normal stress decreases drastically below 30.0 psi, located outside of the tire edge. In this approximately 4.0 inch area (denoted as the “critical zone”), confinement rapidly drops below 30.0 psi, yet shear stress values are relatively high for each SR (greater than 30.0 psi). Converting the 100.0 psi stress applied into an equivalent load indicates the pavement was subjected to 8992.0 lbf. Therefore, estimated load levels at the critical depth of 2.0 inches were 6294.4 lbf (equivalent to 70.0 psi of shear stress).

Similar results were found for the 8.0 inch AC layer structures as indicated in Figures 3-5 and 3-6. As expected, the magnitude of the horizontal shear stress through the depth of the AC layer and located under the edge of the tire is lower than the 4.0 inch AC layer cases. This is due to the reduction of bending as a result of a thicker AC layer, while maintaining the same structure underneath. An area of high shear stress exists between 1.0 to 3.0 inches beneath the surface, with a maximum at the depth of 2.0 inches, comparable to the results for the 4.0 inch AC layer structures. This indicates that at 2.0 inches beneath the pavement surface, horizontal shear stress reaches its maximum value, regardless of AC thickness and the characteristics of the pavement structures analyzed. Figure 3-6 also indicates the existence of a confined zone within the pavement structure located beneath the tire, and ending at the edge of the tire, as in the 4.0 inch AC layer case. Normal stress reached closer to 90.0 psi in this case. This area was then followed by an area in the pavement where confinement was relatively low (reducing drastically from 40.0 to 10.0 psi), but shear stress values were relatively

high (45.0 to 30.0 psi). Since the maximum horizontal shear stresses were much lower than in the 8.0 inch case, the critical zone was approximately 2.0 inches from the edge of the tire.

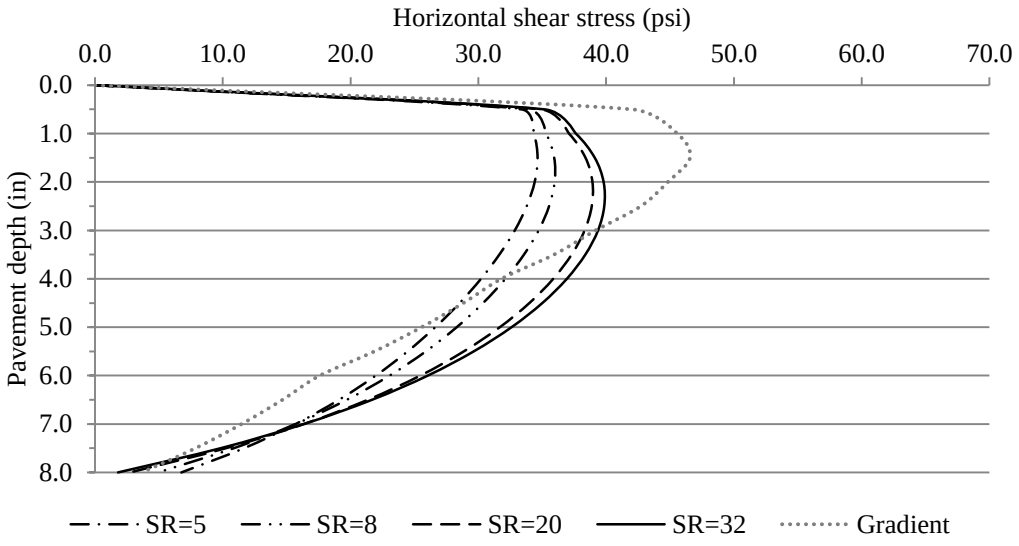

Figure 3-5. Horizontal shear stress through the depth of the 8.0 inch AC layer cases located under the edge of the tire.

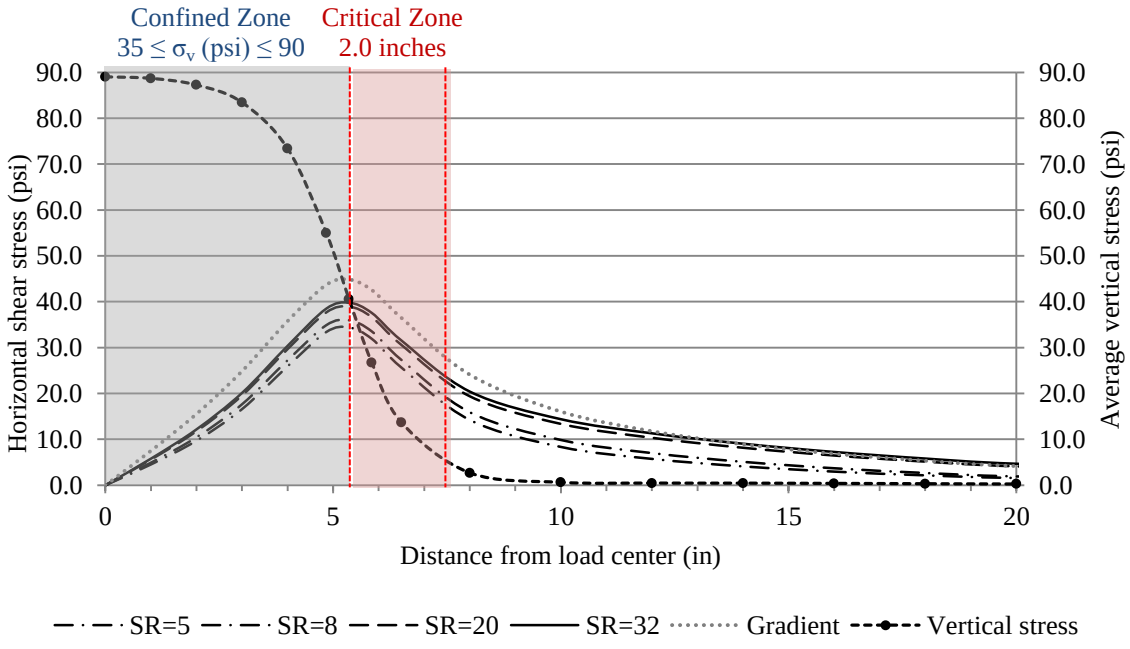

Figure 3-6. Horizontal shear stress and average vertical stress for the 8.0 inch AC layer cases at a depth of 2.0 inches.

3.2.3 Traffic Wander, Tire Size and the Critical Zone

The results of section 3.2.2 indicate that there is the existence of a critical zone of high shear and low confinement at a depth of 2.0 inches in the AC layer extending from the edge of the tire for up to 5.0 inches. This critical zone can potentially promote the development of a debonded area, referred to as a debonding strip, along the tire wheel path. However, traffic does not stay in a singular path along the highway, as drivers in their vehicles tend to display lateral movement within a lane. This lateral movement is referred to as traffic wander, and occurs in the transverse direction of the pavement. Though traffic wander is often unaccounted for in structural design, it has an effect on the pavement response. Previous studies indicate that the lateral position of wheel loads follow a normal distribution with a standard deviation of approximately 4.0 to 11.0 inches within a lane depending on the method used for calculation (Erlingsson et al., 2012).

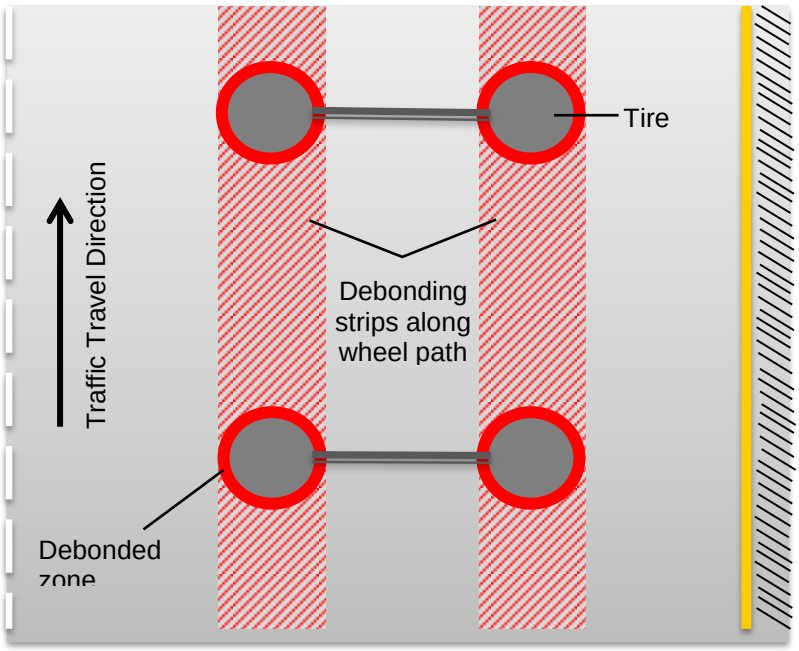

Figure 3-7. Schematic of debonded zone around tire and debonding strip along the tire wheel path within a traffic lane.

The impact of tire wander varies with the type of tire used by truck drivers. As the trucking companies move to increase the use wide-based radial tires due to their fuel efficiency, the impact on effect of wander can increase the debonding strip. Tire contact size can range from a conventional radial tire with a contact width of 8.0 inches, to wide base tires ranging from 12.0 - 18.0 inches of contact (Roque et al. 2011). In combination with wander, the debonding strip width can vary from 20.0 up to 35.0 inches (Figure 3-7), as the trucking industry moves towards using wide-based tires to reduce emissions, improve fuel efficiency and increase load capacity.

3.3 Summary

The elastic layer analysis clearly indicates the existence of a critical zone within the AC layer. In this zone with an applied load of 100.0 psi, high horizontal shear stress up to 70.0 psi can be coupled with low vertical stress (confinement) at a depth of 1.0 to 3.0 inches below the pavement surface, where the most critical depth is approximately 2.0 inches. When pavement interfaces are located within this range of depth, a debonding strip may occur along the interface, even in the case of thick AC layers. In addition, both wander and tire size can impact the debonding strip significantly. Depending on the tire size and breadth of traffic wander conditions, the debonding strip can vary from 20.0 to 35.0 inches in width.

This indicates the need for further analysis of the bond at pavement interfaces, particularly those located near 2.0 inch depths. As indicated in section 2.2.1, shear strength tests are often used to evaluate thin surface AC layers, typically of 0.5 to 1.0 inches in depth. The most critical areas located deeper within the pavement surface, have low confinement which may lead to the onset of debonding. In these areas, pavement bond shear strength may not be the best method of evaluation, as it may not

capture the gradual loss of bond within the pavement structure. This loss of bond may not result from the pavement reaching its ultimate shear strength, but as a result from the repeated application of high horizontal shear stress where confinement is low. In order to assess this concept that may lead to near-surface cracking, a new bond test method is necessary.

CHAPTER 4
MATERIALS AND SPECIMEN PREPARATION

4.1 Materials

The materials in this research represent those typically used in the state of Florida. In order to replicate conditions typically found at interfaces between structural layers a dense-graded mixture was chosen. All mixtures were made with the same aggregate and binder. A Superpave mix designed fine dense-graded asphalt mixture (GA-I2) was selected and the full gradation and mix design are located in Appendix A. The aggregate in the mixture was Georgia granite and local sand with a 12.5 mm (0.492 in) nominal maximum aggregate size. The GA-I2 particle size distribution (gradation) is shown in Figure 4-1. A conventional asphalt binder, PG-67-22, was selected for this mix design with a 4.8% optimal asphalt content. This mixture is commonly used in FDOT projects and serves as a good performing granite mix design.

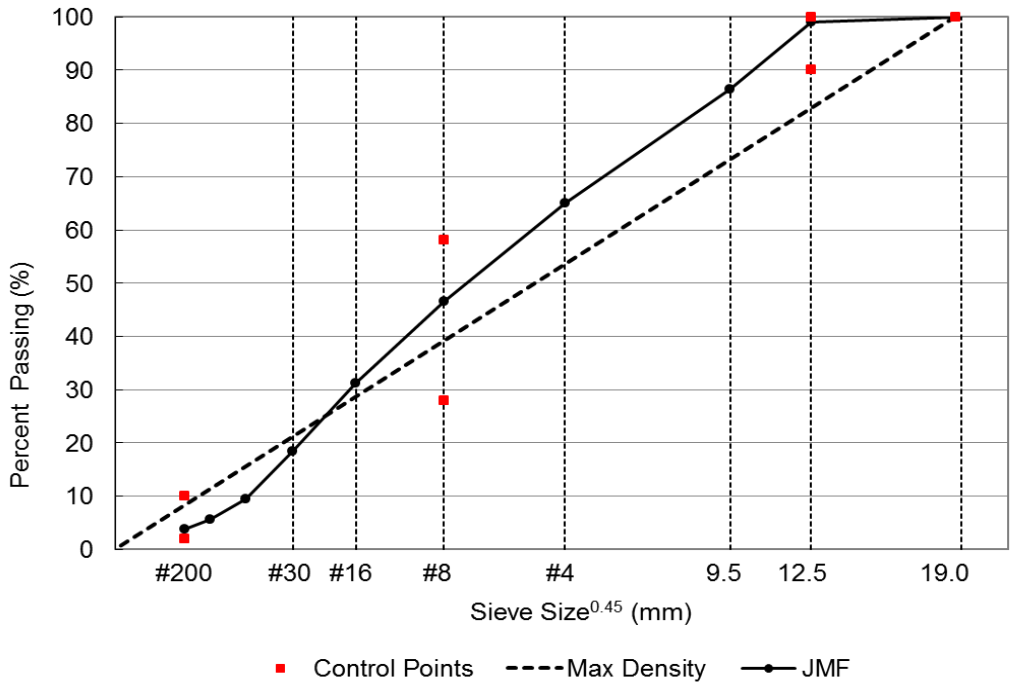

Figure 4-1. GA-I2 dense-graded aggregate mixture.

The aggregate used in this research was obtained from several mines used in the North Florida region. Table 4-1 shows a detailed breakdown of the locations for each material.

Table 4-1. Aggregate sources.

Material	FDOT Code	Producer	Pit No.
#78 Stone	43	Junction City Mining	GA-553
#89 Stone	51	Junction City Mining	GA-553
W-10 Screenings	20	Junction City Mining	GA-553
Local Sand	-	V.E. Whitehurst & Sons	Starvation Hill

Three different tack coat materials were selected for evaluation in this research. All materials were supplied by companies that produce tack coat. As the state of Florida has chosen to almost exclusively use trackless tack (TT) coat in construction, one was selected for use. A conventional tack (SS-1) and a PMAE (PT) were selected for comparison. Since the trackless tack and the PT are proprietary, application rates provided by the manufacturer were chosen. A low (0.02 gal/yd^2) and high application rate (0.155 gal/yd^2) for the conventional tack coat was chosen from the NCHRP 9-40 report. The low rate came as a result of the international survey discussed in the report, whereas the high rate was selected as the rate chosen for their testing (Mohammad, 2012). This would allow for the evaluation of the effect of tack coat material and application rates.

Each tack coat had manufacturer specific storage and application temperatures which were followed to ensure optimal use of the materials. Tack materials were stored

in their original containers and were occasionally stirred according to their storage instructions. Materials for tack coat were obtained from three vendors across the US.

4.2 Specimen Preparation

All specimens were prepared in the laboratory for testing using the device described in section 5.2. Double-layered specimens were prepared for testing by combining half of a full Superpave pill, and an overlay mixture through compaction. A total of 30 specimens were made for trial testing, and 30 specimens were used in final testing, in accordance with the testing plan below in Table 4-2. For final testing, triplicate specimens were produced for the evaluation of each testing method, tack coat, and application rate.

Table 4-2. Testing plan.

Tack coat	Surface type	Application rate	Temp °C	Replicates	Tests	Total specimens
None (NT)	Compacted	0.000 gal/yd^2	25.0 ± 2.0°C	3	2	6
Trackless (TT)	Compacted	0.060 gal/yd^2	25.0 ± 2.0°C	3	2	6
PMAE (PT)	Compacted	0.120 gal/yd^2	25.0 ± 2.0°C	3	2	6
Conventional (CTL)	Compacted	0.020 gal/yd^2	25.0 ± 2.0°C	3	2	6
Conventional (CTH)	Compacted	0.155 gal/yd^2	25.0 ± 2.0°C	3	2	6
Total number of tested specimens						30

4.2.1 Batching and Mixing

A 4500.0 gram batch was produced to create two bottom halves using the gradation found in Appendix A. An overlay batch of 2254.8 grams was produced for

each bottom half. This mass was determined based on a proportional design method described in Appendix B. After batching, asphalt binder and aggregates were placed in an industrial laboratory oven and heated for two hours prior to mixing, at a temperature of 315.0 °F (157.2 °C) (Figure 4-2).

Figure 4-2. Materials and mixing tools inside of the oven. Photo courtesy of author.

After being heated, the appropriate combination of aggregate and binder were mixed in a mechanical mixer (Figure 4-3) until the asphalt covered the aggregate well.

Figure 4-3. Mechanical mixer. Photo courtesy of author.

Mixtures were short term oven aged also at 315.0°F. After an hour in the oven, the mixtures were stirred to ensure uniformity in aging.

4.2.2 Initial Compaction

Specimens were produced by compacting a full Superpave pill using the Superpave Gyratory Compactor (SGC) to 4.0 ±1.0% air voids where N_{design}=27 (Figure 4-4).

Figure 4-4. Device used to produce SGC pills. Photo courtesy of author.

4.2.3 Cutting

Once the pill cooled for 24 hours after compaction, the pills were measured and the halfway point of the cylinder was measured. Using a metallic permanent marker, a line was drawn on the pill to identify the midpoint. A water-cooled masonry saw (Figure 4-5) with a diamond-tipped blade was used to cut each pill. The blade was aligned with the halfway point of each specimen. This process allowed for each pill to create two

bottom halves for future specimens. After cutting, each bottom half was labeled and air dried overnight before further preparation. A fan blew ambient air to help with the drying process. Specimens were elevated on wire mesh stands to allow the air to move underneath as well.

Figure 4-5. Water-cooled masonry saw prior to cutting a specimen. Photo courtesy of author.

4.2.4 Tack Coat Application

Tack coats were removed from their storage containers and slowly transferred into a graduated glass flask. Glass was chosen because it does not interact with the chemicals used in the tack coats, as suggested by a manufacturer. A glass thermometer was inserted into the flask to measure the temperature. Using an insulated portable heater (Figure 4-6), each tack coat was then heated to the appropriate temperature for application.

Figure 4-6. Heater with graduated cylinder containing tack coat. Photo courtesy of author.

Prior to the application of the tack coat, the average of three height measurements was also recorded to provide a reference for future testing for the location of the interface. In addition, the initial weight of the specimen was recorded to ensure the proper amount of tack coat was applied. The scale was then zeroed for the application of the tack coat. The appropriate amount of tack coat was evenly applied with a brush (Figure 4-7) to the compacted side of the base (Figure 4-8). It is important to note that the compacted side of the bottom half was selected to represent a typical new pavement surface. The total mass of the combined initial weight of the specimen and the applied amount of tack coat was recorded.

Figure 4-7. Brush used to apply tack coat. Photo courtesy of author.

Figure 4-8. Tack coat being applied to the bottom half of a specimen on a scale. Photo courtesy of author.

An equivalent mass for each tack coat application rate was calculated based on the percentage of binder using the equations found in Appendix C. After the correct amount of tack coat was applied to the bottom half, the specimens were placed aside to allow for the tack coat to set. The base with tack coat was periodically placed back on the scale to determine if constant weight had been reached. Once the weight stabilized, the bottom half could move to the final stage of specimen preparation, final compaction.

4.2.5 Final Compaction

For the overlay, a batch of 2454.8 grams was prepared to be compacted on top of each bottom half. Once surface preparation of the base and mixing and aging of the overlay were complete, compaction of the base could take place. The base of the SGC mold was removed to insert the base. The base was placed in the SGC mold with the cut surface facing down (Figure 4-9).

Figure 4-9. SGC mold with base insertion in progress. Source: Chen, Y. Composite Specimen Testing to Evaluate the Effects of Pavement Layer Interface Characteristics on Cracking Performance. *University of Florida*, 2011.

Loose mix was subsequently placed on top of the surface of the bottom half, and then the specimen was compacted to 7.0 ±1.0% air voids.

4.2.6 Determining Air Void Content

During the production of trial specimens, the overlay was compacted to a height of 2.2 inches, instead of choosing a gyration number. This resulted in very high compaction effort, where the number of gyrations was between 180 and 280, well over what would be expected in the field. This was due to the variation in height of each bottom half. An analysis of the results for trial specimens can be seen in Figure 4-10. From this analysis, a conservative gyration number was selected for future trial tests and final testing, where N_{design} = 25.

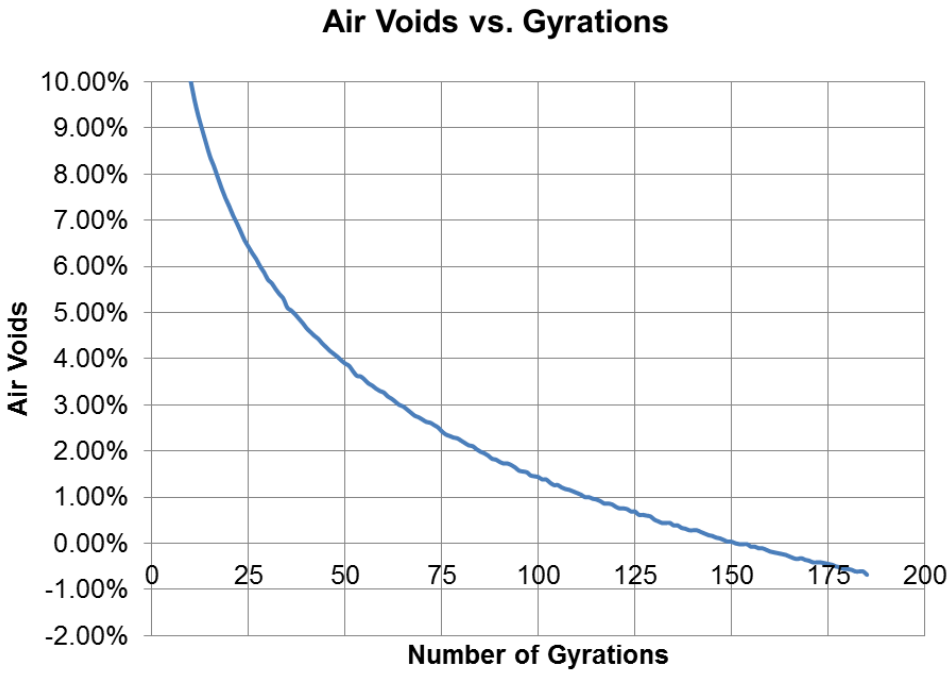

Figure 4-10. Determination of number of gyrations to compact the overlay.

Once the specimen preparation process was complete, specimens were transferred to the Advanced Materials and Characterization lab until testing. Specimens remained at room temperature prior to testing.

CHAPTER 5
TESTING DEVELOPMENT AND DATA INTERPRETATION

A new testing system was developed to analyze a new mechanism of interface bond failure due to repeated load application. Results from this new device were used to compare with the relative results of a typical bond strength test. Ideally the new system would allow for repeated application of shear stress at the interface with little to no confinement, simulating what occurs in real pavement systems as discussed in chapter 3.

A deformation controlled loading mode might provide the most relevant comparison to field conditions, by bringing the interface back to zero deformation after each passing of the load. However, there is no existing knowledge of how to effectively conduct repeated shear testing using a deformation controlled loading mode. The results of the repeated shear testing configuration could provide a measurement of the reduction of effective stiffness at the interface, obtained from by the change in load over a constant deformation.

Ultimately, an initial configuration for a new system was based on the information obtained from the literature review in chapter 2. As mentioned in section 2.2.2, fatigue-type tests can be plagued with complications associated with the testing configuration, loading mode, and time for testing. This chapter primarily focuses on device selection and issues associated with testing and obtaining usable data for interpretation.

5.1 Changes in Florida

As the state of Florida moves towards the sole utilization of non-tracking or trackless tack coats as its bonding method, it was important to evaluate all potential uses for this material. In January 2014, FDOT changed its specifications to implement

trackless tack materials as the only bonding agent for pavement interfaces. However, research in 2011 indicated that brittle systems, like those created by using trackless tack coats, perform poorly by reducing the cracking resistance of materials near the interface (Chen, 2011). However, the work conducted by Chen focused primarily on issues of cracking performance, and not interfacial bond.

This project began as an effort to answer the question of whether or not moving to a stiffer interface system, defined by the implementation of trackless tack systems, was beneficial to interfaces located deeper in the pavement system. The scarcity of information on the potential impacts beyond interfaces located directly beneath thin friction course layers became apparent in the literature review. Moreover, the consequence of only allowing for brittle interface systems in areas where strength may not be the primary contributor to failure is also not addressed.

The FDOT requires the materials chosen by its contractors to reach a minimum bond strength value of 100.0 psi for utilization on its roadways. This value is obtained using bond strength testing, which is the primary method used by many state agencies in the US. Bond strength tests help researchers understand near-surface failures, like delamination. However, bond strength testing may not necessarily provide insight on issues of pavement bond occurring deeper in the pavement system. As mentioned in section 1.1, this type of testing is often conducted to evaluate friction courses and loads located directly beneath the tire, where levels of confinement are highest. These are very high-stress, single-excursion-to-failure episodes, which bond strength tests are able to replicate. However, it represents just one way in which the bond between pavement layers can fail.

Roadways are subject to repeated applications of various stresses. As indicated in chapter 3, critical stress states where pavements experience low levels of confinement and relatively low levels of shear stress exist in the pavement system. No existing test evaluates the resistance of the bond to breakdown over time due to the repeated application of lower magnitude shear stresses, which may be another mechanism by which bond at the interface fails. With a focus on addressing the changes to practice in Florida, the test methods discussed in the remaining sections of this chapter were developed.

5.2 Florida Interface Shear Tester

Given there was no existing device to assess pavement bond resistance to breakdown at the interface, several devices previously used in asphalt research were identified with the initial goal of identifying one that could work in both monotonic and repeated loading modes. This would allow for consistent specimen preparation and evaluation after they were subjected to each loading method. After reviewing the literature, several guillotine-type strength test devices that could be mounted on a universal testing system (ex. MTS) were chosen for comparison. This style of device is very common for evaluation of bond strength and would be familiar to potential future practitioners of the new method proposed by this work (Mohammad et al., 2012). In addition, the specimens produced for this type of test are commonly used. They were cylindrical, and could either cored from the field, cored from laboratory prepared slabs or produced in the laboratory using a SGC.

Schematic drawings of three potential devices were obtained to determine whether or not they could withstand repeated application of shear stress or be modified to do so. Ultimately the LISST (Figure 2-5) and the FDOT Shear Tester (Figure 2-2)

served as inspiration for the new device (Figure 5-1). These devices were discussed in more detail in chapter 2.

The Florida Interface Shear Tester (FIST) was produced by Associated Technologies & Manufacturing (ATM) in Louisiana (Figure 5-1). The FIST was a modification of the LISST device, designed to our specification to allow for repeated load. The FIST was installed on a MTS servo-hydraulic load frame to allow for accurate measuring of the material response (Figure 5-2). The FIST included the addition of a thicker and elongated bottom plate to reduce the eccentricity of the load, increase flexural strength of the device, and provide a better location to attach it to the MTS system. Its primary components are a loading frame that is allowed to move vertically, and a reaction frame that is stationary, each with a removable top collar.

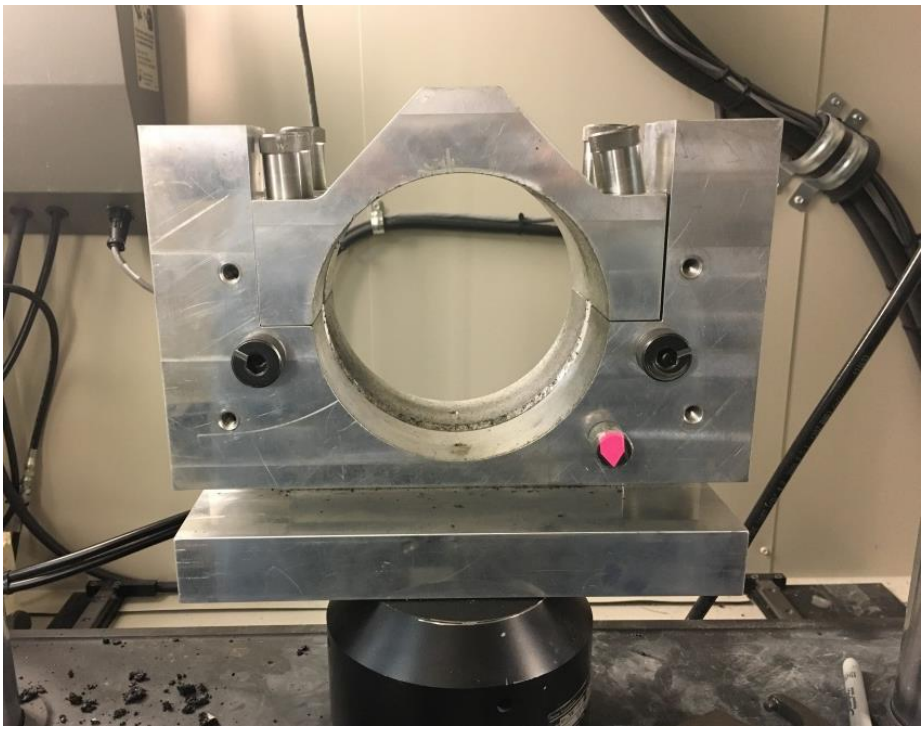

Figure 5-1. Image of the FIST. Photo courtesy of author.

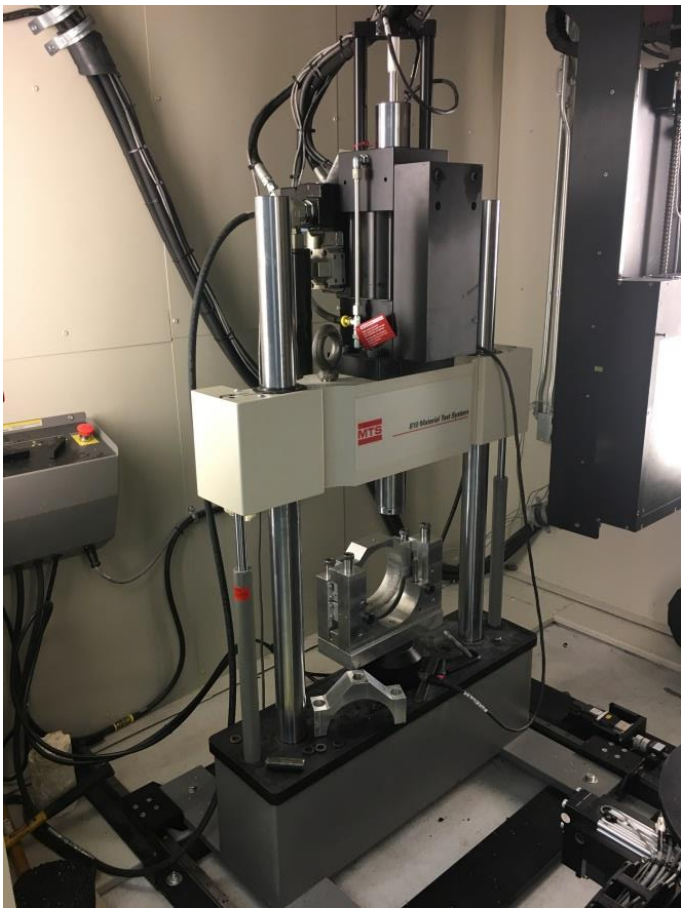

Figure 5-2. Image of FIST mounted on the MTS system. Photo courtesy of author.

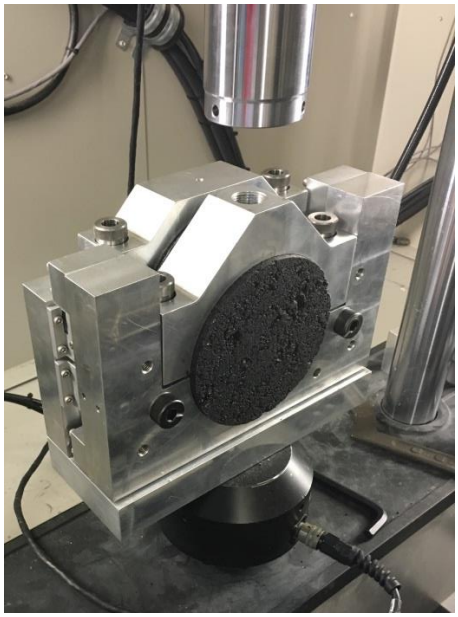

Figure 5-3. Close up view of a specimen loaded in the FIST. Photo courtesy of author.

The frames were designed with a 0.5 inch gap. The two collars are removed in order to properly place the specimen, allowing for the interface to be aligned within the gap. Two locking pins were provided to attach each collar to the base of the loading and reaction frames. The pins are tightened around threaded rod couplings (originally designed with a finger grip) which allows the device to tighten the around the specimen. As shown in Figure 5-3, the top of the loading frame collar comes in contact with the MTS actuator.

A modification of additional steel was added to the top of the loading frame collar to provide a more even distribution of the load where the collar contacts the specimen. In addition, the added height prevents the actuator from coming into contact with the reaction frame. The additional material also provides space for a threaded bolt to be attached, which can fully link the loading frame collar to the MTS system actuator, allowing them to act as one (if desired). Multiple collar inserts were provided by ATM to allow for the testing of 150.0 mm (5.905 inches) and 4.0 inch diameter specimens. Only 150.0 mm diameter specimens were used in this research.

The following sections discuss several iterations of testing and their corresponding results. For each loading method (monotonic and repeated), several trial tests were run to identify the optimal testing conditions. In some cases, the optimal testing conditions required device modifications. As issues that contributed to loss of energy applied at the interface became apparent, their sources were eliminated. These energy losses were either due to the device itself or the chosen testing mode. Ultimately a final test method was decided upon for both monotonic and repeated testing, of which the findings will be presented and discussed.

5.3 Energy Losses and Their Solutions

Since the FIST was a modification of an existing bond strength test, monotonic loading was chosen for initial testing. Using information provided by researchers at the LTRC facility, a program was developed in the MTS MultiPurpose TestWare (MPT) software to apply a strain rate of 50.8 mm/min (2.0 in/min). Specimens chosen for initial testing had interfaces, but no tack coat applied. Initial values were in the 300.0 psi range, nearly double the anticipated results based on previous tests with specimens of the same geometry (Mohammad et al., 2012). It is important to note that there was no reference made to the types of materials used for the mix design of the specimens in the NCHRP 9-40 report, though the authors discuss using a variety of mix designs. Researchers at the LTRC facility were contacted to obtain a more detailed explanation of their operating procedures for their device. According to researchers at LTRC, bond strength testing procedures adopted for the FIST were consistent; however there was little confidence in this response, as it remained unclear what led to the increase in stress.

A secondary set of tests were performed to compare with another loading rate. The loading rate was adjusted in an attempt to achieve results similar those obtained by the FDOT (Sholar et al., 2004). This was also useful for addressing the changes to Florida's specifications, as the materials used in this this research are consistent with materials used in the state. Thus, the loading rate was reduced from 50.8 mm/min (2.0 in/min) to 2.54 mm/min (0.1 in/min). Though the results became more similar to those found by Sholar et al., upon further inspection the specimens were not failing directly through the interface. This indicated that the measured response was not only that of

the interface, but also the mixture itself. This led to the investigation of the influence of gap width on shear strength test results.

5.3.1 Gap Width

After observing several tests with the 0.5 inch gap width, failure was seen propagating from a contact point where the inside corners of the collars touched to the specimen and through the mixture. From this point, cracks moved through the mixture and ultimately reached the interface. The results of these tests were suspected to be of in-layer shear behavior and not necessarily representative of the interface. The right side of Figure 5-4 shows specimen T-S2B that failed through the mixture during trial testing instead of through the interface, as shown on the left side with specimen CL-S3.

Figure 5-4. Two specimens failed with different gap widths on the FIST. Photo courtesy of author.

The device specification called for a 0.5 inch gap between the collars on the device. Upon a more critical investigation, a chamfered edge on the interior side of each collar added 0.125 inches to each side. This meant that the gap width was effectively 0.75 inches, much larger than what has been previously found in the literature. Figure 5-5 shows the full extent of the beveled edge on a collar insert, which is difficult to show on the FIST due to its location.

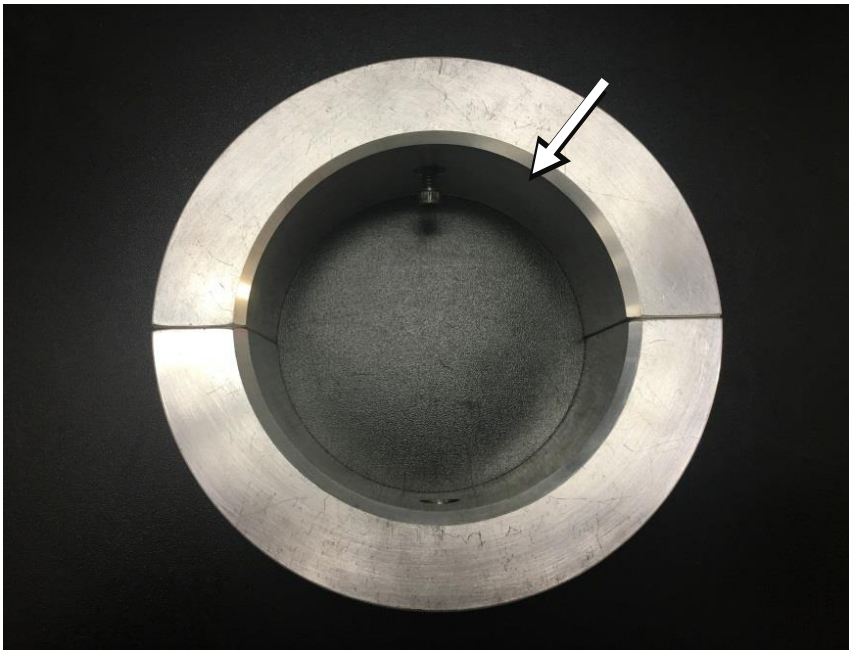

Figure 5-5. Collar insert that shows the beveled edge on the FIST. Photo courtesy of author.

Despite the existence of several modified shear bond testing devices, there remains limited evidence relating to why a specific gap width was chosen. A study on gap width that investigated interlayer versus in-layer shear behavior also noted a lack of previous research on gap widths (Raab et al., 2010). This work was in response to concerns raised in response to the modifications made by the United Kingdom (UK) for standardization of European testing. The UK wanted to ensure that devices would allow for specimens to be properly aligned between shearing rings in direct shear tests. Raab

et al. investigated 0.0, 2.5 and 5.0 mm gap widths and compared bond strength between the pavement layers. Specimens were comprised of four layers, with the top layer being stone mastic asphalt (SMA), and all subsequent layers being asphalt concrete, in accordance with Swiss standards. Five to seven 150.0 mm diameter cores were tested at 20.0°C on a Leutner Shear Test (Raab et al., 2010), which is a guillotine style device, for each gap width with loading rates of 2.5 mm/min and 50.0 mm/min being evaluated.

Results from this work indicated that eccentricity is increased as gap width increases. This eccentricity leads to a bending and shear stress state. Additionally, the authors mentioned that zero gap width would be ideal, but not practical. Their research indicated that the gap width on existing direct shear devices should not be greater than 2.5 mm. The results also showed that in-layer shear forces were higher than shear forces at the interface. Though there is limited research on the effect of gap width on interface shear bond results, these results confirmed that adjusting the gap width was important, particularly since the gap width of the FIST was nearly an order-of-magnitude larger than the largest gap width used by previous researchers.

Large gap widths can be associated with lack of a defined failure plane, resulting in failure occurring at the weakest point in the material (Raab et al., 2010). This was visually confirmed in Figure 5-4. Previous research also indicates that eccentricity is increased as gap width increases (Raab et al., 2010). The eccentricity caused by the larger gap width allows for bending in the specimen, thus the results are a combination of bending and shear stress. Thus, reducing the gap width of the FIST device became necessary to improve how the load was being transferred to the specimen.

The FIST gap width was reduced to allow for the comparison of results between those obtained from previous FDOT Shear Bond testing (Sholar et al., 2012). It was ultimately reduced to 0.25 inches (6.35 mm), which is larger than the width suggested by Raab et al. This width allows for some irregularity in the interface surface, so that the interface can be aligned within the shear plane, but also reduced eccentricity in the specimen during loading. This reduction also involved the removal of the chamfered edge dimension on either side of the device.

SGC pills (specimens without an interface) were subsequently tested to obtain an in-layer shear stress value. The comparison of the results from a typical pill and a typical no tack specimen with an interface is shown in Figure 5-6. Although the response is similar to what was seen for no tack specimens, it is believed that the slight increase in peak stress was due to the specimen failing through the mixture first.

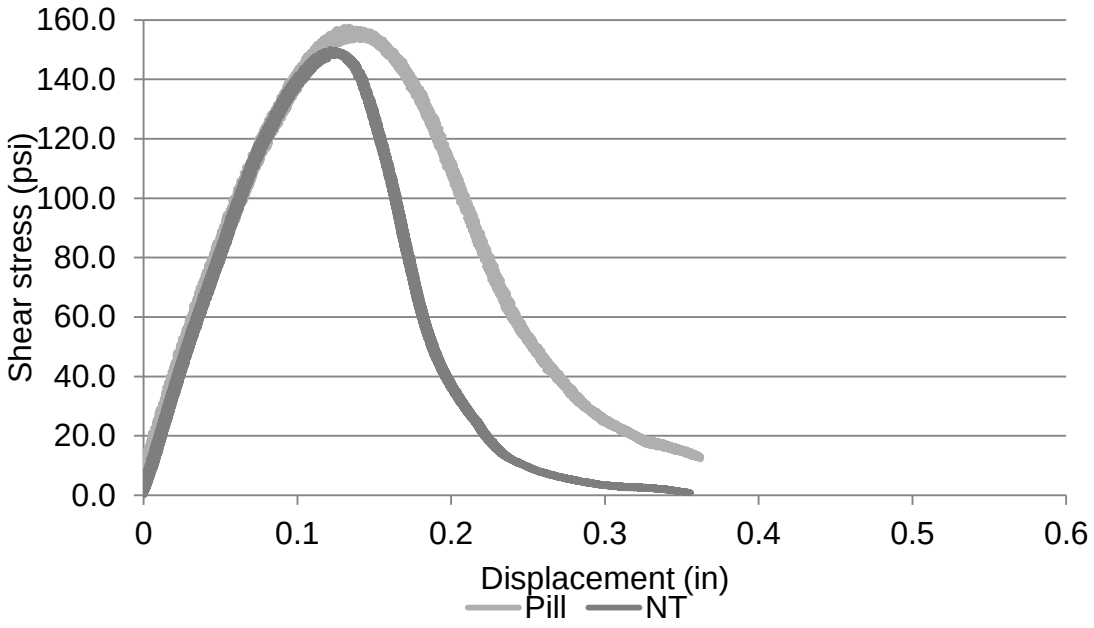

Figure 5-6. Comparison of shear stress response of a pill and specimen with no tack.

After the gap width was reduced, specimens failed along the interface, as originally anticipated. The right side of Figure 5-4 shows specimen CL-S3 which failed through the interface after the gap width was adjusted for final testing.

5.3.2 Bond Strength Testing

Strength testing was conducted using the FIST device for evaluation of the various interface conditions indicated in chapter 1. Specimens were prepared according to the steps in section 4.2, and for each interface condition, three replicates were evaluated. The following steps were taken prior to testing:

- Bring the loading and reaction frames to the same level and use the pin to secure them in place
- Place the specimen in the FIST, aligning the interface marking with the gap. The bottom half of the specimen should be on the reaction frame side, and the top half on the loading frame side
- Draw the direction of loading on the specimen
- Lock the specimen in the collar by tightening the locking pins using the knurling until finger tight and ensure cams are completely tight
- After checking the specimen to ensure it is still properly aligned, remove the pin and begin testing.

The program starts by the actuator applying a 10.0 lbf seating load, after which the operator can begin testing. The actuator then moves down at a constant rate of displacement 2.54 mm/min (0.1 in/min) until the predetermined displacement limit of 0.1 inches is reached. Once the displacement limit is reached, the actuator retracts and the specimen can be removed from the device. Each test took four minutes on average to complete. The resulting shear-displacement curves for each interface condition are shown in Figures D-1 to D-5. During testing, operator error caused the results of a replicate to be invalid (Figure D-3). The pin used to align the loading frame with the

reaction frame was left in place during testing. The results are therefore not included in the analysis.

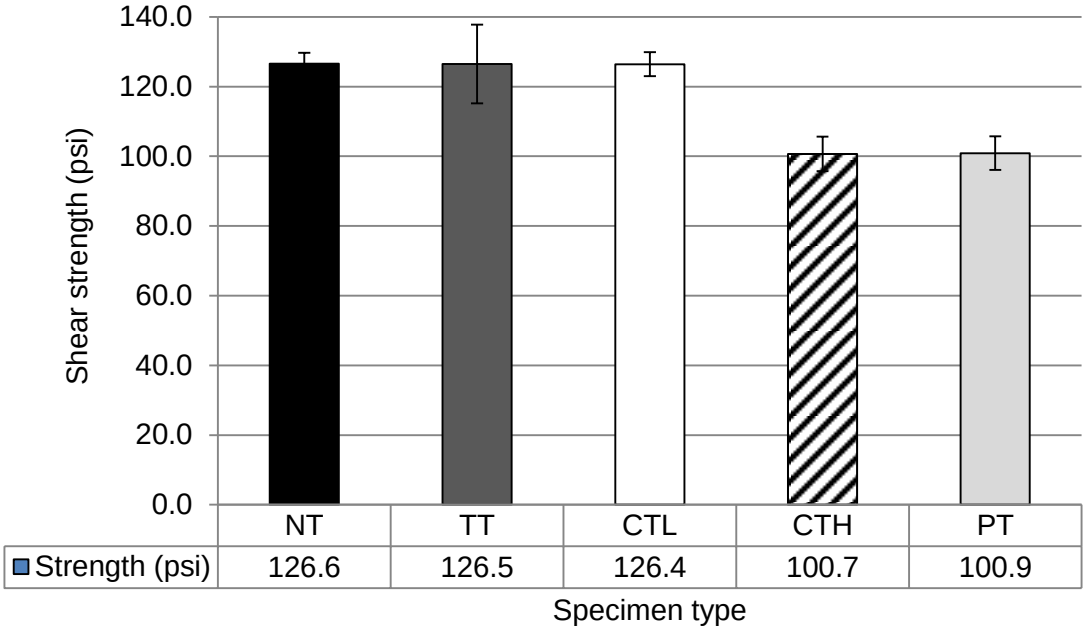

Figure 5-7. Average of the maximum shear stress for various tack coats.

Figure 5-7 shows the average maximum shear stress for specimens with different tack coat. The results of the strength tests indicate that the specimens with no tack coat (NT), trackless tack (TT) and a low application rate of conventional tack coat (CTL) exhibited the highest shear strengths. This is consistent with the results of previous studies on bond strength (Sholar, 2004; Mohammad et al., 2012).

It is important to note that application rate played a role in the results. From Figure 5-7, it is clear that brittle, low application rate materials exhibited higher strength. The NT, TT and CTL shear strengths were 25.7% greater than the PMAE tack coat (PT) and the high application rate of conventional tack coat (CTH) specimens on average reaching 126.6, 126.5 and 126.4 psi respectively. The high application rates of the PT and CTH yielded very similar results of 100.9 and 100.7 psi respectively, indicating that

higher rates of tack coat can diminish the performance of the interface in single action, high stress failures. This also supports previous research conducted on bond strength testing (Sholar, 2004; Mohammad et al., 2012).

5.3.3 Complications with Repeated Testing Modes

For repeated shear stress testing (RST), determining the appropriate testing mode was a major topic to address. Previous research described in section 2.2.2 indicates practitioners of similar fatigue-type analysis have found difficulty with effectively obtaining data for evaluation. Many researchers limit testing time, and extrapolate data for analysis. These considerations went into the process of developing the repeated testing method that would give insight into the breakdown of bond at the interface. However, it is important to note that this previous work was not in an effort to characterize the resistance to the breakdown of the bond at the interface.

The UF MTS servo-hydraulic system allows for both load and deformation controlled repeated testing schemes to be programmed within the MPT software. With any testing mode, it is important to identify an appropriate level of load. Concerns with the ability to estimate and control the amount of load applied to the interface under deformation controlled conditions led to the decision to attempt testing using a load controlled mode. Applied load levels were determined from the elastic layer analysis in chapter 3, in tandem with the results of the strength data presented in section 5.3.2. Several attempts of load controlled testing were made, primarily due to difficulties identifying an appropriate load level that would result in failure of the specimen within a reasonable time frame.

For each variation of the Load Controlled RST (LC-RST), the full loading sequence was one second. The loading period was 0.1 seconds (0.05 sec load, and 0.05 sec unloading), followed by a rest period of 0.9 seconds.

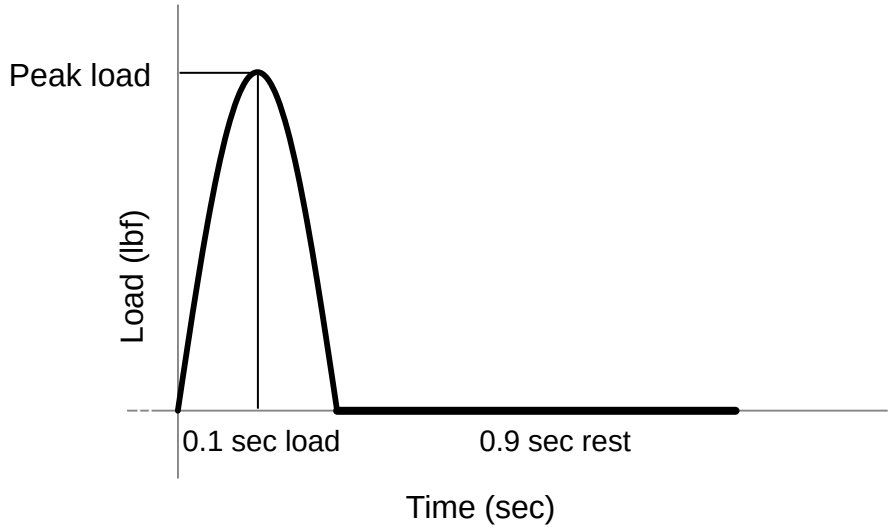

Figure 5-8. Repeated loading period.

The loading period was selected to allow for the relaxation of the materials at the interface, unlike in monotonic testing. A half-sine load was the shape of the load applied as illustrated in Figure 5-8. All tests were performed at room temperature (25.0 ± 2.0°C). The initial design of the LC-RST program applied a 10.0 lbf seating load. Then the chosen load was applied. The actual applied load was varied with each attempt of the test from 1000.0 lbf up to 2250.0 lbf, which will be discussed more in detail in this section. The LC-RST program ran until the displacement limit of 0.50 inches was reached or the operator terminated the program. At this point, the actuator was retracted and the raw data was saved.

5.3.3.1 Data Interpretation

This section provides a general overview of the techniques used to analyze the data evaluated in section 5.3.3, as well as section 5.4. Previous research indicates that at least 500 points per second is required to capture the effects of repeated load (Chen, 2011). For RST evaluation, data was acquired every three minutes, with 512 points acquired every second for 6 seconds (cycles). The measurements obtained were load (applied), deformation (measured from loading head movement) and time. These measurements were sent to a .DAT file created by the MPT software. Data was subsequently exported into Microsoft Excel for post-processing and further interpretation. Typical plots of the repeated loading and axial displacement are shown in Figures 5-9 to 5-12.

As shown in Figures 5-11 and 5-12, several 6-cycle data made up the full data set that was ultimately used for interpretation. The number of 6-cycle data that were acquired depended on how many cycles it took to reach the established displacement limit of 0.5 inches which terminated the test. It is important to note that similar to as shown in Figure 5-12, the point at which the displacement limit was reached was not acquired by the software, as data was only acquired for 6.0 seconds every 3.0 minutes.

Data reduction was necessary to analyze the results provided from the MPT software. Depending on the length of the test the number of data points could range from 400000.0 to 950000.0 for each of the outputs. The complexities of handling this size of data required the development of a routine in Microsoft Excel for data reduction. Axial displacement data provided by the MPT software was used to identify the total, permanent, and resilient deformation information. The routine identified the maxima (total deformation) and minima (permanent deformation) of the 6-cycle data.

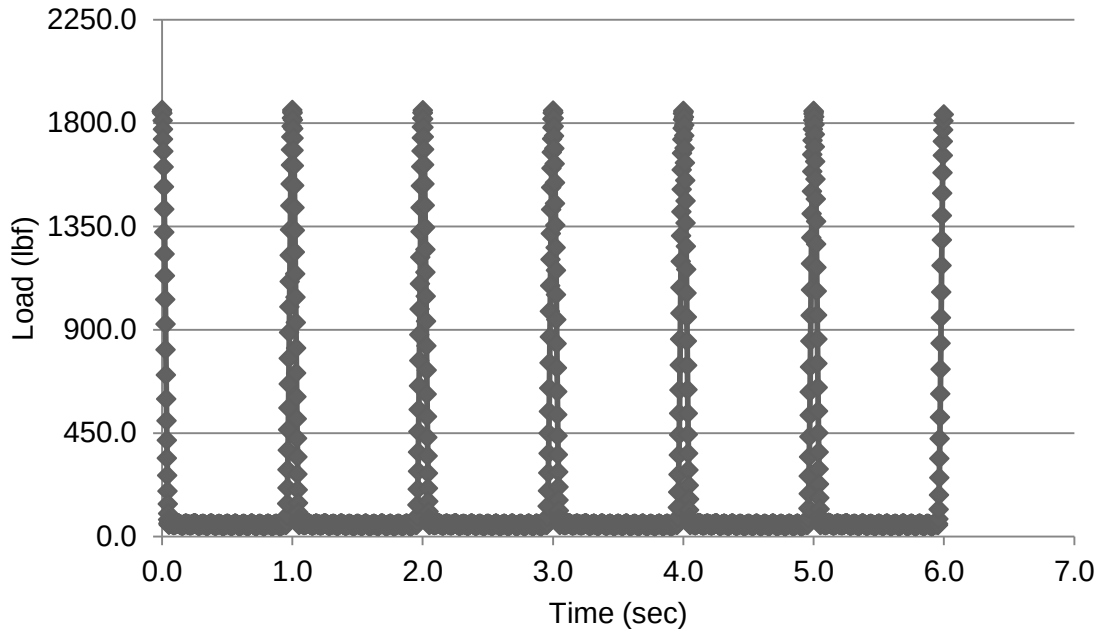

Figure 5-9. Typical raw data for repeated loading versus time.

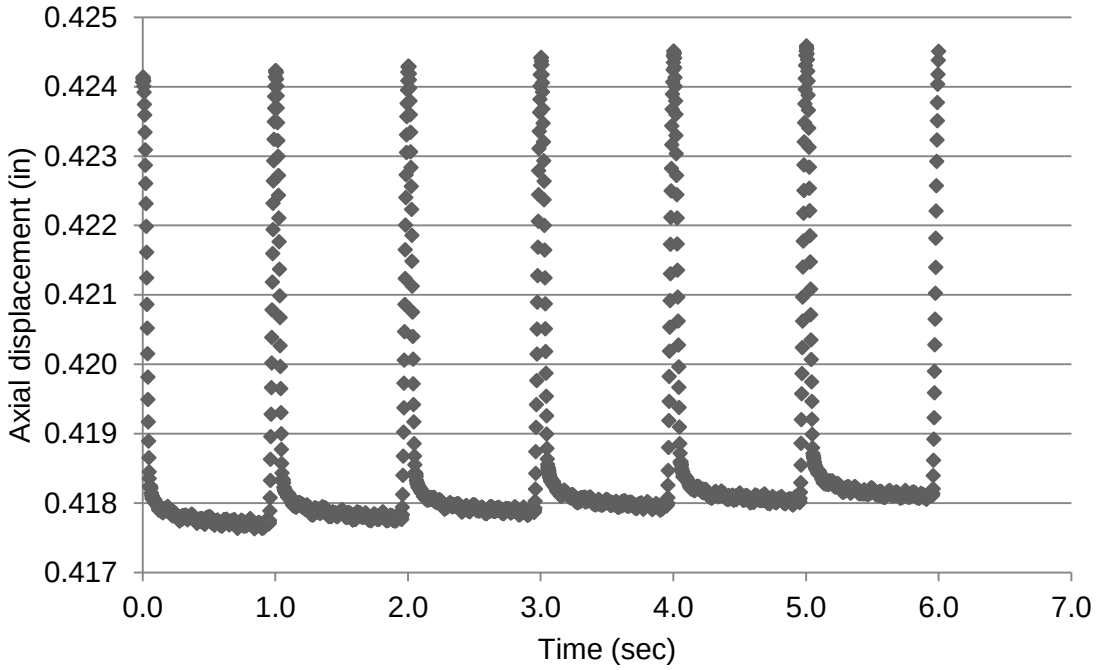

Figure 5-10. Typical raw 6-cycle data of axial displacement versus time.

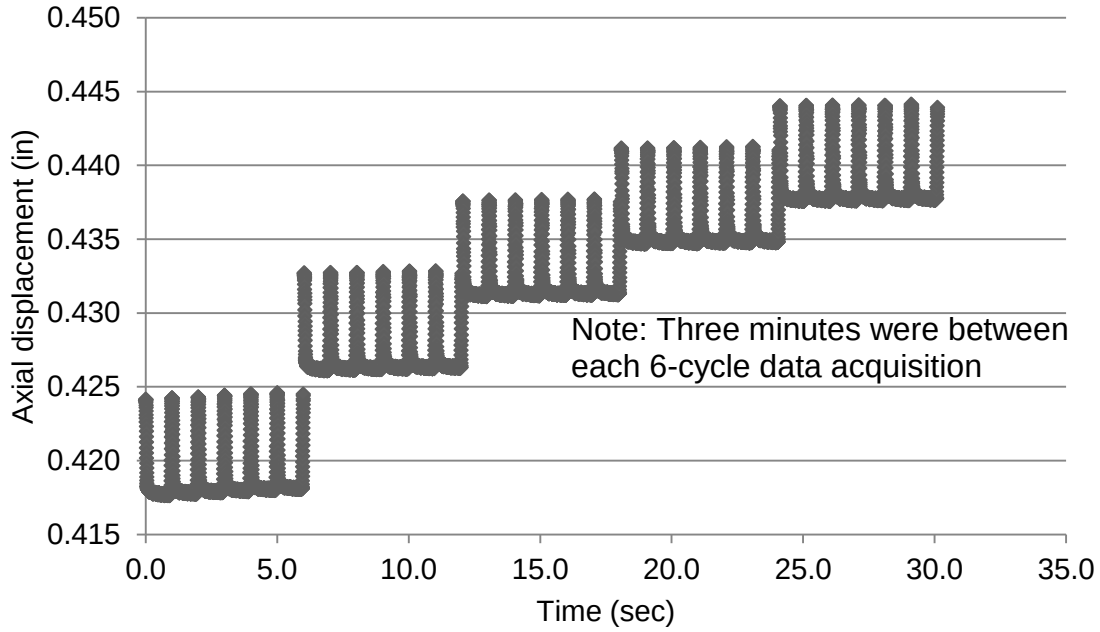

Figure 5-11. Progression of displacement for five acquisitions of 6-cycle data versus time.

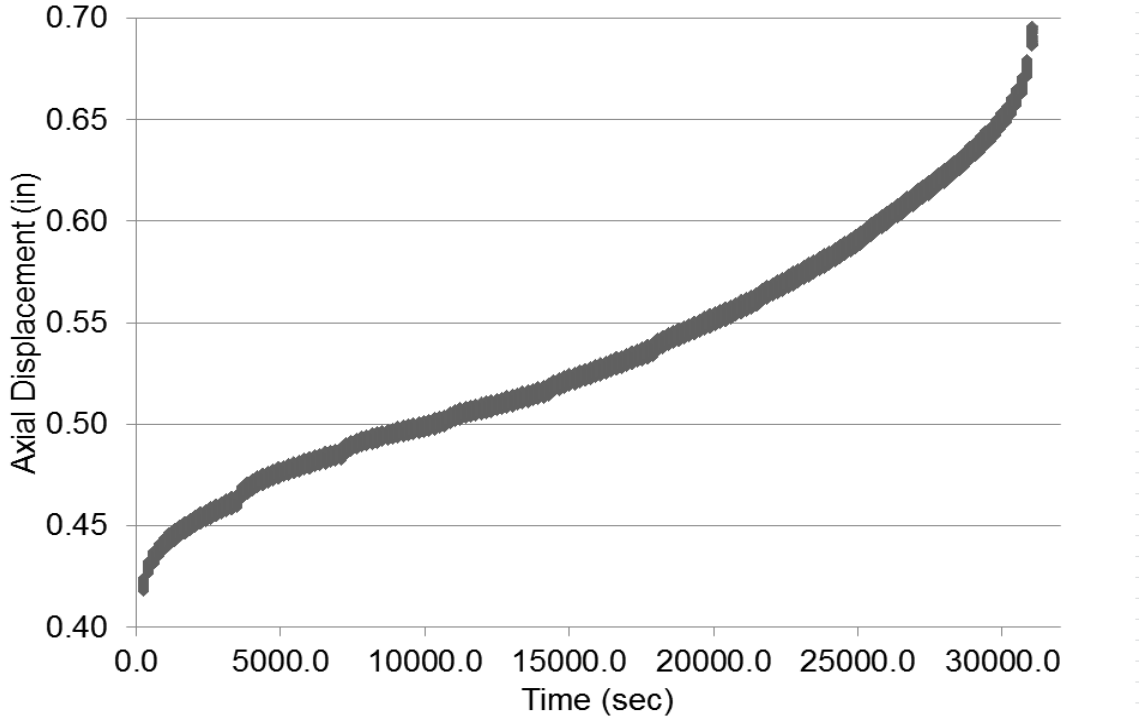

Figure 5-12. Typical full data set of axial displacement data.

Four full cycles (i.e. the first and final cycles were removed) for each acquisition time was averaged together. This value would represent the deformation (total or

permanent) for the time at which the data was acquired. The difference between the total and permanent deformation, referred to as resilient deformation, was also calculated. A similar calculation was made to confirm the applied load was consistent throughout testing. Table 5-1 shows typical values for a specimen tested using the load controlled analysis.

Table 5-1. Typical deformation obtained from Microsoft Excel analysis

Deformation (in)	Cycle 1	Cycle 2	Cycle 3	Cycle 4	Average
Total (max)	0.4242	0.4243	0.4244	0.4245	0.4244
Permanent (min)	0.4178	0.4178	0.4179	0.4180	0.4179
Resilient (max-min)	0.0064	0.0065	0.0065	0.0065	0.0065

Resilient deformation and load data were used to determine the stiffness (lbf/in) of the material. Normalized values of the stiffness were calculated by dividing the stiffness values by the initial stiffness value. Stiffness reduction has been well recognized as a way to measure damage induced in a specimen. Often, a stiffness reduction of 50.0% serves as a measure of failure in asphalt testing. Typical calculations of stiffness and normalized stiffness are shown in Table 5-2.

Figure 5-13 shows a typical normalized stiffness for the no tack specimen evaluated at 1500.0 lbf. From the graph it is clear that the specimen's stiffness did not show a significant decrease until it was beginning to fail. This information was insufficient for observing the resistance of breakdown in this and other specimens tested at this load level.

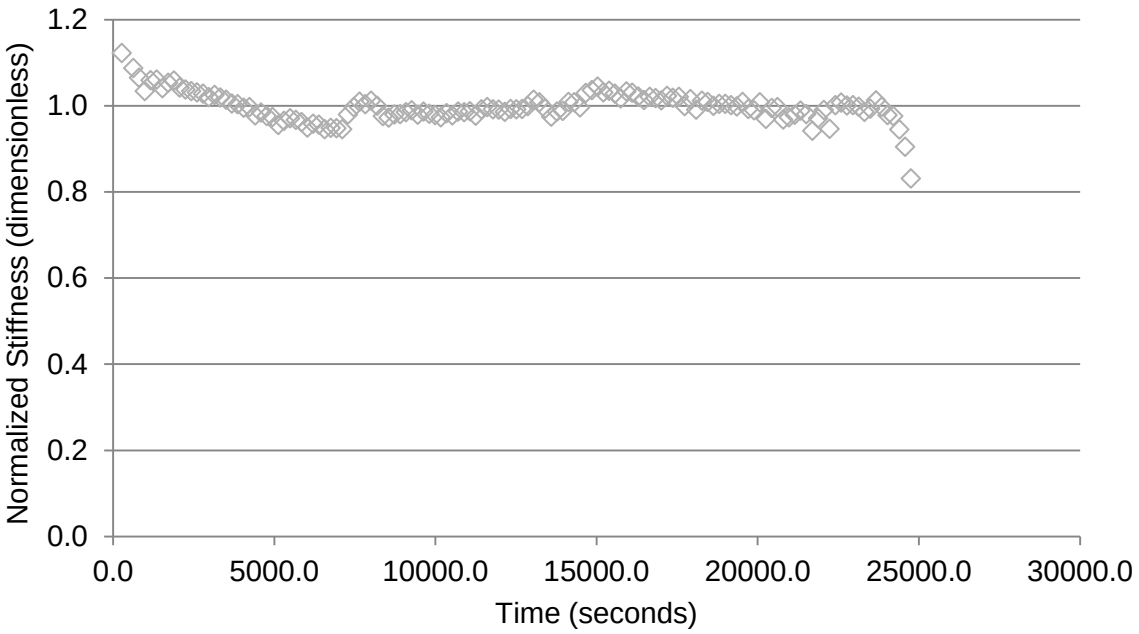

Figure 5-13. Normalized stiffness for 1500 lbf LC-RST NT specimen.

Table 5-2. Typical stiffness obtained from Microsoft Excel analysis

Time (sec)	Load (lbf)	Resilient deformation (in)	Stiffness (lbf/in)	Normalized stiffness (dimensionless)
0.0	1854.1	0.0065	285246.15	1.000
3.0	1857.1	0.0066	281378.79	0.986

The results of the elastic layer analysis in chapter 3 indicated that for a typical pavement structure, shear stress at structural interfaces was 30.0 psi to 60.0 psi with an applied stress of 100.0 psi. This led to the selection of 1000.0 lbf (36.5 psi) for initial testing. This load represented 28.8% of the average shear strength for lowest performing specimens and 36.3% for the highest performing specimens in the bond strength tests as described in section 5.3.2. After testing at the 1000.0 lbf (990.0 lbf and 10.0 lbf seating load) load for two hours, the specimens remained intact with minimal

external signs of damage and very limited reduction in stiffness. This indicated that the load, and/or the amount of time for testing would need to be increased to induce failure.

Subsequently, the load was increased to 1500.0 lbf, which represented 43.3% of the average shear strength for lowest performing specimens and 54.4% for the highest performing specimens. After conducting several trial tests for four hours, the specimen exhibited minimal signs of damage. The damage that was visible was located where the specimen and the collar were in contact. It was determined that the locking pins were loosening as a result of the compaction of the exterior of the specimen. The locking pins were subsequently tightened every two hours to ensure the collars remained in constant contact with the specimen.

The decision was made to proceed with the load controlled method by maintaining the load-level but increasing the time of loading. The next set of LC-RST trials were run with an applied compressive load of 1500.0 lbf (1490.0 lbf and 10.0 lbf seating load). The time of load application for these tests was increased to eight hours, in an attempt to induce more damage at the interface. The results of these trials are presented in Figures E-1 to E-3. Stiffness reduction for all of the specimens was less than 20.0% prior to specimens failing. The TT specimen exhibited the highest reduction in stiffness (19.9%), but did not fail during testing. The results of this attempted LC-RST evaluation were inconsistent, potentially due to a number of factors including the movement of the specimen in the device and compaction of the mixture at the collars.

In summary, using 1000.0 and 1500.0 lbf load controlled method could not achieve the typically desired 50.0% reduction in stiffness that was initially chosen to be a measure of failure within a reasonable time-frame. The data indicated that specimens

were exhibiting a limited loss of stiffness prior to failure. Additionally, some specimens were unable to fail within the allotted testing time. To encourage failure of the specimen, higher load-levels were required.

5.3.3.2 Progressive LC-RST

In an attempt to improve upon the previous method, a progressive loading scheme was conceived where the applied load went from 1500.0, 1750.0, 2000.0 and 2250.0 lbf sequentially (10.0 lbf seating load and 1490.0 lbf, 1740.0 lbf, 1990.0 lbf and 2240.0 lbf), with each load being applied for two hours (Figure 5-14). NT, TT and PT were all tested using this method. During data interpretation, the effect of the load changes was visible as seen in Figure E-4 to E-6. To aid in analysis, lines were placed on each graph to indicate where the load level changes occurred. No changes were made to the data interpretation as the Microsoft Excel routine accounted for the load changes.

Results showed that the NT, TT and PT specimens had 16.5%, 17.3% and 23.7% reduction in stiffness, respectively. While the NT and PT specimens failed before the end of testing, the TT specimen remained intact. It was speculated that the specimens might be failing due to high load-levels approaching the specimen's relative strength as the PT specimen failed within the load 3. Not apparent from the graphical data shown in Figures E-4 through E-6, is that the TT specimen remained intact after testing. Table 5-3 provides the comparison between the measured strength of the surface treatments obtained from section 5.3.2 with the chosen applied loads for the RST analysis.

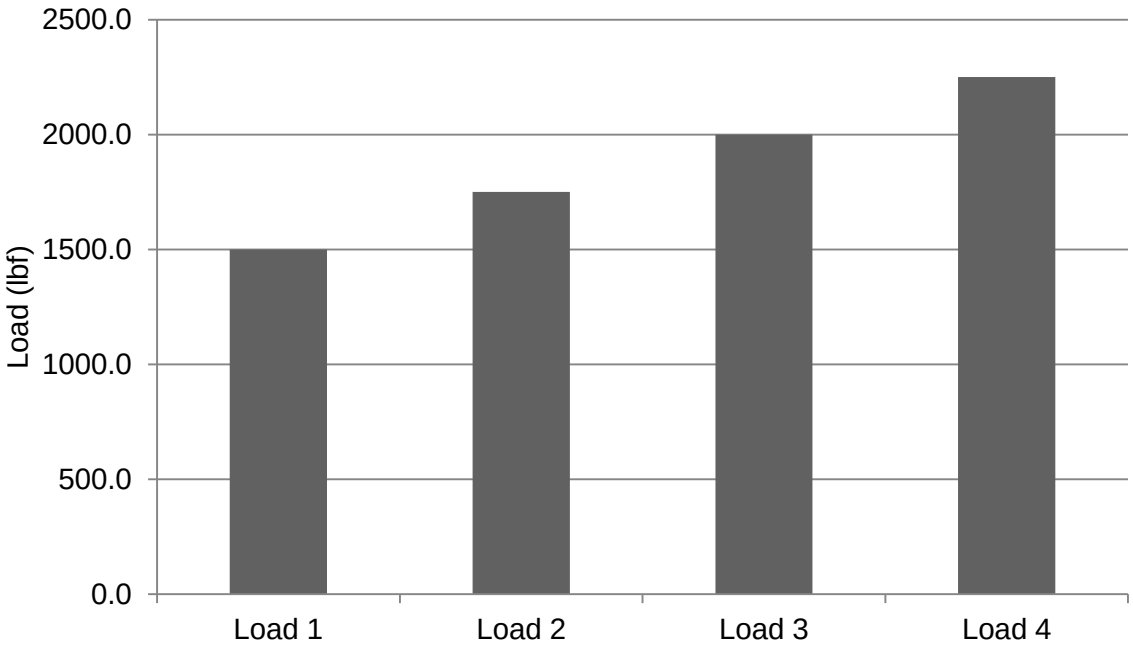

Figure 5-14. Loads used for progressive loading method.

Table 5-3. Percent of measured bond strength reached with applied RST stress.

Applied load (lbf)	Applied stress (psi)	Specimen type (average shear strength)		
		NT (127.0 psi)	TT (133.6 psi)	PT (106.6 psi)
1500.0	54.8	43.1%	41.0%	51.3%
1750.0	63.9	50.3%	47.8%	59.9%
2000.0	73.0	57.5%	54.6%	68.5%
2250.0	82.2	64.7%	61.5%	77.0%

As the applied loads reached the measured shear loads of the specimens tested, specimens began to fail due to lack of bond strength. This was particularly visible while evaluating the PT specimen, since it failed much earlier than the NT and TT specimens. The PT specimens exhibited the lowest shear strength, and thus failed in an earlier loading period than the TT and NT specimens. During the third load level, the PT specimen experienced reached 68.5% of its bond strength, while the TT and NT specimens were at 54.6% and 57.5%, respectively.

Evaluating the mechanism of bond strength failure was never the intention of the repeated shear testing. As discussed in the elastic layer analysis conducted in chapter 3, interfaces deeper in the pavement can experience load levels up to 70.0% of applied stress. It was important to take this into account when determining whether or not the loads were characteristic of what might occur at deeper pavement interfaces. However, the majority of the pavement systems evaluated experienced stress levels closer to 30.0% to 60.0% of the applied stress. Thus, the method was altered by applying each load for three hours to approximate the 60.0% maximum stress. The resulting test could then be up to nine hours, if the specimens were able to last until then. Also, the final load (load 4) was removed from the analysis to be certain that the specimen shear strength or load levels beyond the predicted values from the elastic layer analysis would not be reached.

With the new progressive loading scheme, the LC-RST was able to induce failure. Each of the specimens evaluated were also able to reach the final loading stage, unlike the previous attempt with four load levels. This allowed for a better comparison between the results, but also increased the length of testing. The results of these tests are shown in Appendix E, Figures E-7 to E-9. Ultimately the results indicated that the NT, TT and PT specimens evaluated exhibited 19.2%, 15.2% and 28.1% reduction in stiffness, respectively. However, this data was determined to not be fully representative of the breakdown of the bond at the interface. During a visual inspection of FIST device with the progressive loading method, the locking pins were again found loose after testing. In addition, several specimens failed through the mixture, instead of through the interface. This was attributed to the specimens moving during testing as a result of the

looseness of the collars. While a negligible amount of dilation could be expected due to aggregate shifting during testing as specimens were not confined, the observed movement of the entire specimen was undesired.

The attempts at the LC-RST were not producing results that were representative of the breakdown of the interface. With specimens failing with a shear strength response, the progressive method was also abandoned. A re-evaluation of the methodology for the test was conducted. It was determined that the options moving forward could be a higher single load controlled option or a displacement controlled RST could be implemented. The displacement controlled method was subsequently pursued.

5.3.3.3 Displacement controlled RST

The results of the LC-RST evaluations led to the implementation of a deformation controlled method. The benefit of having the LC-RST results meant that average deformation associated with each load level could be obtained. It was assumed that this deformation controlled method would better represent field conditions where the elastic energy within the real pavement system would bring the deformation back to zero. The value of 0.0085 in was identified from the average total deformations from the 1500.0 lbf RST data. It was a middle-ground representation of the 1500.0 lbf applied load.

A conditioning period of one hour was put in place in an attempt to reduce the loosening from the specimen compressing due to the collars, which was identified in the progressive LC-RST analysis. For conditioning, a LC-RST program was run at 1500.0 lbf. The device was then fully tightened before starting the deformation controlled analysis removing the space caused from specimen compression at the collars. Because of this conditioning, tightening every two hours during testing was eliminated,

as it was assumed the system would remain fully tight. A seating load of 10.0 lbf was applied before the deformation controlled program could proceed. Again a load pulse of 0.1 seconds and a rest period of 0.9 seconds were chosen, as shown in Figure 5-15. Three trial tests including an SGC pill (no interface), TT and NT specimens were evaluated. Displacement controlled data analysis was conducted using the same Microsoft Excel routine as discussed in section 5.3.3.2. The difference between the analyses is found in the load data. Over time, the load acquired during the deformation controlled analysis reduced. A typical representation of this is shown in Figure 5-16. The figure also clearly shows the conditioning period. This data was removed for the calculation of deformation, stiffness and normalized stiffness. Figure 5-17 shows a typical stiffness plot with the conditioning period data removed

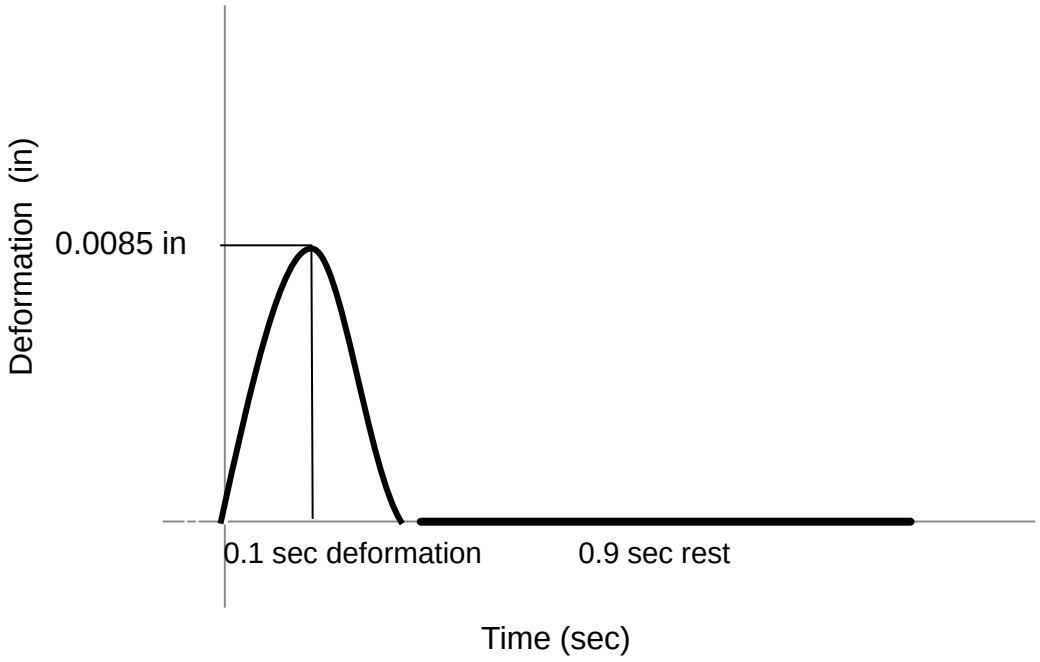

Figure 5-15. Repeated applied deformation schematic.

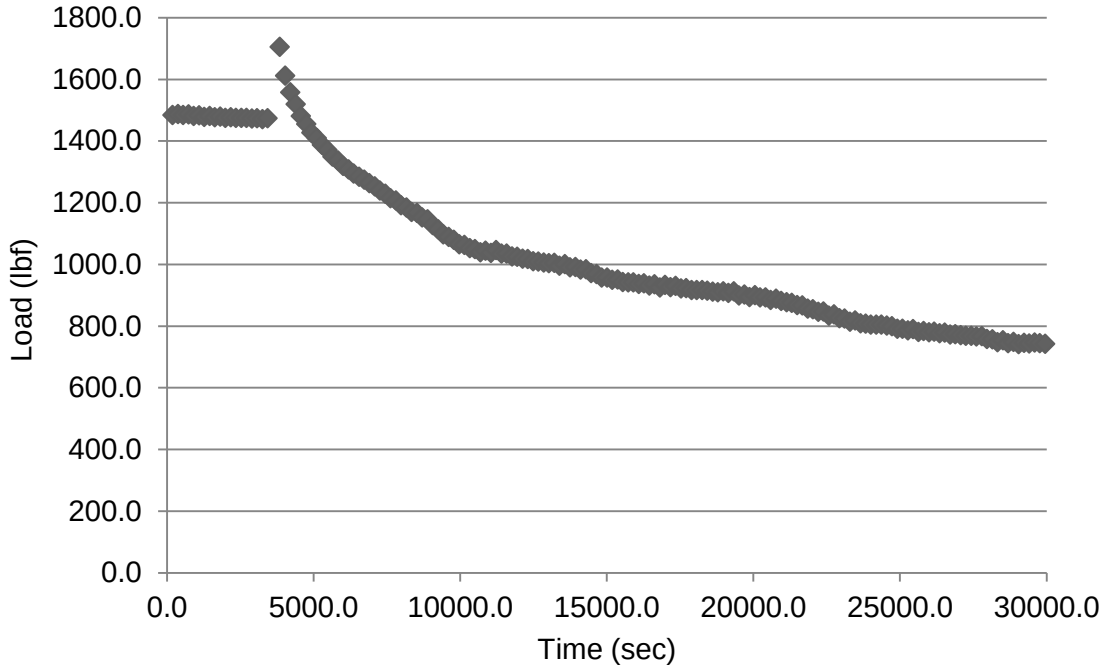

Figure 5-16. Load reduction for typical displacement controlled RST evaluation.

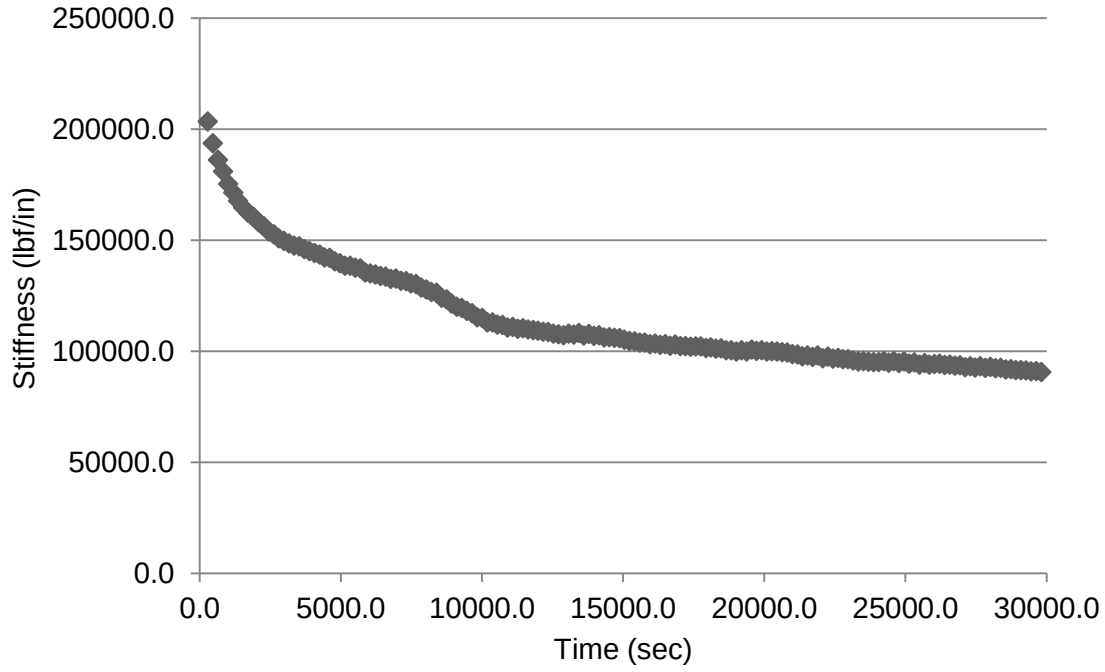

Figure 5-17. Stiffness reduction for typical displacement controlled RST evaluation.

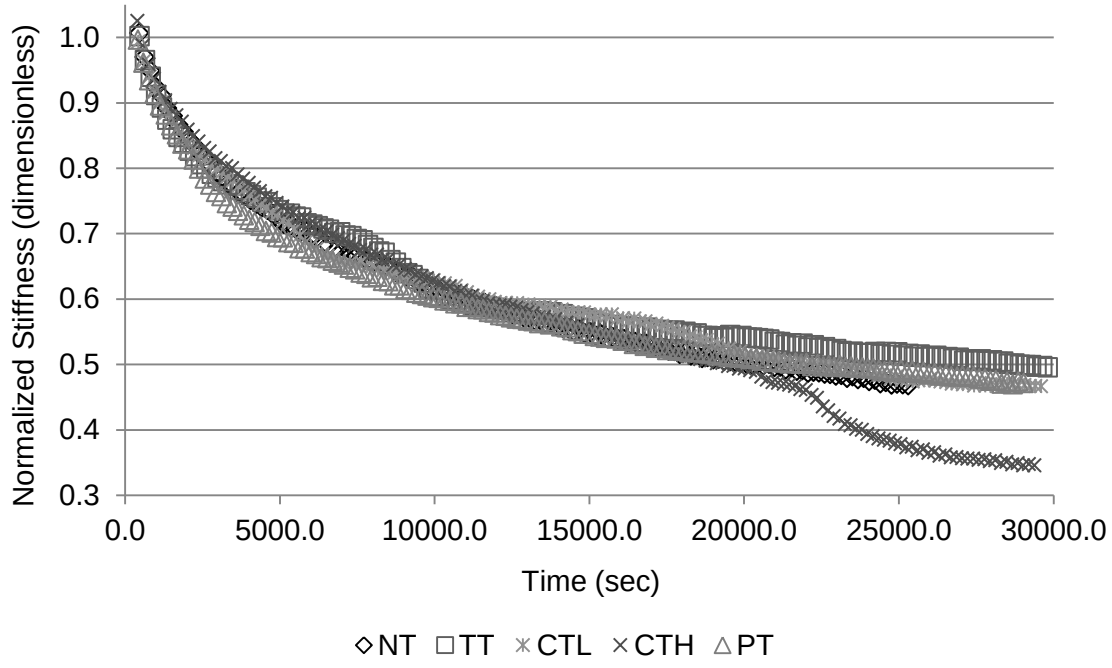

Figure 5-18. Displacement controlled RST normalized stiffness results for all specimens.

Results indicated a 33.0% higher reduction in stiffness than the load controlled tests, which was consistent across all of the initial specimen types evaluated during trial testing. With these apparently promising results, analysis of the other specimen types was conducted. Normalized stiffness results for all specimens are shown in Figure 5-18, and the data shows a consistent trend across the specimens, with each dropping beyond the 50.0% reduction in stiffness just after 4.0 hours of testing. Normalized stiffness results show little variation between the conditions, with exception of the CTH specimen, which experienced a secondary drop in stiffness at around 6.5 hours into testing. Though the data appeared to be more consistent, the loosening of the device controlled the response obtained from the MPT software. Thus, the results could not be evaluated.

After thoroughly inspecting the specimens tested under deformation controlled RST, compression of the mixture caused by the collars was found to be more pronounced than in the load controlled test. These indentations allowed the specimen to work its way loose during testing contributing to even more movement than specimens evaluated during LC-RST tests. It was determined that the indentations were caused by the free motion of the specimen and not by loading. Data also indicated most of the displacement occurred under little to no load. This was consistent across all tests. Over time the load felt by the specimen had effectively reduced to zero and the play in the device increased.

Ideas on how to improve the deformation controlled method were extremely complex to implement with the existing FIST design. It might have required more intuitive software for identifying a zero reference to return the device to after a displacement pulse. For example, applying a seating load, then a deformation and finally releasing the load until it would reach zero could successfully work as a method, but this design would also increase testing time. Ultimately the deformation controlled RST was abandoned as a methodology because of the inability to control the device with the existing setup.

5.3.4. Discussion on the Solutions for Energy Loss

Throughout all of the testing conducted with the device, it became clear that energy was not being fully transferred from the loading head to the location of interest to evaluate interface bond performance. During strength testing, the gap width of the device led to an abnormally high shear stress response from the materials. After reducing the gap, data became more consistent with the anticipated results from the literature. Six attempts were made at developing a test to evaluate resistance to

breakdown of the interface during this testing phase. With each attempt, information on how energy was lost during testing gave insight into the complexities of cyclical/fatigue-type testing in asphalt pavement.

Of particular note was the issue of the loosening of the collars of the FIST device. Since previous tests were plagued with loosening of the locking pins, new threaded hex nuts were purchased to improve tightening the device, in addition to circular curved disc spring washers (Figure 5-19) to help mitigate excess vibration. These washers compress as load is applied as the round threaded rod coupling on the pins is tightened, actively maintaining a desired load within the pin shaft. Sixteen washers were placed on the device, four per pin shaft. As they are compressed, a light load the washers exert prevented the pins from loosening due to the vibration of the FIST. Washers were stacked in series, to further stiffen the washers allowing for the hex nuts to remain tightened for longer periods. Additional washers were added to adjust for the height difference between the shorter Allen nuts and the taller original locking pins.

Figure 5-19. Curved disc spring washers stacked in series. Photo courtesy of author.

Additionally, capture screws were installed on each of the cams to prevent their movement. The capture screws effectively locked the cams in place during testing,

preventing them from loosening. This was identified as a problem during trials prior to final testing which will be discussed in section 5.4.

Each of the aforementioned changes also culminated in a discussion on the need for the RST method to induce failure in specimens. In several of the trial testing methods used, specimens were able to fail. The failure of these specimens was often not related to interfacial bond breakdown, as previously reported in section 5.4.3. In an ideal test, failure of the specimen would mean that the geometry of the interface changed due to the surface detaching. However in previous attempts, data acquired with failure of the specimens were often not related to the interface. None of these failures were relevant for answering how the bond at interfaces breakdown due to repeated applications of shear stress. Thus, visible failure of the specimen was no longer a requirement for or indicator of a successful test.

Reduced gap width, curved disc spring washers, and the capture screw were all device modifications that resulted in the collection of more consistent data for final RST method. Determining what could correlate with RST stiffness from the strength test data was also not apparent. Thus, continuing to use stiffness as a measurement would be problematic moving forward, as one of the goals of this study was to compare relative rankings of tack coat performance.

Load controlled testing was chosen as the final RST method with the changes presented in this section, as data could be consistently obtained. All of these solutions were implemented in the final LC-RST testing discussed in section 5.4. Ultimately the findings of the trial RST methods led to an improved method of the LC-RST evaluation at a single load.

5.4 Final Repeated Shear Stress Testing

The new testing methodology for the LC-RST is described as follows. An 1850.0 lbf compressive load (50.0 lbf seating and 1800.0 lbf load pulse) was selected, which represents 60.0% of the average strength of the specimens assessed in section 5.3.1 using monotonic load. Every hour, the hex nuts were tightened to 35.0 inch-pounds using a drive click torque wrench to ensure a constant grip on each specimen. The loosening associated with this testing could be attributed to a loss of compression in the springs over time. This new method prevented movement, which allowed for the majority of the load exerted on the specimen to be targeted to the interface.

A set of trial tests were run on specimens without tack coat and with trackless tack coat to see how the results would improve based on these and other changes described in section 5.3. During these tests, the cams became loose, allowing the collar to move minimally. A capture screw was installed on the cams as a preventive measure to mitigate loosening. This was the final change to the FIST design. This design, while still requiring frequent tightening of the hex nuts, allowed for consistent data acquisition between tests.

Several factors were considered for data analysis approaches for this LC-RST data. Though the original intent was to use reduction in effective stiffness as a measurement of the breakdown of the bond at the interface, the response from tightening the device appeared to be quite visible within the resilient deformation data (which was used for the stiffness calculation). The influence of the tightening is shown in Figures 5-20 and 5-21, which depict the resilient deformation and stiffness data for a typical specimen. The average reduction in stiffness for all of the tests was 9.5% with the maximum reduction of 23.4%. The standard deviation of the stiffness reduction was

7.2%. The data was inconsistent between tests for each specimen type as shown in Table 5-4. Stiffness could not be effectively implemented for the comparison of the relative results from the RST analysis to the shear strength analysis. The same can be said for number of cycles to failure, which could only be obtained for the RST analysis.

Table 5-4. Stiffness reduction of LC-RST specimens.

Specimen ID	Stiffness reduction (%)
NT 1	14.0
NT 2	2.0
TT 1	6.9
TT 2	13.9
CTL 1	0.0
CTL 2	23.4
CTH 1	0.0
CTH 2	11.8
PT 1	15.6
PT 2	7.4

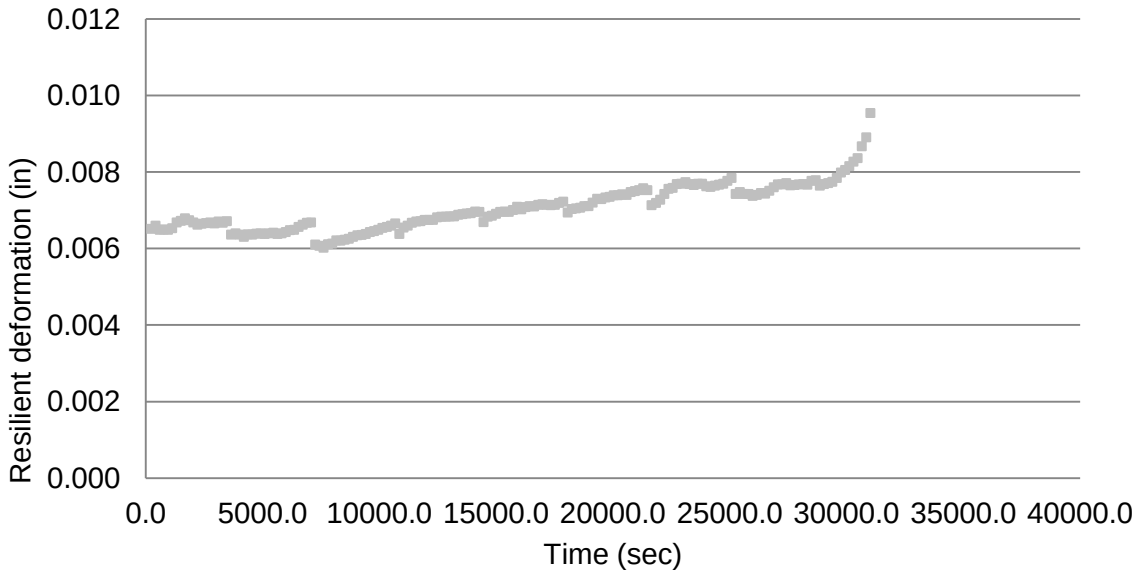

Figure 5-20. Typical resilient deformation data for final LC-RST evaluation.

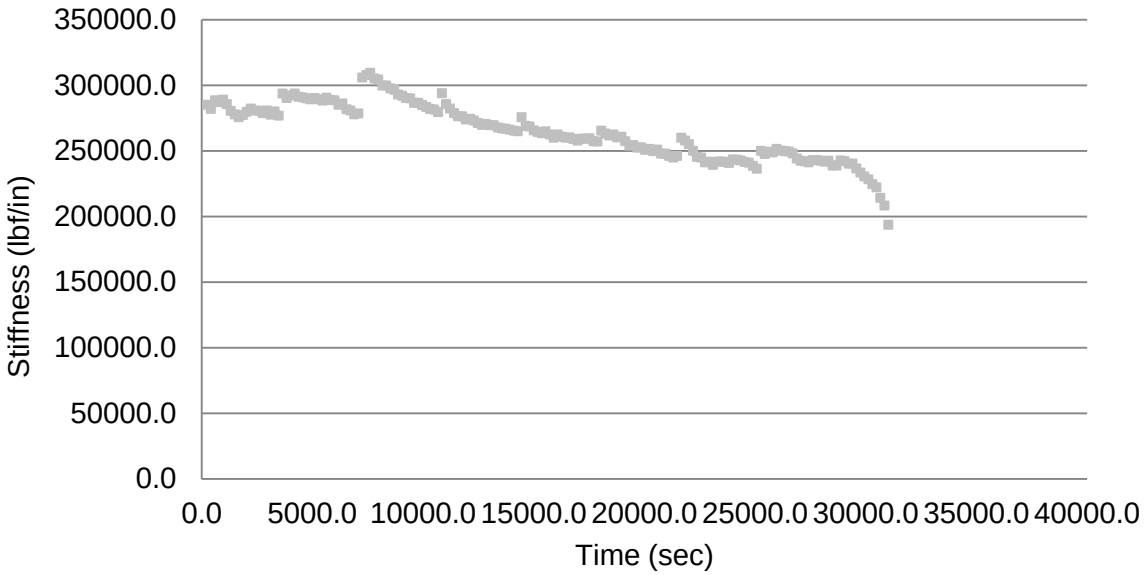

Figure 5-21. Typical stiffness data for final LC-RST evaluation.

Figures 5-22 to 5-24 show typical load, total and permanent deformation data acquired for the LC-RST final analysis. The average applied load throughout testing varied only 0.21%. As shown in Figure 5-22, the load obtained for the test was consistently near 1850 lbf.

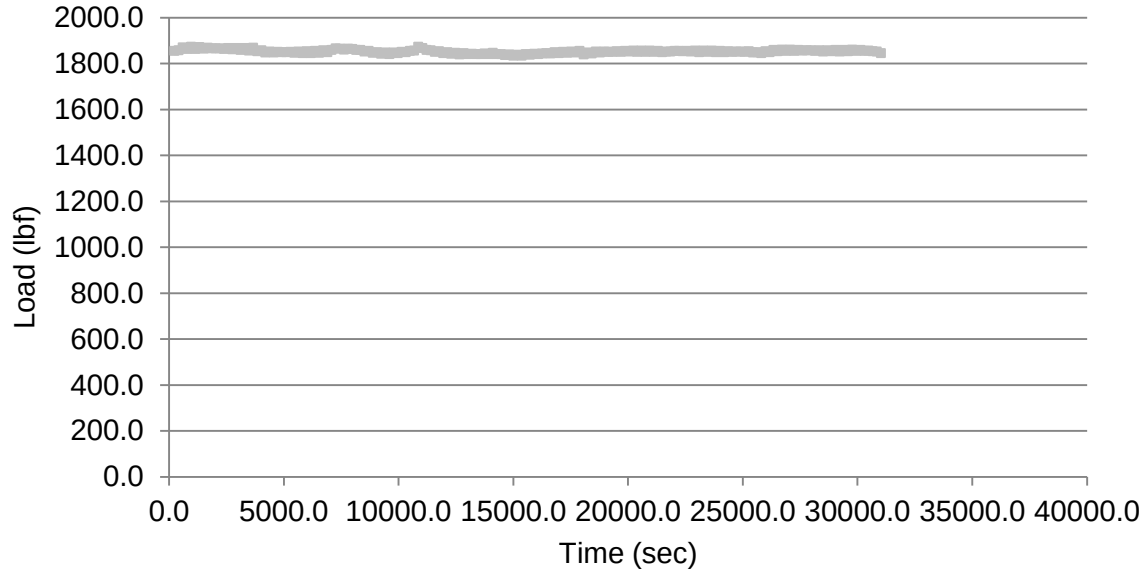

Figure 5-22. Typical load data from LC-RST evaluation.

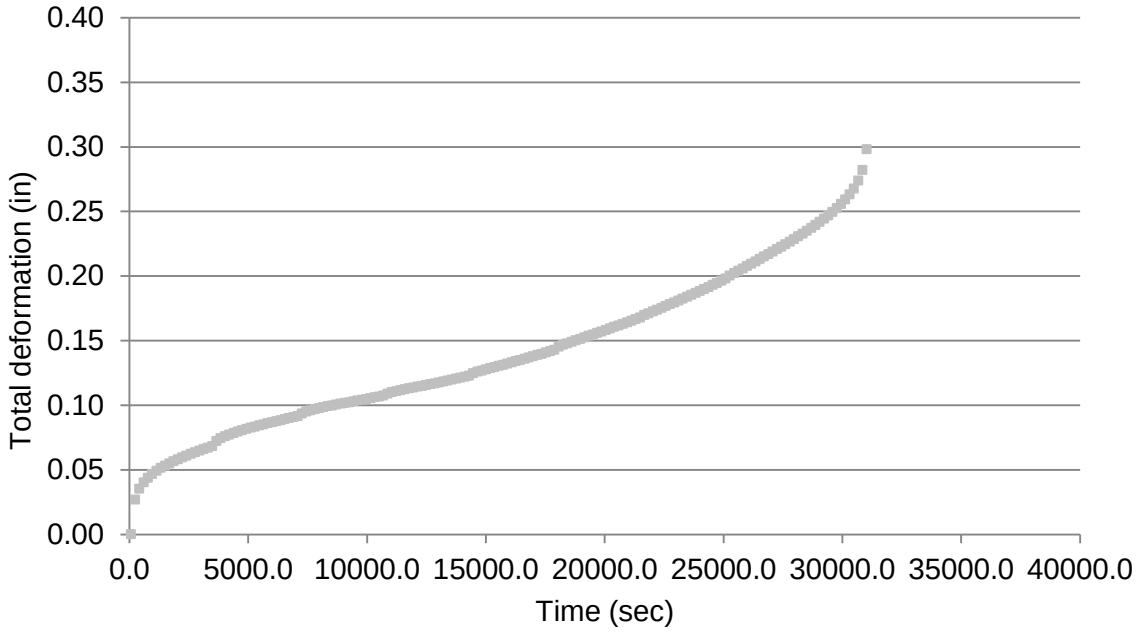

Figure 5-23. Typical total deformation data from LC-RST evaluation.

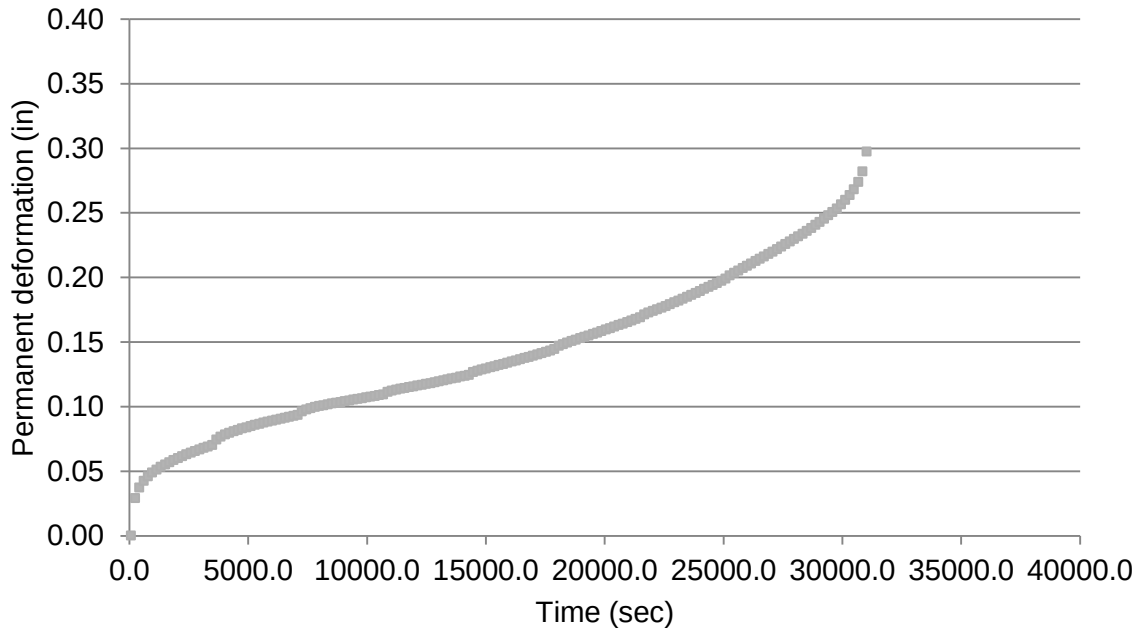

Figure 5-24. Typical permanent deformation data for final LC-RST evaluation.

With the load controlled RST method, the deformation data were the only changing measurement that could provide insight into bond degradation occurring at the

interface. With the variations found in the resilient deformation, both total and permanent deformation data was more closely evaluated. Permanent deformation data was chosen as it provided the most insight into the breakdown of the bond at the interface. As shown in Figure 5-24, tightening the device did not show up in the permanent deformation data.

Ultimately an energy analysis approach, presented in section 5.4.1, was chosen as the method for evaluating the results of RST analysis. The energy analysis also provided the best comparative analysis between RST data and the strength test data, as energy could also be calculated from shear strength test data. Graphical representation of the permanent deformation results from the final RST analysis is presented in Figures F-1 to F-10.

5.4.1 Energy Analysis

In order to compare the relative values from the strength analysis (section 5.3.2) to the LC-RST analysis, energy from each test was calculated and compared. To make this calculation, the permanent deformation curves of each specimen (Figures F-1 to F-10) were used to identify the cumulative permanent deformation found in the steady-state region of the curve. This value is multiplied by the load to calculate the energy. A typical permanent deformation curve where the steady state portion is identified is presented in Figure 5-25. The permanent deformation curve can be divided into three stages: the initial stage, which involves local damage due to the collars, changes in temperature and elastic and delayed elastic responses; the second stage, where relevant permanent deformation associated with the breakdown of the interface is located; and the final stage, where debonding propagates through the specimen causing a detachment of the two surfaces and the specimen breaks. The steady-state

portion of the curve provides the insight into the breakdown of the bond at the interface. The circle in Figure 5-24 indicates the location of the y-intercept for the steady state portion of the curve, which is used in the energy calculations.

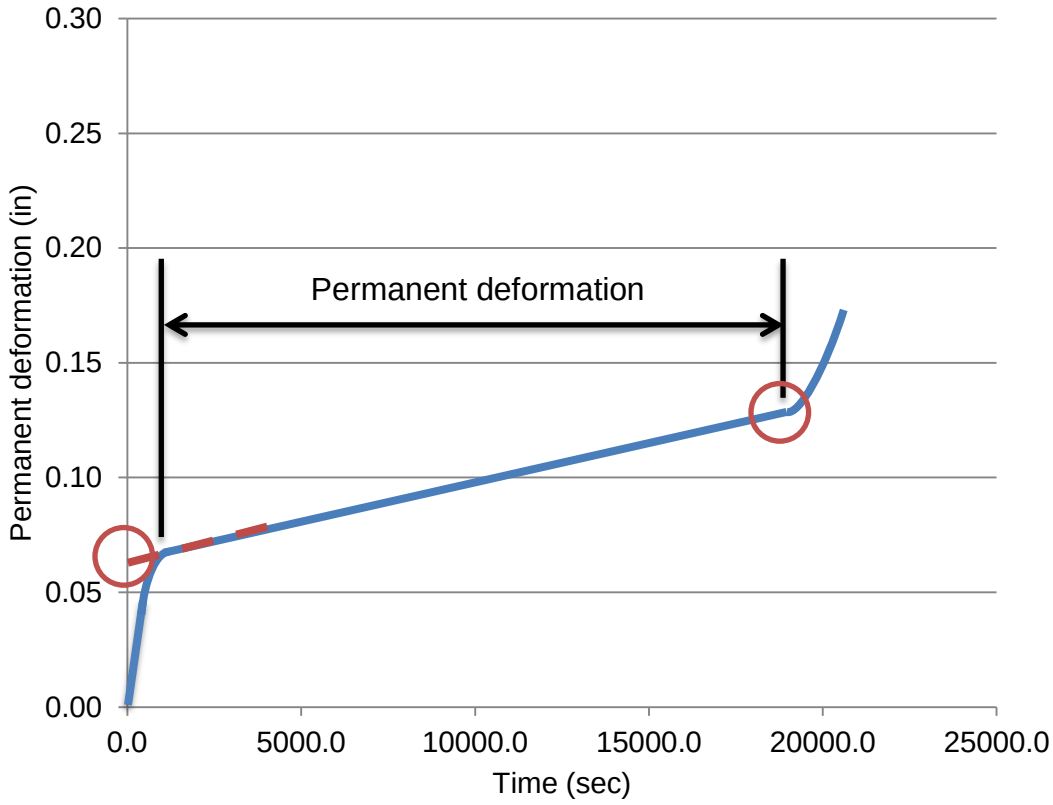

Figure 5-25. Identifying permanent deformation data from a typical curve.

To identify the initial point of the steady-state region of the permanent deformation curve, the rate of change (slope) between two consecutive data points until the midpoint of the data. Using the first hour of this slope data, the initial point of analysis for the steady state region was selected by visual inspection. A typical slope plot is shown in Figure G-1, where the chosen initial point is circled. Similarly, the slopes between last full hour of data points and any points thereafter until the end of the test were plotted to identify the final point of steady-state, as shown in Figure G-2. Once

these points were identified, a new permanent deformation plot of the steady-state data could be analyzed.

A third-order polynomial was fit to the steady-state permanent deformation curve. Using the equation for this curve, the inflection point of this data was identified using Equation 5-1.

$$x_{inflection} = -\frac{b}{3a} \quad (5\text{-}1)$$

Where,

The cubic equation is defined as ax^3+bx^2+cx+d; and

The coefficients a, b, c and d are real numbers.

An example graph of the steady state data is shown in Figure G-3. A table of the inflection point data is found in Table G-1. The permanent deformation between the initial point and the inflection point were subsequently plotted, and a linear regression was fit to the points to identify a y-intercept value. Using this point, the energy can be calculated. The energy is described by Equation 5-2.

$$Energy_{RST} = (y_{final} - y_{intercept}) \times 1850 \quad (5\text{-}2)$$

Where,

y_{final}= final point of the steady state portion of permanent deformation data; and

$y_{intercept}$= the y-intercept linear regression fit from the initial point to the of the inflection point of the permanent deformation data.

The results of this analysis are presented in Figures G-5 and G-6.

The results indicate that PT specimens performed best with an average of 363.4 in-lbf of energy, while the CTH specimens performed worst with 260.6 in-lbf of energy on average. Interestingly, the CTL specimens were the second best performer with

335.5 in-lbf of energy. This indicates that application rate of the tack coat had little impact on the energy of the specimens tested using the LC-RST method. TT specimens were the second worst performers in the test, with 274.3 in-lbf of energy, while NT specimens fell in the middle with 316.1 in-lbf of energy. Statistical analysis was conducted to determine statistical significance, if any. Those results can be found in section 5.4.2.

To compare the results of the LC-RST data to the strength data, energy needed to be calculated for the strength test results. A simple approximation of the energy from the strength test data was chosen for this evaluation. Using the maximum recorded load and its corresponding displacement from the data obtained for each strength test, a triangular calculation (Equation 5-3) for the energy was made for each specimen and averaged for each specimen type.

$$Energy_{Strength} = 0.5 \times d_{peak} \times P_{peak} \quad (5\text{-}3)$$

Where,

d_{peak}= the displacement at the maximum load recorded; and

P_{peak}= the maximum load (lbf) recorded from the strength test data.

Graphical representation of this equation can be found in Figure 5-26. This novel approach to calculating energy provided a comparable value to assess the energy obtained for reach material analyzed in the bond strength testing. The results of this analysis show a different trend than the energy results of the LC-RST data. The energy calculated from the strength data indicate that the TT specimens show higher energy than any other specimen, with 249.4 in-lbf of energy on average. The CTH specimens exhibited the lowest average energy from the strength data, followed by the PT

specimens with 128.8 and 144.9 in-lbf of energy respectively. The full results of the energy analysis of the strength data is reported in Figures G-7 and G-8.

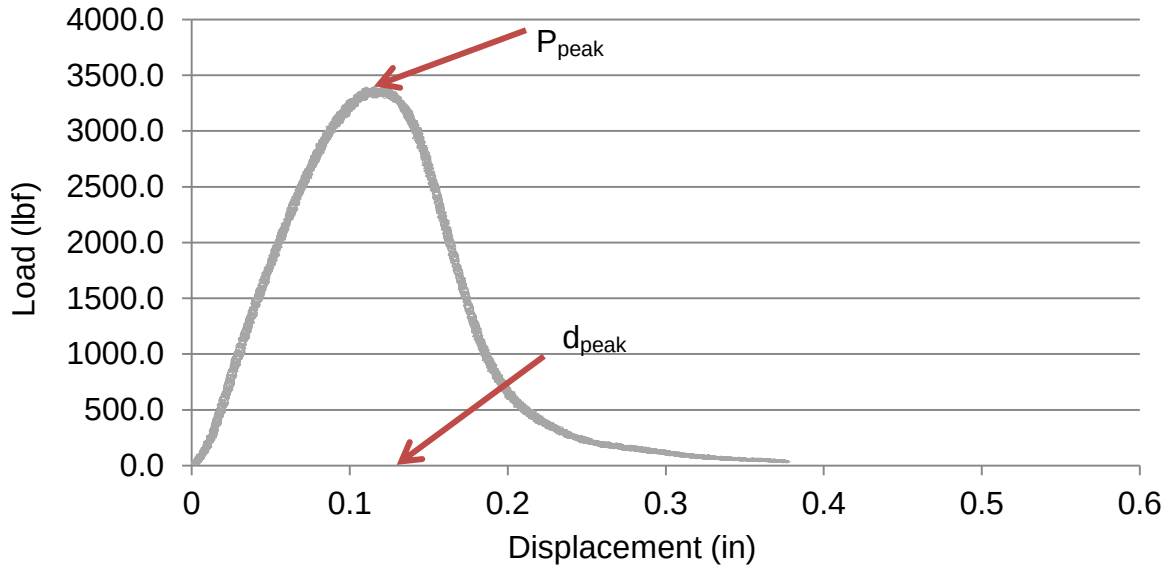

Figure 5-26. Graphical representation of energy calculation of typical strength test data.

Figure G-9 shows a scatterplot of the data from both energy analyses with a line of equality. With the data gathered away from a line of equality, results indicate these tests do not provide the same comparison of the tack coat types. The PT specimens are furthest away from the line of equality, indicating that the strength test is the worst indicator of its performance. This supports the hypothesis of this research as it was hypothesized that the performance of the materials used at the interface is improperly evaluated when based primarily on the outcomes from bond strength tests.

5.4.2 Statistical Analysis

Statistical data was calculated for the purpose of comparing the data found in the energy analysis of the LC-RST data. Due to the limited data evaluated in the LC-RST analysis, the initial statistical analysis was done manually, employing a normalization technique commonly used in previous asphalt research conducted at the University of

Florida. In order to construct confidence intervals for the LC-RST data, this normalization approach was used. The energy of replicates of a specimen type was averaged (Equation 5-4), and then the energy of the individual specimen was normalized to that average.

$$Mean\ (Average) = \frac{\Sigma(x)}{n} \quad (5\text{-}4)$$

Where,

x=Energy of the specimens (in-lb.);

n=Number of specimens evaluated.

The VAR.P function was used to find the variance of all of the normalized energy values. The population variance of the energy data from the LC-RST tests were calculated using Equation 5-5 using the VAR.P function. The population variance is a statistical measurement often used to identify the amount values vary from the average within a population.

$$Variance\ (VAR.P) = \frac{\Sigma(x-\overline{x})^2}{n} \quad (5\text{-}5)$$

Where,

x=Energy of the specimens (in-lb.);

$\overline{x}$=Average energy of all of the specimens evaluated (in-lb.); and

n=Number of specimens evaluated.

The population standard deviation was also calculated using the STDEV.P function. The population standard deviation is the measure of how widely values are distributed from the average (mean) within a population (Equation 5-6).

$$\textit{Standard Deviation (STDEV.P)}=\sqrt{\frac{\Sigma(x-\overline{x})^2}{n}} \quad (5\text{-}6)$$

Where,

x=Energy of the specimens (in-lb.);

$\overline{x}$=Average energy of all of the specimens evaluated (in-lb.); and

n=Number of specimens evaluated.

From the standard deviation and mean (for normalized data the mean is 1.0), the coefficient of variation for the population was calculated. The coefficient of variation (CV) is described by Equation 5-7.

$$\textit{Coefficient of Variation (CV)}=\frac{\sigma}{\mu}\times 100\% \quad (5\text{-}7)$$

Where,

σ=Standard deviation of the specimens (in-lb.); and

μ=Average energy of all of the specimens evaluated (in-lb.).

The calculated population CV for the LC-RST energy test data was 6.95%. Using the mean for each specimen type, a normalized standard deviation was calculated by multiplying it by the population CV. Confidence intervals were then constructed using the appropriate Z-value. Table 5-5 shows the data for the confidence interval calculations.

Graphs of the confidence intervals of the data are also shown in Figures H-2 to H-3. It appears from Figure H-2 that there is significance between some, but not all of the data at a 90% confidence interval. At an 85% confidence interval, the data does not

overlap indicating overall statistical significance. Additional post-hoc analysis was conducted to determine statistical significance between the specimen types.

Table 5-5. Confidence interval data for LC-RST energy analysis.

Specimen Type	Mean (in-lbf)	Normalized Standard Deviation (in-lbf)	Confidence Intervals		
			95% Z=1.96	90% Z=1.645	85% Z=1.44
NT	316.12	21.96	13.61	11.42	10.00
TT	274.29	19.05	11.81	9.91	8.68
CTL	335.52	23.31	14.45	12.12	10.61
CTH	260.63	18.11	11.22	9.42	8.25
PT	363.44	25.25	15.65	13.13	11.50

Due to the limited number of specimens available to run trial testing, additional statistical analysis was conducted to evaluate the consistency of the results from the final LC-RST. Data was analyzed using Microsoft Excel Data Analysis Tools, which are part of the Analysis Toolpak Add In. The ANOVA function was used to determine if there was any statistical significance within the overall population. The alpha chosen for this analysis was 0.10. Using the data from the energy analysis, the resulting P-value from the ANOVA was 0.11 (see Tables H-1 and H-2 in Appendix H). This confirms that the data overall is not significantly significant at a 90% confidence interval. ANOVA analysis does not identify whether or not there is any significance between the sample groups (specimen types). A post-hoc analysis was subsequently conducted at an alpha of 0.10 to determine if there was significance between the sample groups.

When a sample size is less than 30 ($n < 30$), the t-distribution is appropriate for determining significance between sample groups. To identify the correct t-test to run using Microsoft Excel, an f-test for two sample variances was conducted to determine

whether or not the variances of the compared data sets were equal or unequal. The null hypothesis assumes that the variances are equal. An alpha of 0.10 was assumed for this analysis. If the resulting P-one-tail from the f-test results was greater than alpha (the null hypothesis is accepted), a two-sample t-test assuming equal variances was conducted. If the resulting P-one-tail was less than alpha (the null hypothesis is rejected), a two-sample t-test assuming unequal variances was run. The alpha used for the t-test analysis was also 0.10. T-test data results indicate that the TT and PT specimens show significant difference between the means (Figure H-19). The resultant data from each of the sample groups is reported in Figures H-3 to H-22.

5.5 Device Limitations

It is also important to mention that the FIST has limitations that cannot be avoided due to its design. The major issue as described in section 5.3 was the difficulty associated with ensuring the applied load is transferred directly to the interface. The second is that since the focus of this research was to provide a simple comparison of results for existing bond strength test data, specimens traditionally evaluated using those tests should be accommodated by the FIST. This work only used laboratory prepared specimens, eliminating some of the variability of the location of the interface. Cores from real pavements may have interfaces that are not perfectly in plane with the surface of the road. With a gap of only 0.25 inches, ensuring the interface is aligned within the gap could be a challenge with the FIST device.

CHAPTER 6
RESULTS AND CONCLUSIONS

6.1 Summary and Findings

In this research, the Florida interface shear tester (FIST) was developed to evaluate the resistance to breakdown of the bond for various bonding agents and application rates used for asphalt pavement layer interfaces. This type of failure is believed to occur deeper in the pavement system, where the mechanism of interface bond breakdown is difficult to evaluate. In order to properly assess this potential mechanism of failure, an elastic layer analysis was conducted to determine stress states deeper in the pavement system than previous research efforts. The results of the elastic layer analysis indicated the existence of critical stress states, supporting the need for this research.

The FIST device was used in both monotonic and repeated loading modes to provide insight into how various interface conditions performed under each mode. Using the monotonic loading mode the shear strength of the bond at the interface was determined. Double-layered cylindrical specimens made with a dense-graded mix design were prepared with and without tack coat for evaluation. Three tack coat materials were tested including a conventional tack coat, trackless tack coat and a polymer modified asphalt emulsion (PMAE). The conventional tack coat was applied at two rates (low and high), while the PMAE and trackless tack coats were applied at rates suggested by their manufacturers.

Initial attempts to determine the shear strength of the specimens indicated that specimens were not failing through the interface .This led to the reconfiguration of the gap width of the FIST device, allowing for consistency in results. The findings from the

elastic layer analysis and the shear strength tests were used to determine the initial level of loading required for failure due to repeated application of shear stress.

Much of the focus of this research ultimately shifted towards the development of the new RST testing method, as several iterations of analysis were conducted to attempt to reduce the loss of energy associated with mixture compaction and loosening of the device. A load controlled repeated shear application method was developed that resulted in an energy associated with the breakdown of the bond at the interface. This energy provided insight into the various tack coat types and application rates evaluated in this study. These results were able to show the relative performance of these interface conditions and their resistance to the breakdown of the bond over time. Ultimately, using an energy calculation, the results were compared to the existing monotonic loading method traditionally used to evaluate interface bond strength. The findings associated with this research are summarized as follows:

- Critical stress states conducive to debonding exist 1.0 to 3.0 inches depth beneath the pavement surface, with the most critical depth being 2.0 inches.
- Bond strength test results grouped the stiffer interface systems together with the NT, TT and CTL specimens exhibiting the highest shear strength. The PMAE tack coat and the CTH had the lowest shear strength.
- Using the FIST device, tack coats applied at rates of 0.06 gal/yd^2 or less had a negligible effect on interface shear strength, whereas higher application rates, greater than 0.12 gal/yd^2, reduced shear strength 25.7%.
- Monotonic testing is not relevant for assessing the bond degradation deeper in the pavement system. Repeated loading systems should be used to identify how materials at the interface will perform at depths of greater than 1.0 inches.
- RST analysis indicates PMAE tack coat exhibits the highest energy, while trackless tack displays the lowest energy. Strength test energy indicates that trackless tack displays the highest energy, while the low application rate of the conventional tack exhibits the lowest energy.

- Materials with stress relaxation properties (high application rates of PMAE) appear to resist breakdown of bond at the interface better than stiffer systems (little to no tack coat). This is directly counter to the results obtained from monotonic shear strength testing in this research and found in the literature.

- Overall the results indicate that shear strength cannot be used as the sole method of evaluation of interface performance.

In conclusion, it is clear that bond strength testing cannot capture how pavement bond degrades due to repeated applications of lower magnitude shear stresses. Thus, monotonic load tests improperly predict interface bond performance of various tack coats applied in locations deeper in the pavement system, where strength may not be the primary failure mode. Ultimately this work indicates the FIST device and RST method developed for this research can be used to evaluate the relative performance of pavement layer interface conditions.

6.2 Recommendations

Based on the work completed in this research, the following is recommended for investigation:

- As this was the first study developed to specifically evaluate characteristics associated with the interface between structural layers of asphalt concrete, additional surface characteristics should be investigated to determine the effects they have on the breakdown of the bond including: milled vs. new, wet vs. dry, and additional tack coat types. In addition, variations of the mixture types should be evaluated. This could lead to the determination of optimum materials used for structural interface condition.

- The gap width for guillotine-type shear stress testing devices is an important factor to consider in test development. Further investigation on the influence of gap width on the results from shear bond testing should be conducted. There is limited data and understanding of effect of gap width on various types of tack coat materials and application rates. Optimizing the gap in the FIST or other shear bond devices could lead to better prediction of pavement performance.

- A new iteration of the design of this device that could restrict vibration of the FIST device would provide more accurate data for analysis. Curved disc spring washers helped dampen the vibration on the system. However, a better system that reduced vibration altogether could potentially results. This design could

incorporate a method for fully encasing the specimen in a rigid tube, leaving only the interface free to move.

- Due to the difficulty experienced with managing the data output files from this type of analysis in Microsoft Excel, an algorithm that could reduce the large data sets would improve the analysis portion of this work for future research.

APPENDIX A
ASPHALT MIXTURE INFORMATION

Table A-1. Dense gradation for base job mix formula (JMF).

Sieve Size	Percent Passing				
	33% # 78 Stone	7% #89 Stone	50% W-10 Screenings	10% Sand	100% JMF
3/4”	100.0	100.0	100.0	100.0	100
1/2”	97.0	100.0	100.0	100.0	99.0
3/8”	58.5	100.0	100.0	100.0	86.4
#4	8.1	30.1	100.0	100.0	65.1
#8	3.0	4.0	70.2	100.0	46.6
#16	1.0	2.0	42.4	94.0	31.2
#30	1.0	1.0	25.5	53.0	18.5
#50	1.0	1.0	15.9	11.0	9.5
#100	1.0	1.0	9.9	3.0	5.7
#200	1.0	1.0	7.0	0.0	3.9
Gsb	2.809	2.799	2.770	2.626	2.770

Table A-2. Dense gradation for base (cumulative).

Sieve Size	Retained Weight, g			
	# 78 Stone	#89 Stone	W-10 Screenings	Sand
3/4”	0.0	1471.0	1785.1	4050.0
1/2”	44.6	1471.0	1785.1	4050.0
3/8”	609.8	1471.0	1785.1	4050.0
#4	1352.3	1690.6	1785.1	4050.0
#8	1426.5	1772.5	2460.1	4050.0
#16	1456.2	1778.8	3090.1	4050.0
#30	1456.2	1782.0	3472.6	4077.0
#50	1456.2	1782.0	3690.0	4261.5
#100	1456.2	1782.0	3825.0	4450.5
#200	1456.2	1782.0	3892.5	4486.5
Pan	1471.0	1785.1	4050.0	4500.0

Table A-3. Dense gradation for overlay (cumulative).

Sieve Size	Retained Weight, grams			
	# 78 Stone	#89 Stone	W-10 Screenings	Sand
3/4”	0.0	799.2	969.8	2200.4
1/2”	24.2	799.2	969.8	2200.4
3/8”	331.3	799.2	969.8	2200.4
#4	734.7	918.5	969.8	2200.4
#8	775.0	963.0	1336.6	2200.4
#16	791.2	966.4	1678.8	2200.4
#30	791.2	968.2	1886.7	2215.0
#50	791.2	968.2	2004.8	2315.3
#100	791.2	968.2	2078.1	2418.0
#200	791.2	968.2	2114.8	2437.5
Pan	799.2	969.8	2200.4	2444.8

Table A-4. Volumetrics for GA-I2 granite.

G_{mm}	G_b	P_b	G_{sb}	G_{se}	P_{ba}	P_{be}	VMA (%)	VFA (%)	V_a	DP
2.579	1.03	4.8	2.770	2.791	0.3	4.5	14.9	73.2	4.0	0.93

Table A-5. Specific gravity for GA-I2 materials.

Stone	G_{sb}
#78 Stone	2.809
#89 Stone	2.799
W-10 Screenings	2.770
Local Sand	2.626

APPENDIX B
OVERLAY MATERIAL CALCULATION

To calculate the amount of overlay material needed to reach 2.2 inches the following equation was used.

$$M_{overlay} = V_{asphalt+aggregate} \times Gmm_{overlay}$$

Where,

$$V_{asphalt+aggregate} = A_{pill} \times (H_{overlay}).$$

It is important to note that all lengths are converted to cm for calculation. Therefore,

$$M_{overlay} = \pi \times (D/2)^2 \times H_{overlay} \times (1 - AV_{overlay}) \times Gmm_{overlay}$$

$$M_{overlay} = \pi \times (15/2)^2 \times 5.588 \times (1 - 0.07) \times 2.579$$

$$M_{overlay} = 2368.44\ grams.$$

To determine the mass of the aggregate required for the overlay, the following calculation is required:

$$M_{aggregate} = M_{overlay} - M_{asphalt}$$

$$M_{aggregate} = M_{overlay} - (M_{overlay} \times AC)$$

$$M_{aggregate} = 2368.44 - (2368.44 \times 0.048)$$

$$M_{aggregate} = 2254.8\ \text{grams}$$

APPENDIX C
APPLICATION RATE CALCULATION

To calculate the mass equivalency of the application rate of tack coat used for a Superpave gyratory compacted specimen the following formulas were used:

$$mass = Application\ rate \times Area \times G_b$$

Calculate the surface area of the pill where the tack coat will be applied:

$$A = \pi r^2 = \pi \times 7.5^2 = 176.71 cm^2$$

Convert the application rate from gal/yd^2 to centimeters:

$$1\ gallon/yard^2 = 3785.41 cm^3 / 8361.27 cm^2 = 0.453\ cm$$

The equivalent mass of tack coat applied is then,

$$mass = application\ rate \times 0.453 \times 176.71 \times G_b$$

Where G_b is the specific gravity of the tack coat. This value can be found from the fact sheets provided by the source of the tack coat material. A typical value for G_b is around 1.00. It is also important to note the tack coat's percent binder residue, which must be factored into the equation to determine the appropriate mass. Therefore the final equation used for calculation is as follows:

$$Emulsion\ mass = (application\ rate \times 0.453 \times 176.71 \times G_b) \times \left(\frac{100}{\%residue}\right)$$

For the trackless specimen, with a 0.06 application rate, G_b=1.03 and 50% binder residue, the mass of emulsion applied to the base is:

$$mass = 0.06 \times 80.0496 \times 1.03 = 4.95\ grams$$

$$Emulsion\ mass = 4.95\ \times \left(\frac{100}{50}\right)$$

$$= 9.9\ grams\ of\ emulsion.$$

APPENDIX D
SHEAR STRENGTH TEST DATA

Table D-1. Maximum shear strength data.

Specimen ID	Maximum Shear Strength (lbf)	Maximum Shear Stress (psi)
NT-S1	3400.4	124.1
NT-S2	3563.1	130.1
NT-S3	3436.9	125.5
TT-S1	3110.0	113.5
TT-S2	3687.4	134.6
TT-S3	3596.1	131.3
PT-S1	2669.5	97.5
PT-S2	2856.6	104.3
PT-S3	3209.3	117.2
CTL-S1	3567.7	130.3
CTL-S2	3435.1	125.4
CTL-S3	3385.4	123.6
CTH-S1	2721.0	99.3
CTH-S2	2642.9	96.5
CTH-S3	2907.0	106.1

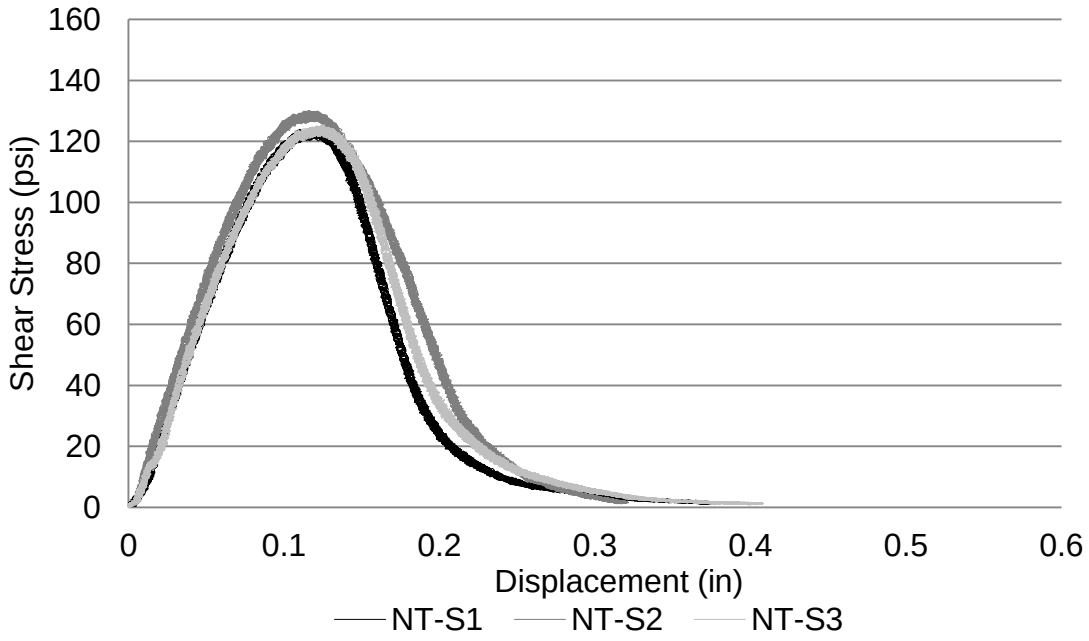

Figure D-1. Shear stress of specimens with no tack coat.

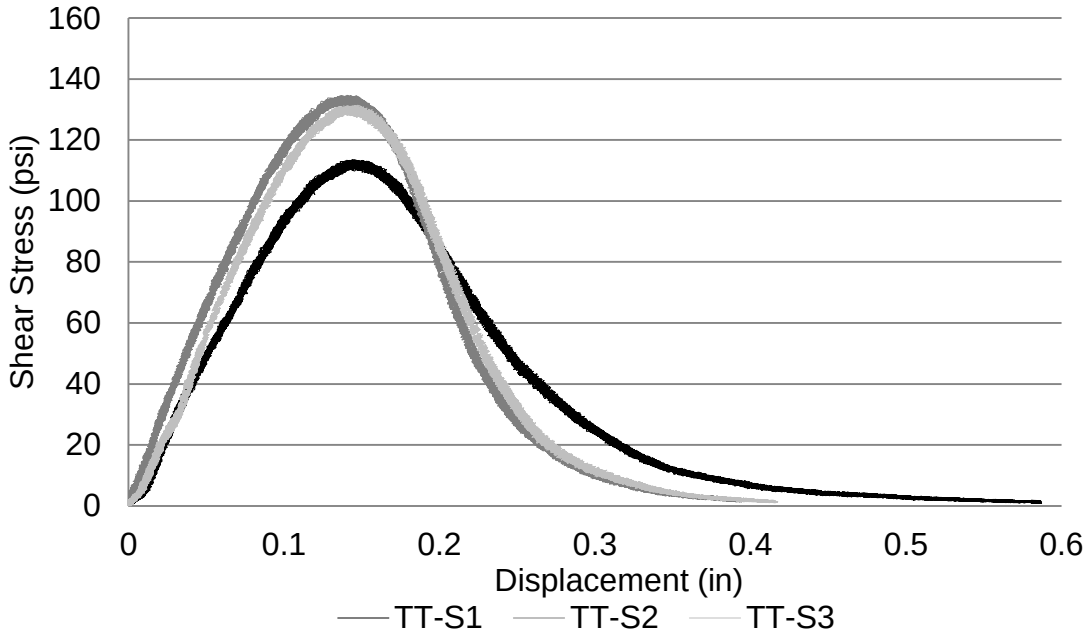

Figure D-2. Shear stress of specimens with trackless tack coat.

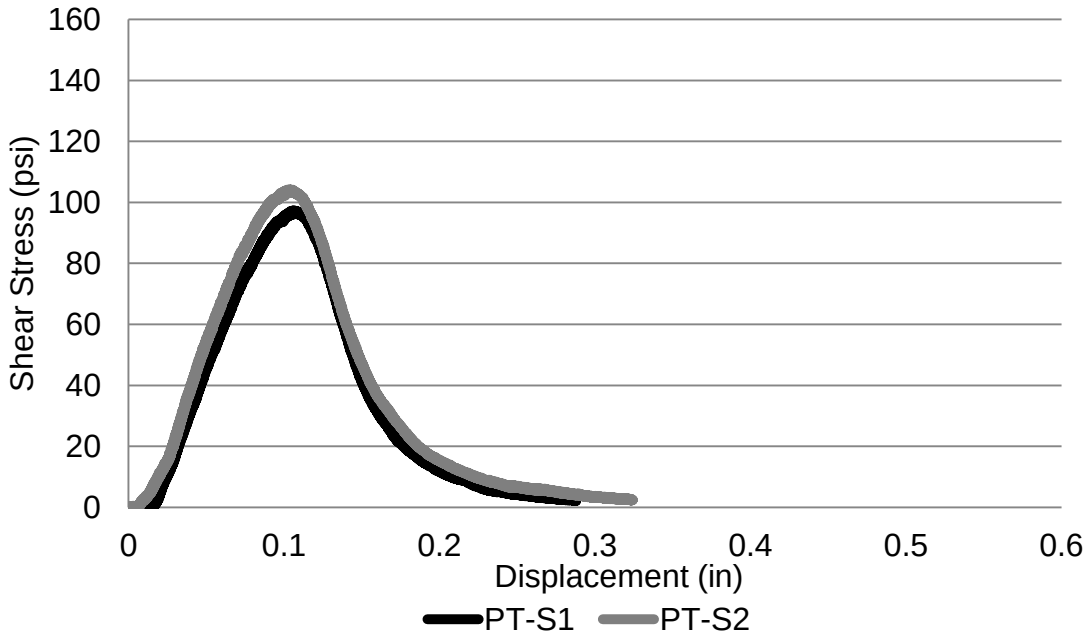

Figure D-3. Shear stress of specimens with PMAE tack coat.

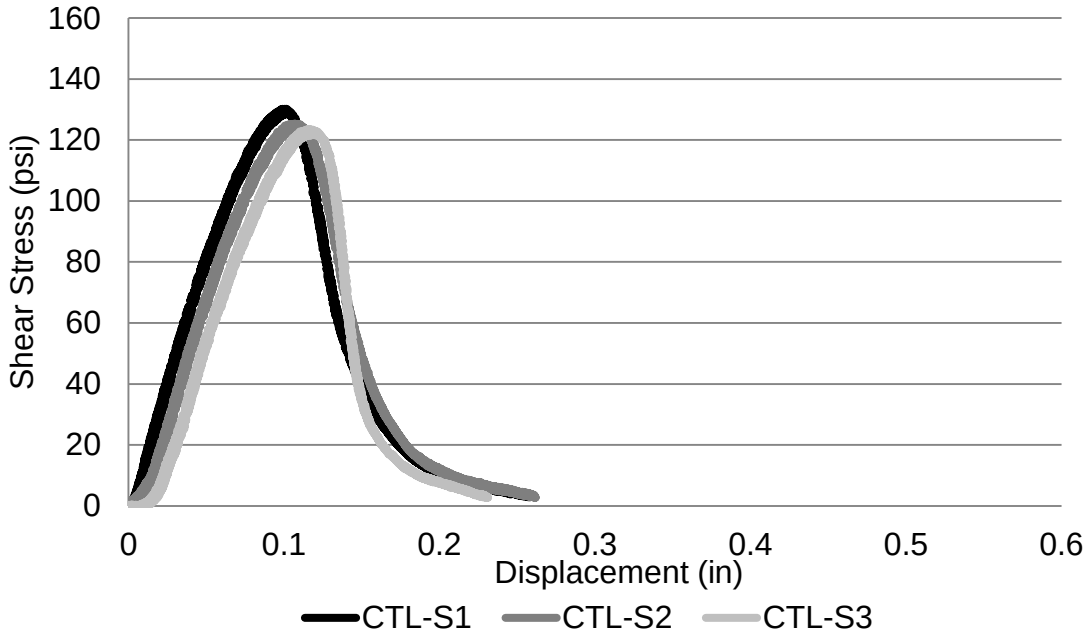

Figure D-4. Shear stress of specimens with conventional tack coat applied at a low rate.

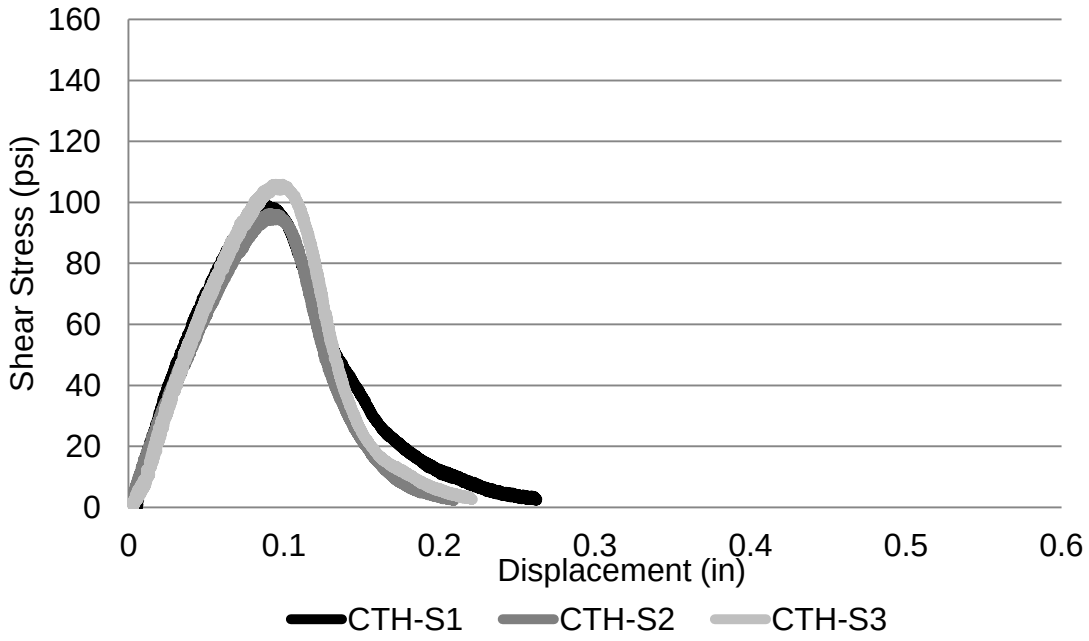

Figure D-5. Shear stress of specimens with conventional tack coat applied at a high rate.

APPENDIX E
REPEATED SHEAR STRESS TEST DATA

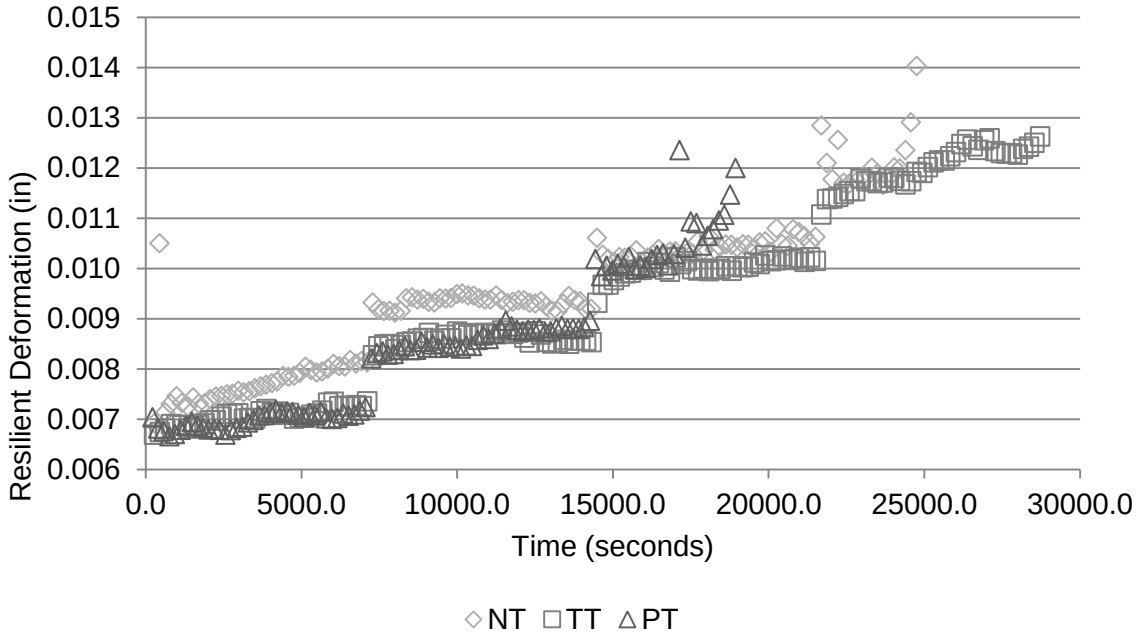

Figure E-1. Trial LC-RST resilient deformation data at 1500.0 lbf.

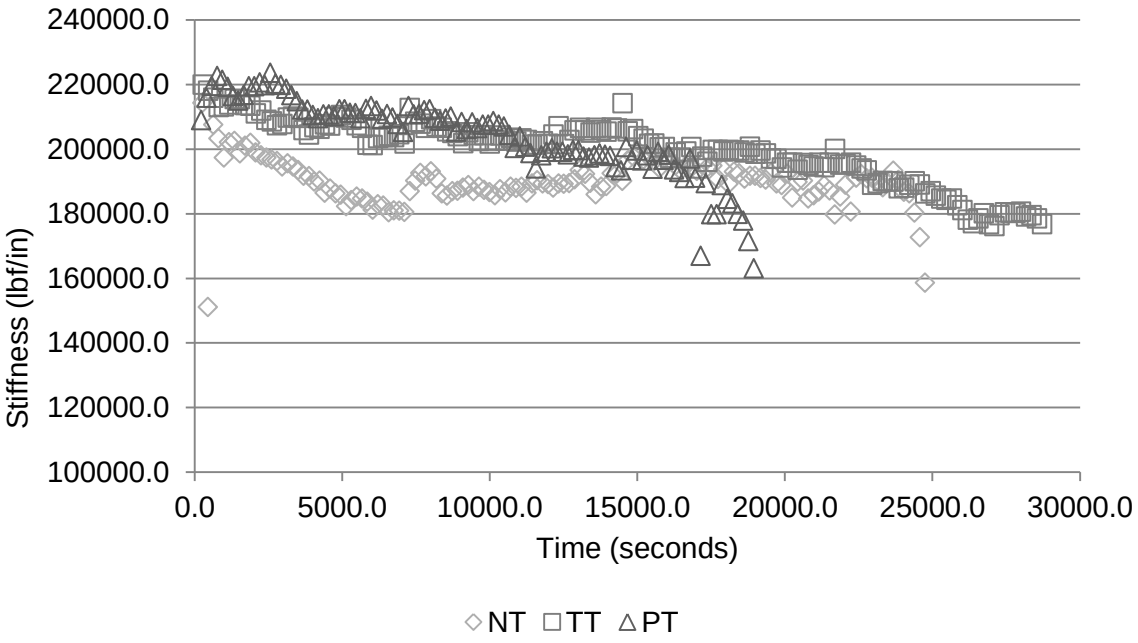

Figure E-2. Trial LC-RST stiffness data at 1500.0 lbf.

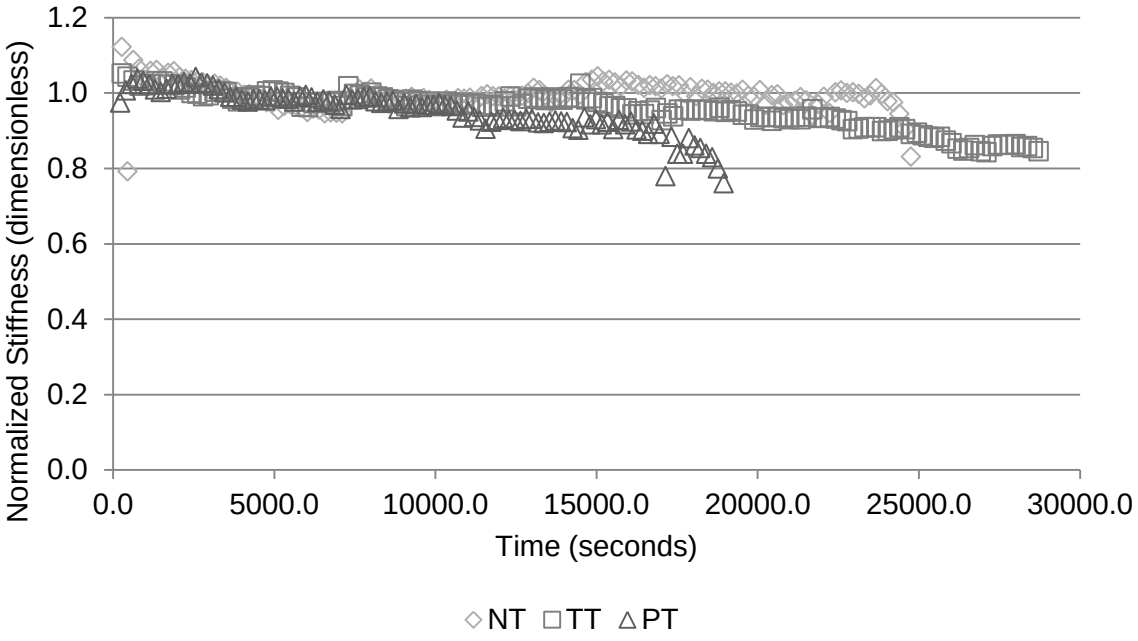

Figure E-3. Trial LC-RST normalized stiffness data at 1500.0 lbf.

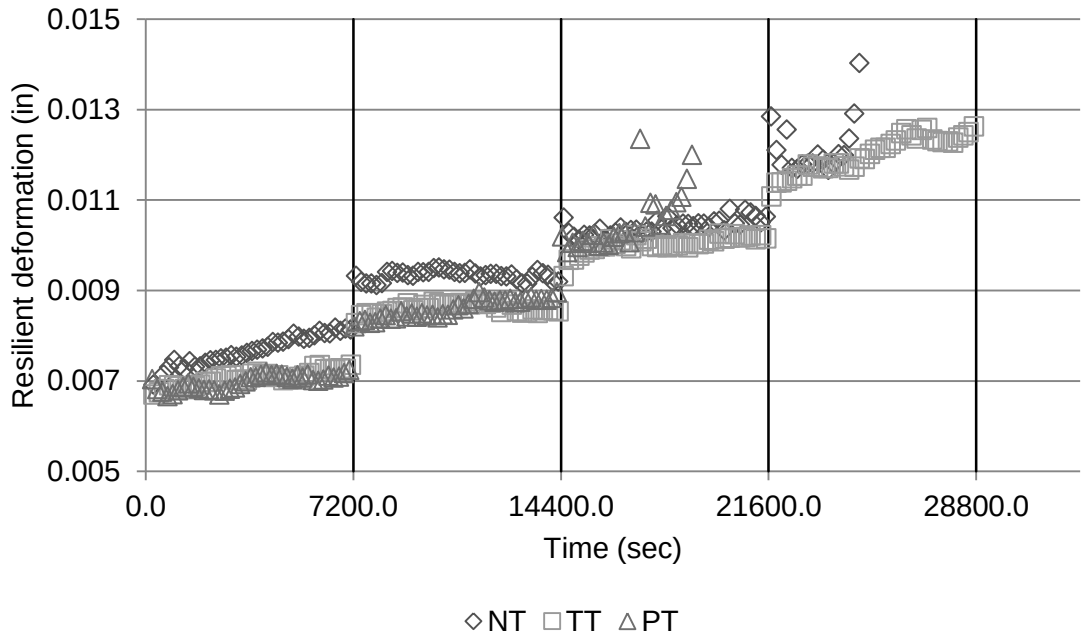

Figure E-4. 8 hour LC-RST progressive loading trial resilient deformation data.

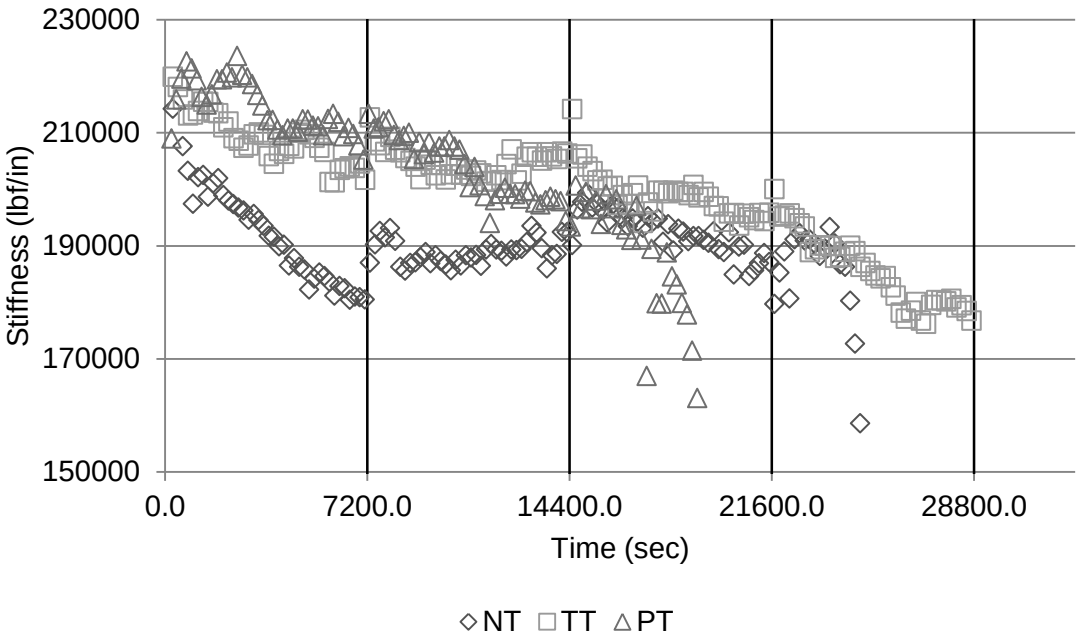

Figure E-5. 8 hour LC-RST progressive loading trial stiffness data.

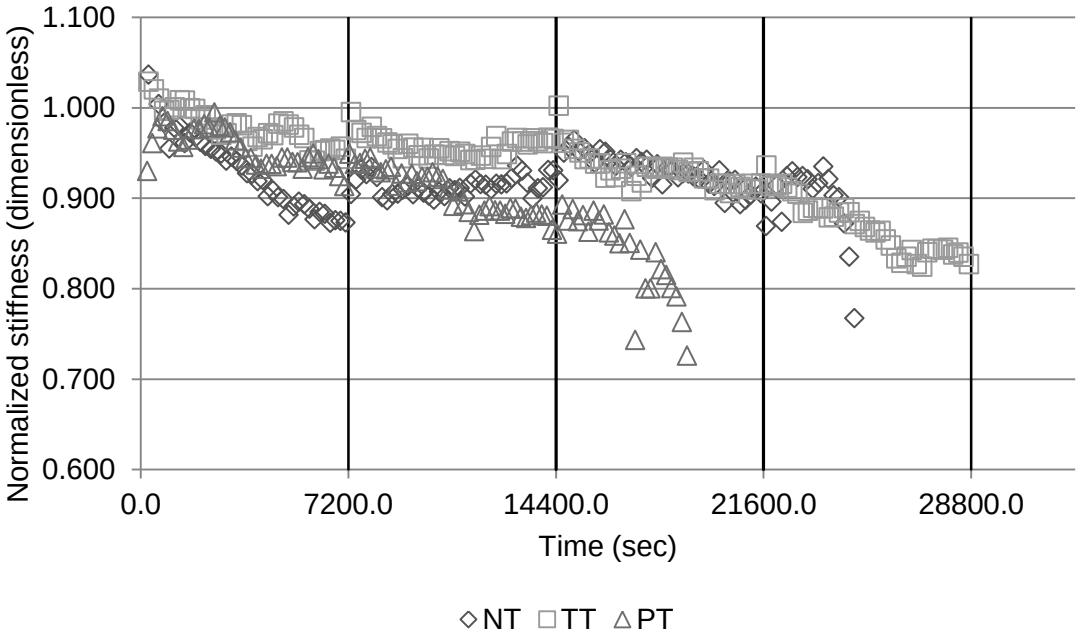

Figure E-6. 8 hour LC-RST progressive loading trial normalized stiffness data.

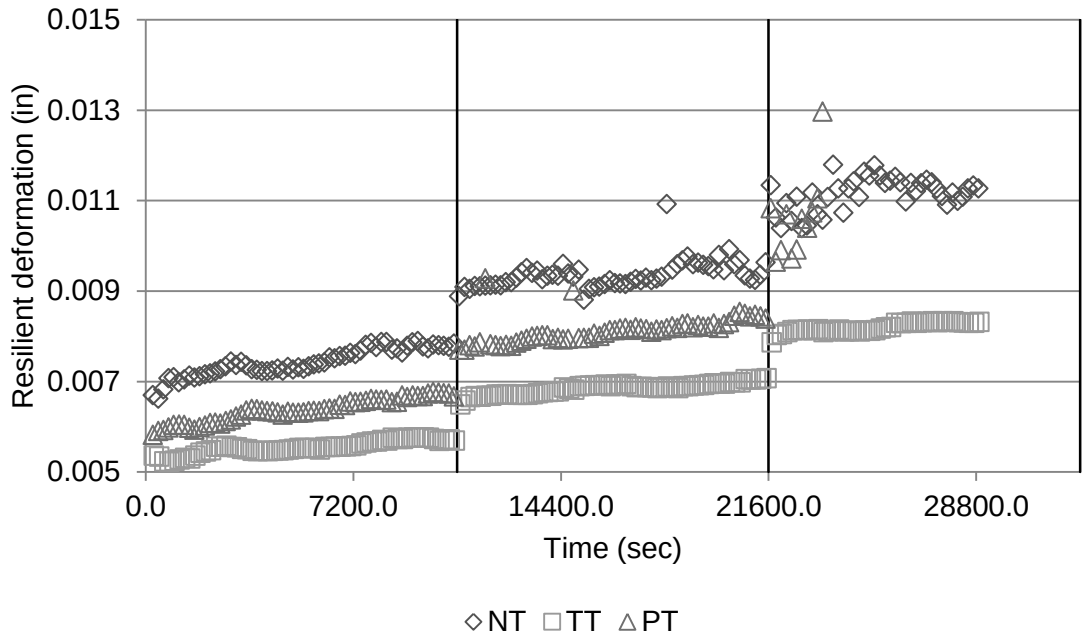

Figure E-7. 12 hour LC-RST progressive loading trial resilient deformation data.

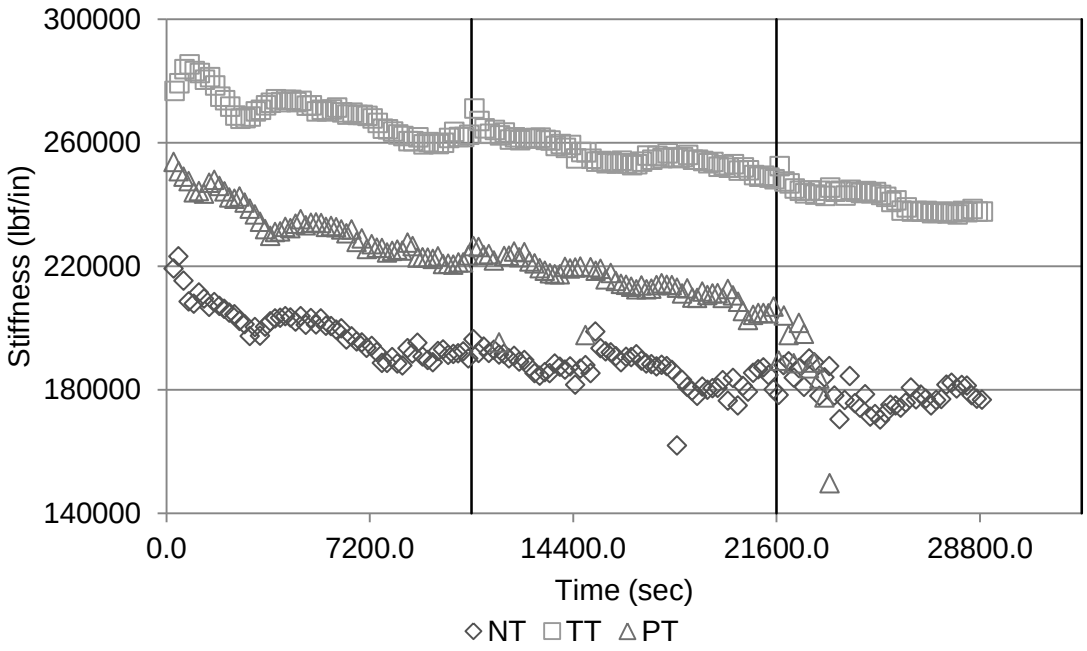

Figure E-8. 12 hour LC-RST progressive loading trial stiffness data.

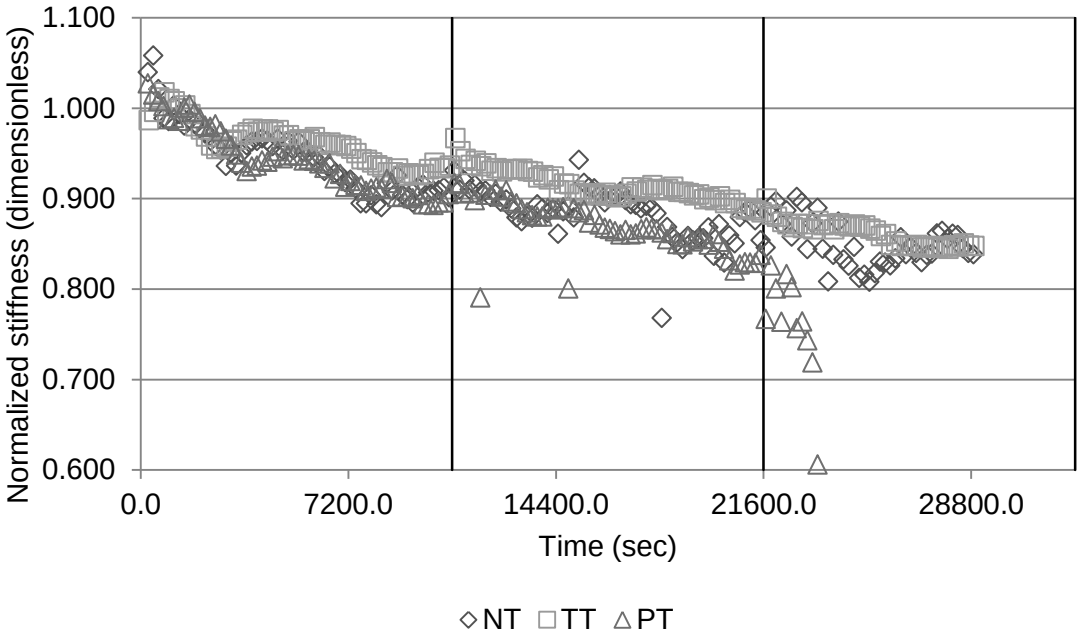

Figure E-9. 12 hour LC-RST progressive loading trial normalized stiffness data.

APPENDIX F
FINAL LC-RST DATA

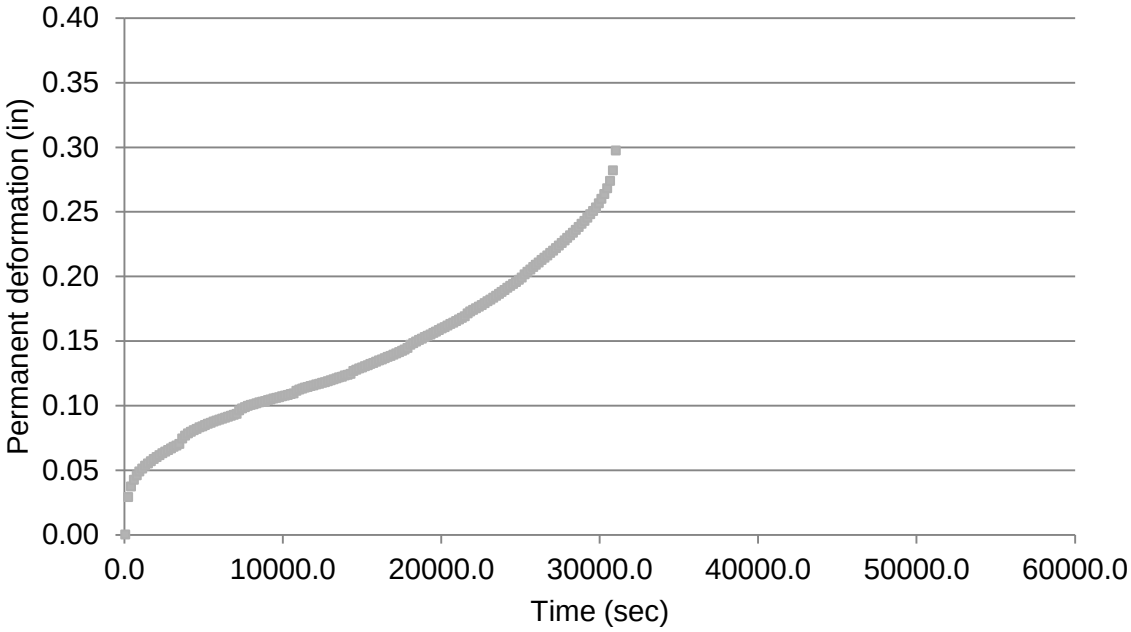

Figure F-1. Permanent deformation data from LC-RST specimen NT-1.

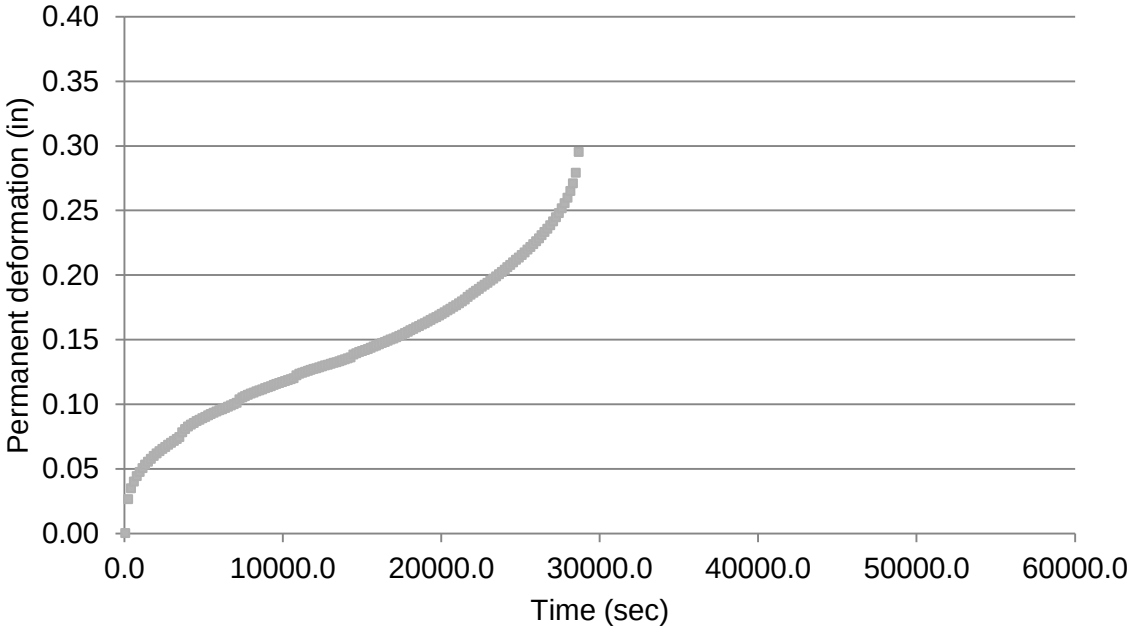

Figure F-2. Permanent deformation data from LC-RST specimen NT-2.

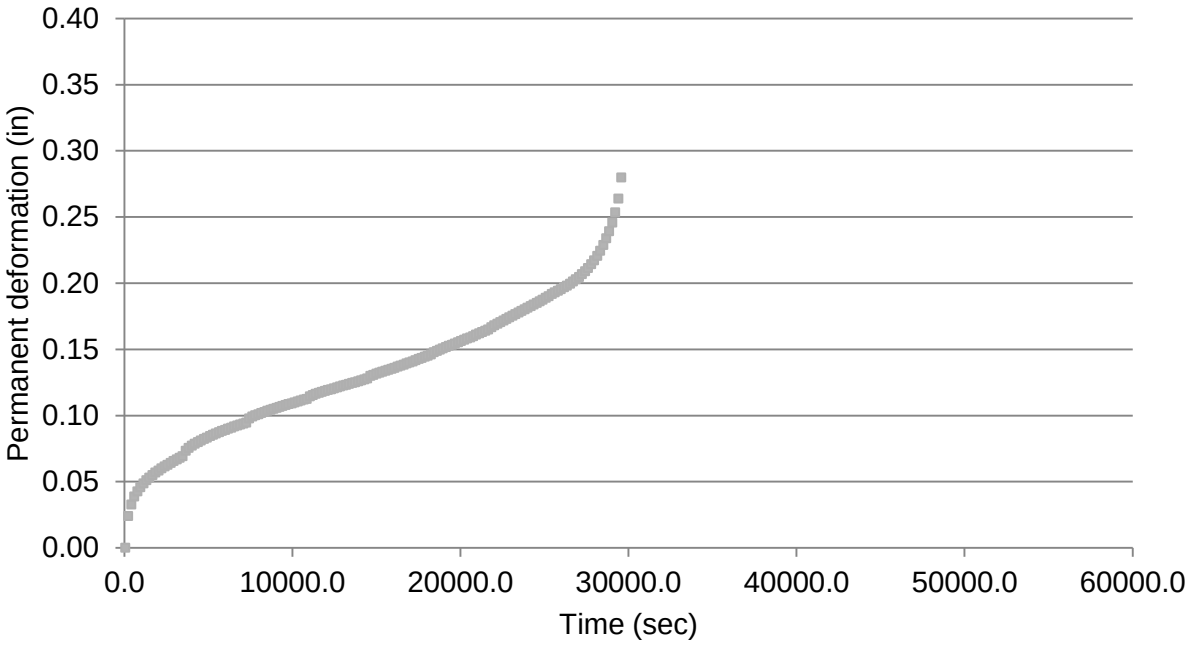

Figure F-3. Permanent deformation data from LC-RST specimen TT-1.

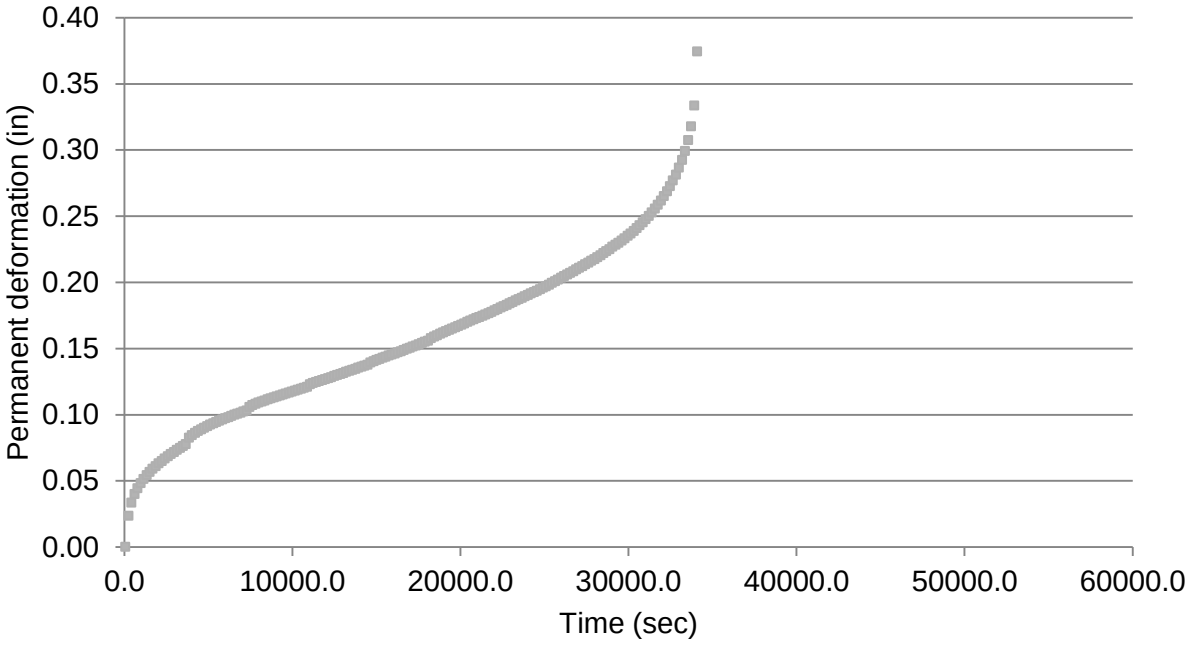

Figure F-4. Permanent deformation data from LC-RST specimen TT-2.

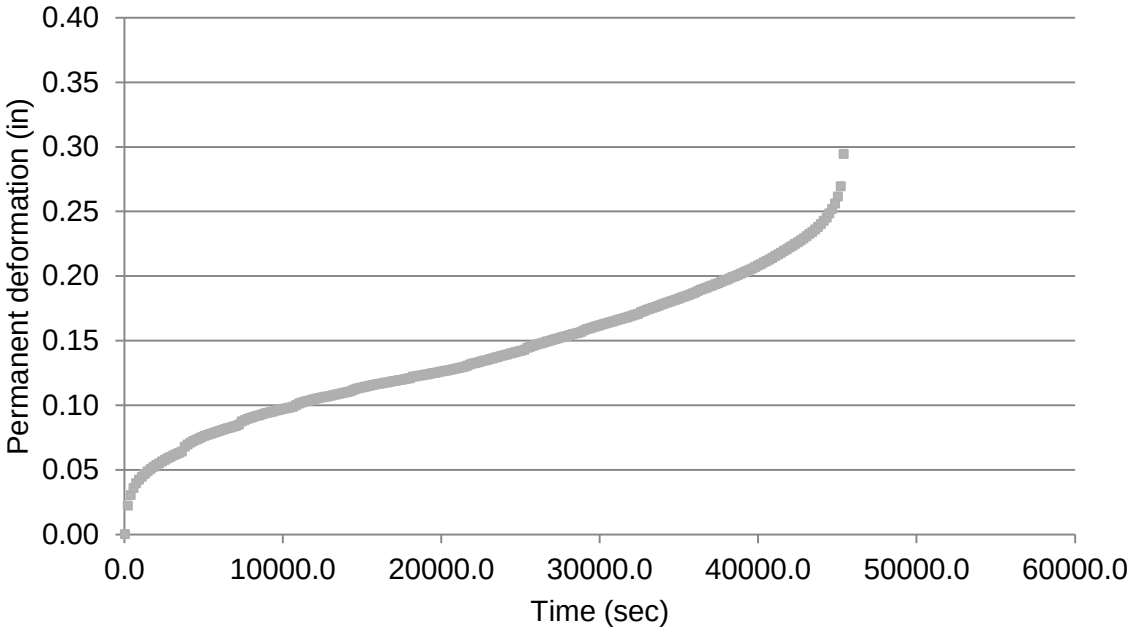

Figure F-5. Permanent deformation data from LC-RST specimen CTL-1.

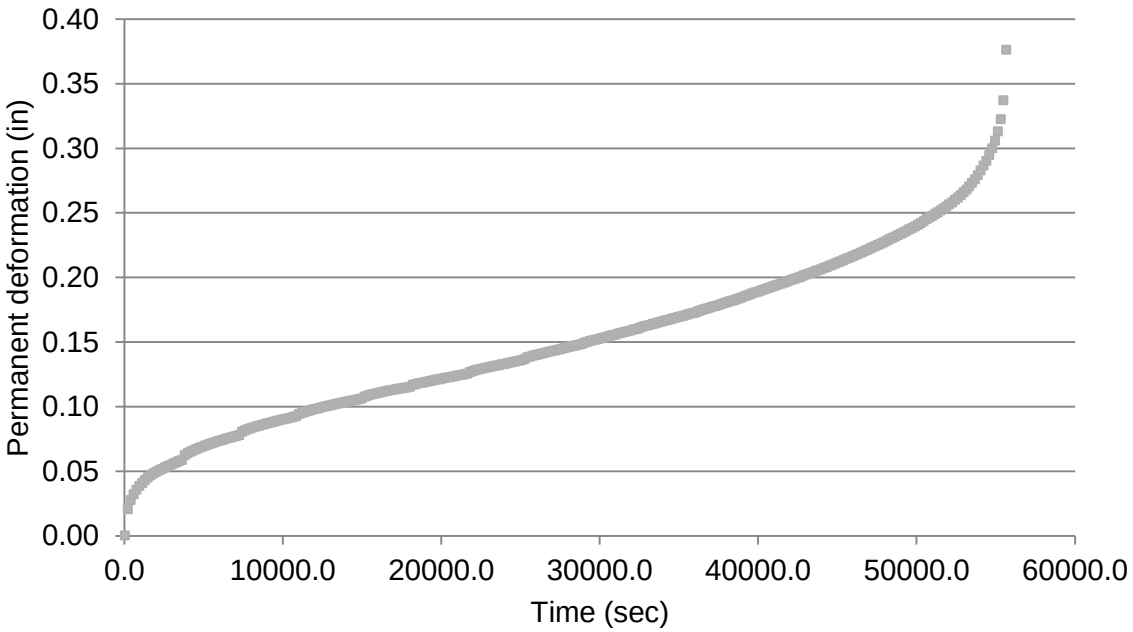

Figure F-6. Permanent deformation data from LC-RST specimen CTL-2.

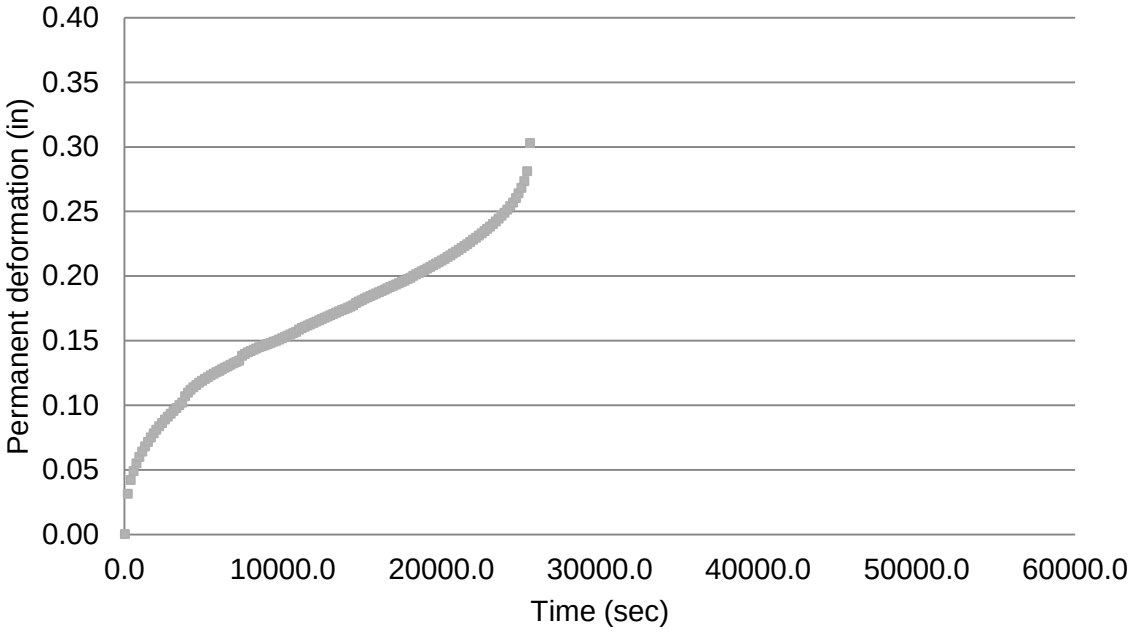

Figure F-7. Permanent deformation data from LC-RST specimen CTH-1.

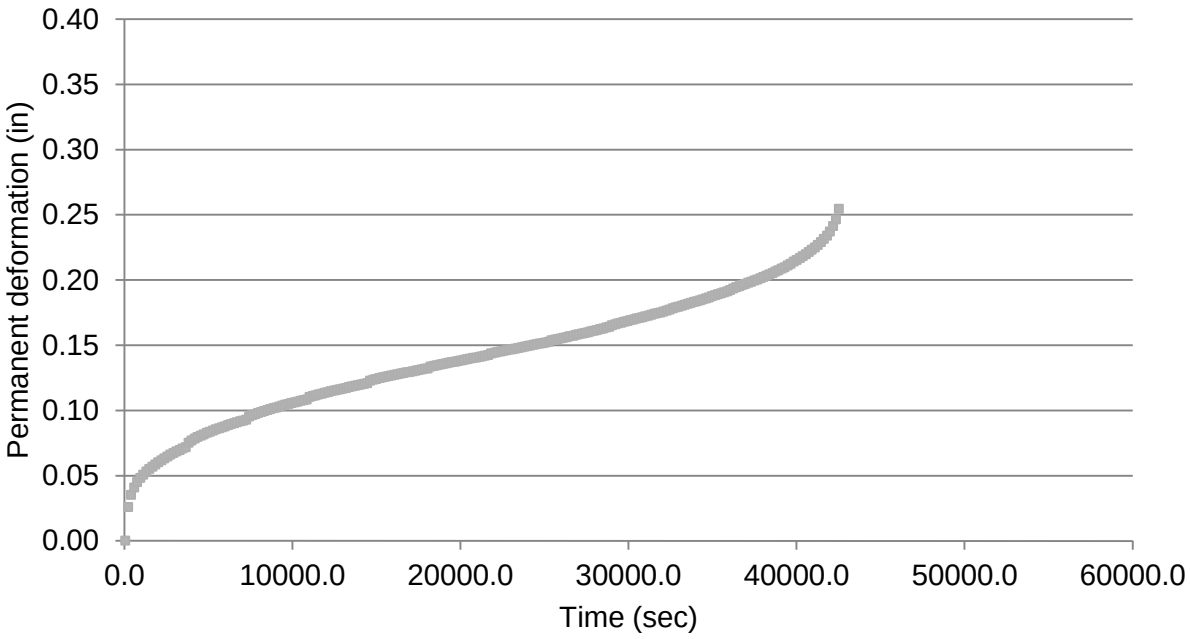

Figure F-8. Permanent deformation data from LC-RST specimen CTH-2.

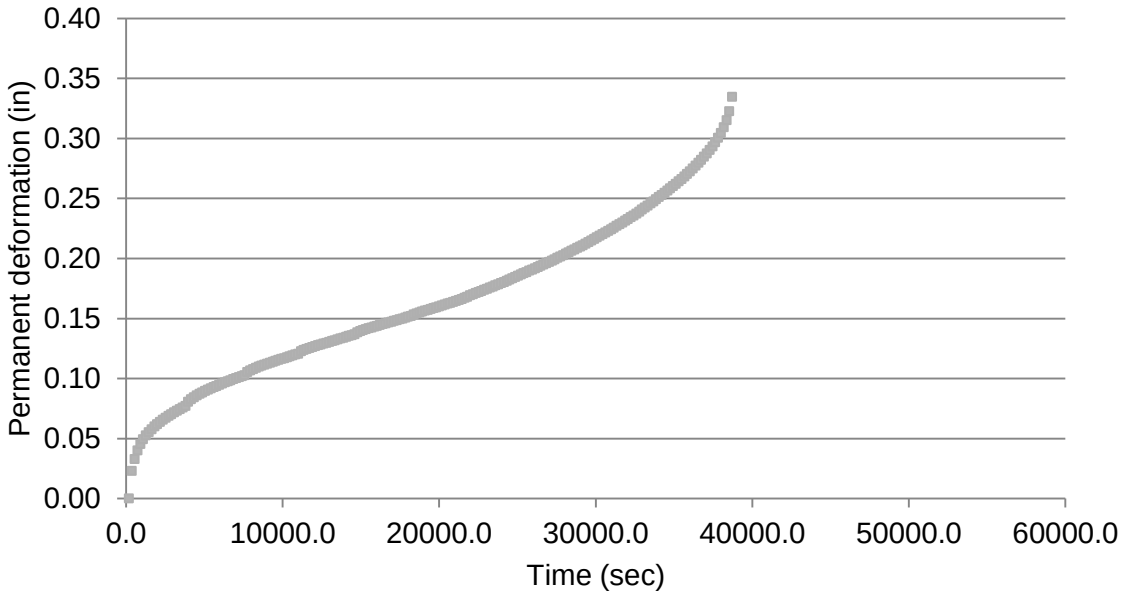

Figure F-9. Permanent deformation data from LC-RST specimen PT-1.

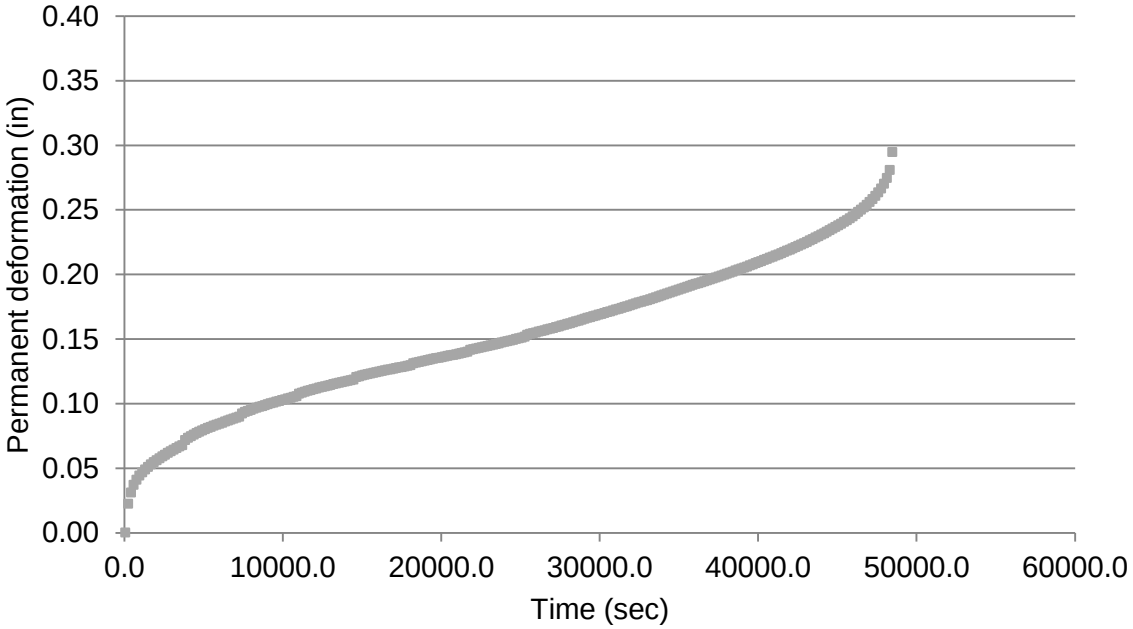

Figure F-10. Permanent deformation data from LC-RST specimen PT-2.

APPENDIX G
ENERGY ANALYSIS

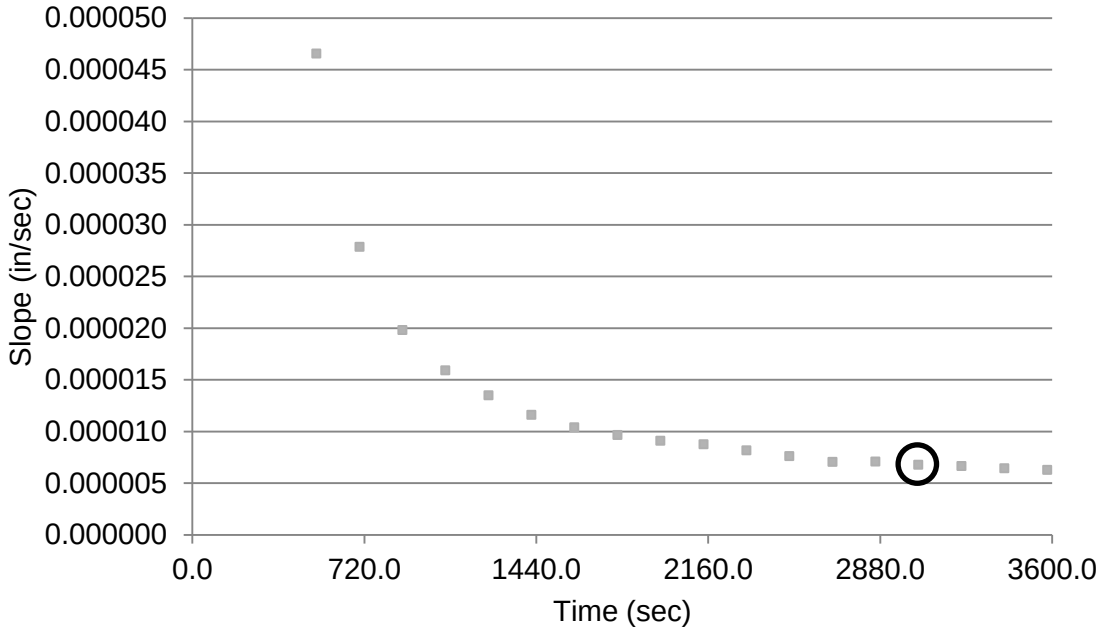

Figure G-1. Typical slope of LC-RST permanent deformation data for initial point.

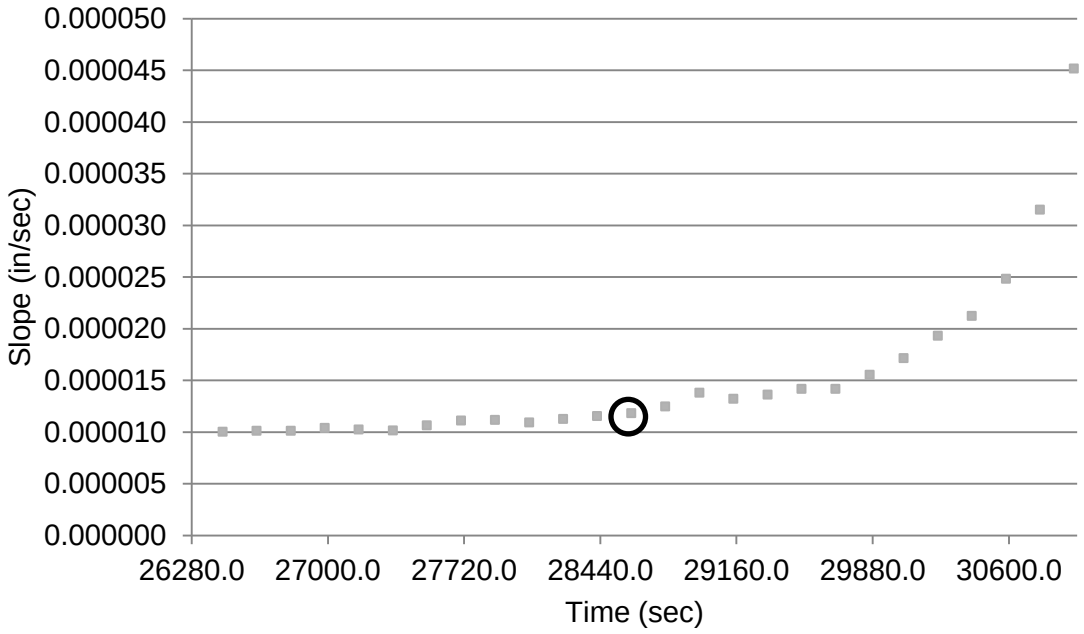

Figure G-2. Typical slope of LC-RST permanent deformation data for final point.

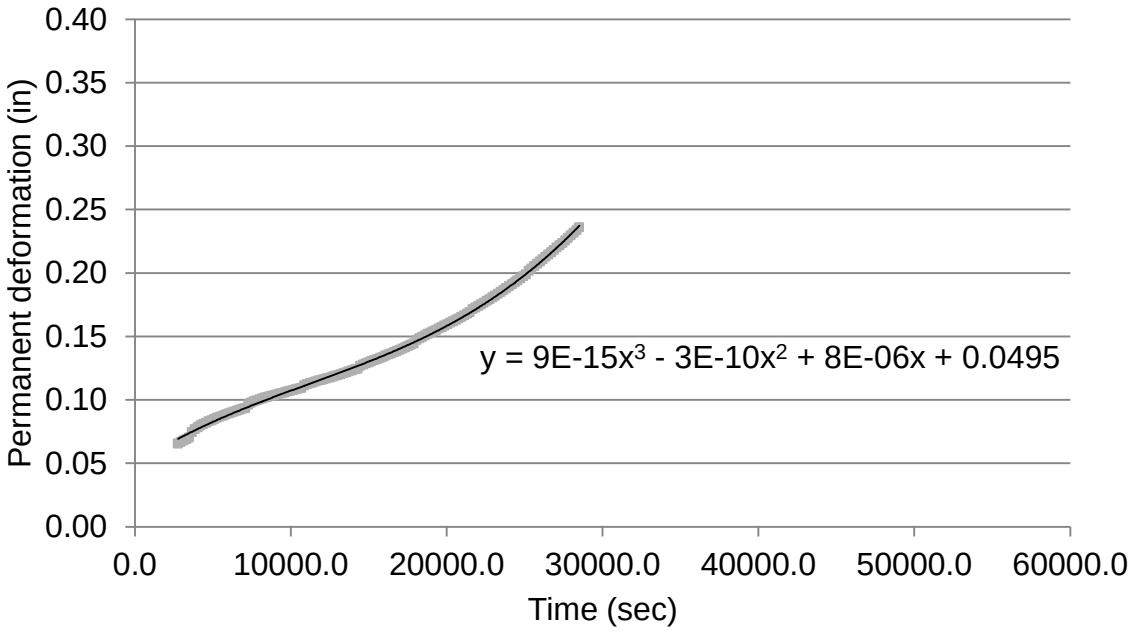

Figure G-3. Cubic function fit to steady state of NT-1 permanent deformation data.

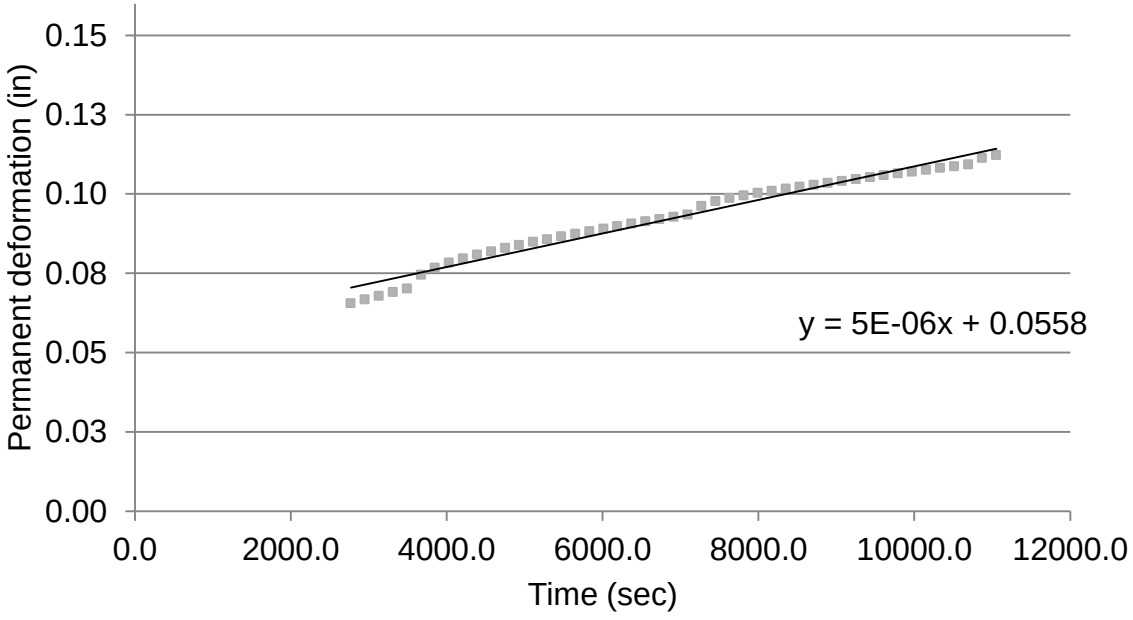

Figure G-4. Linear regression line fit to NT-1 permanent deformation data.

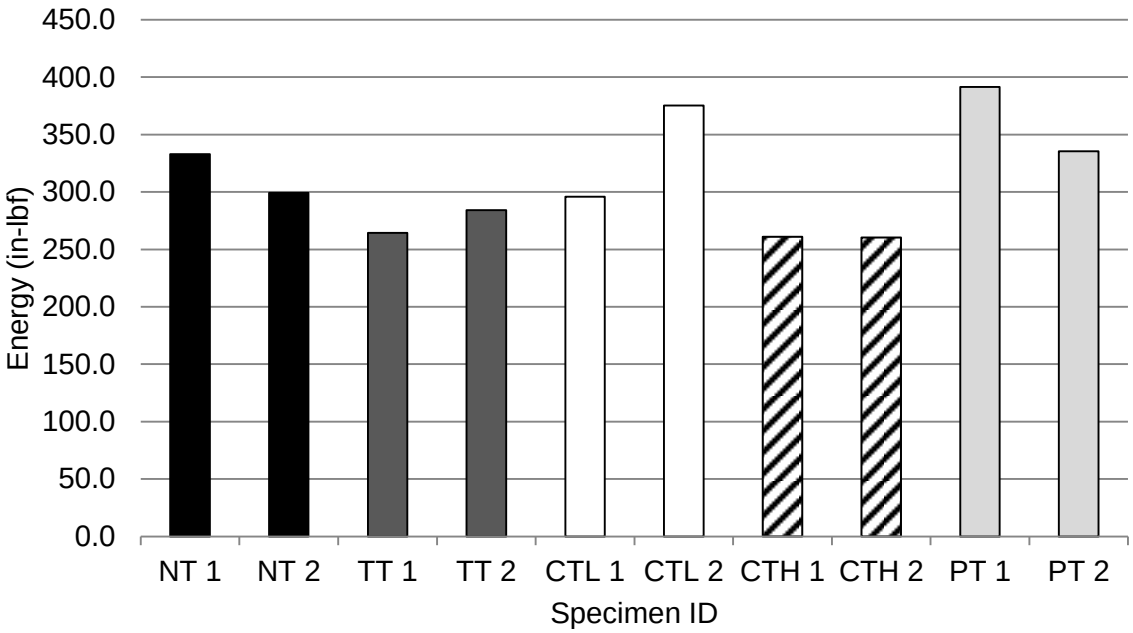

Figure G-5. Energy of LC-RST specimen results.

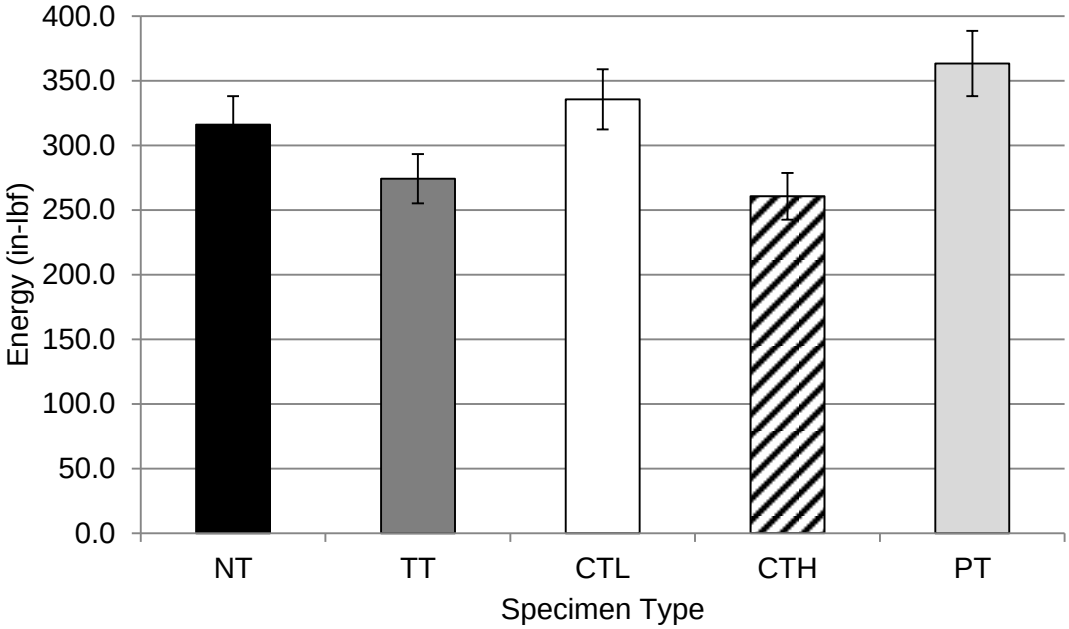

Figure G-6. Average energy of LC-RST specimen results.

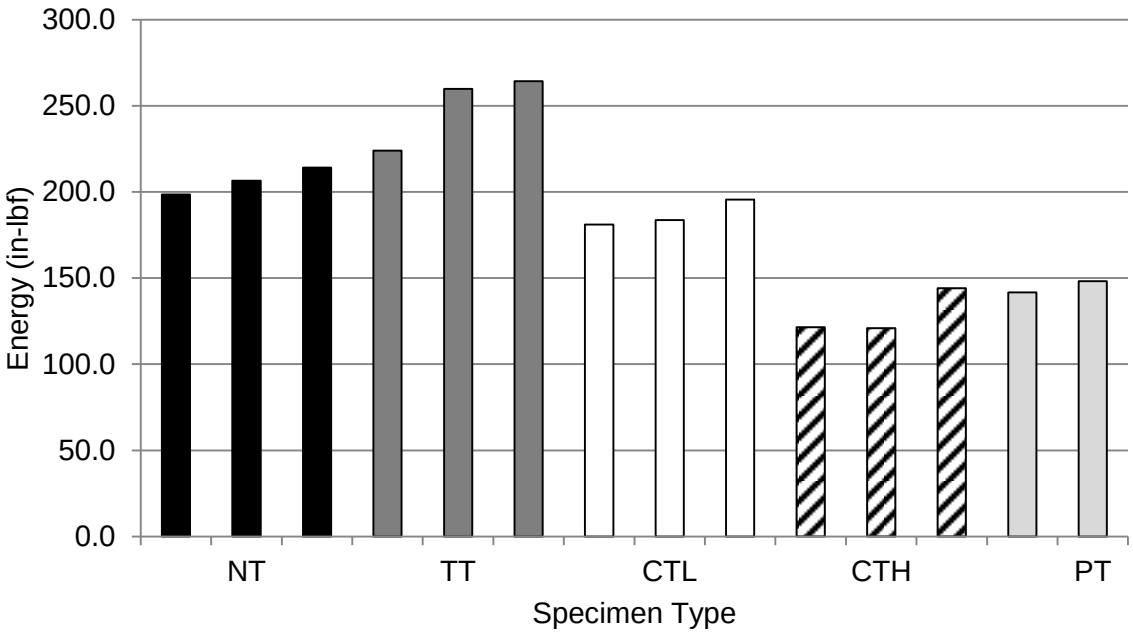

Figure G-7. Energy of strength test specimen results.

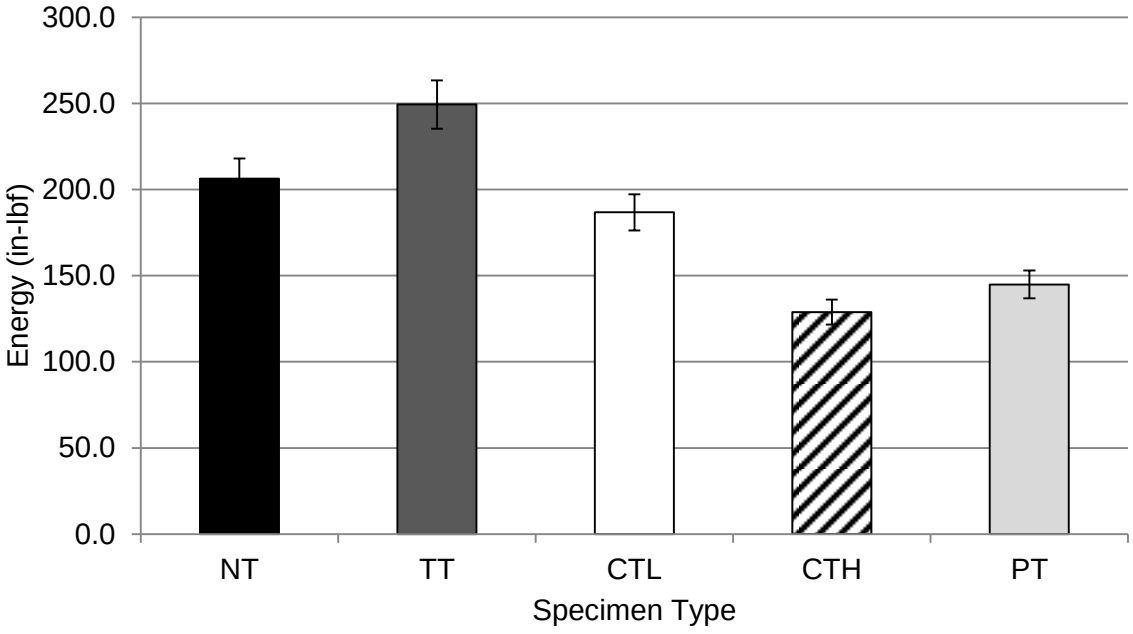

Figure G-8. Average energy of strength specimen results.

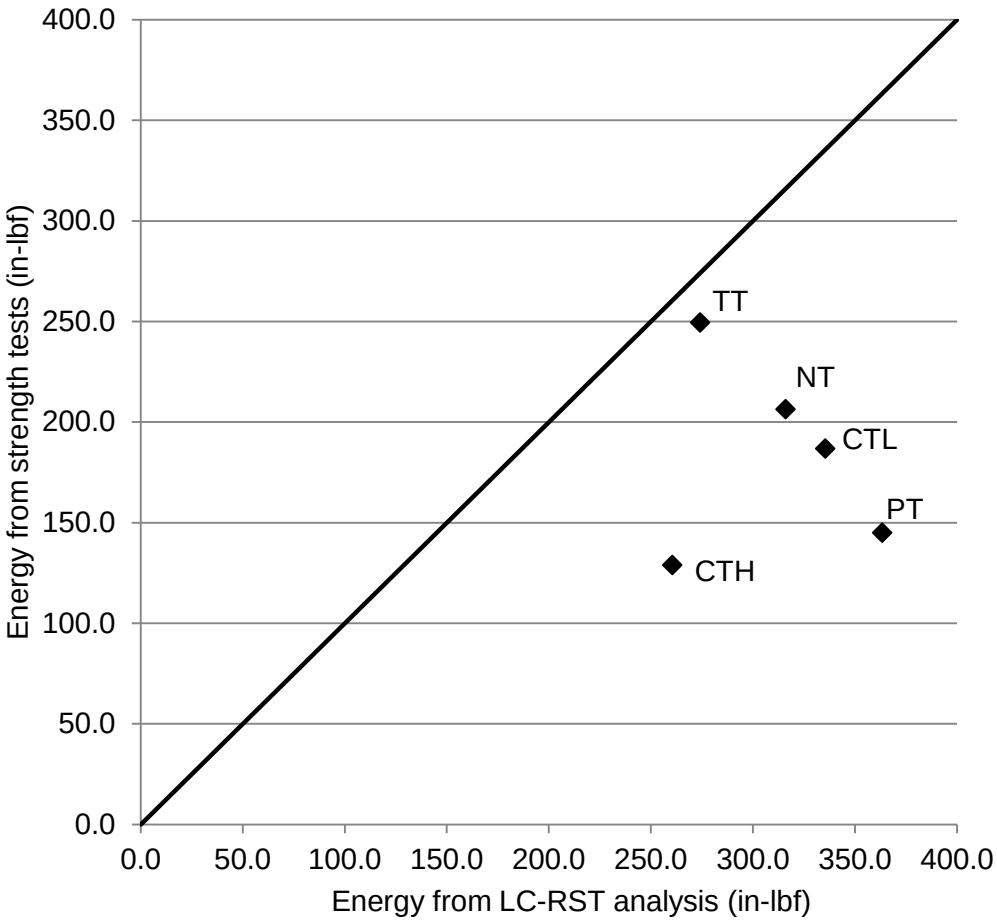

Figure G-9. Line of equality for energy data.

Table G-1. Inflection points for each LC-RST specimen.

Specimen ID	Inflection Point (in)
NT-1	11111.1
NT-2	10000.0
TT-1	13333.3
TT-2	16666.7
CTL-1	11111.1
CTL-2	16666.7
CTH-1	11666.7
CTH-2	22222.2
PT-1	16666.7
PT-2	16666.7

APPENDIX H
STATISTICAL ANALYSIS

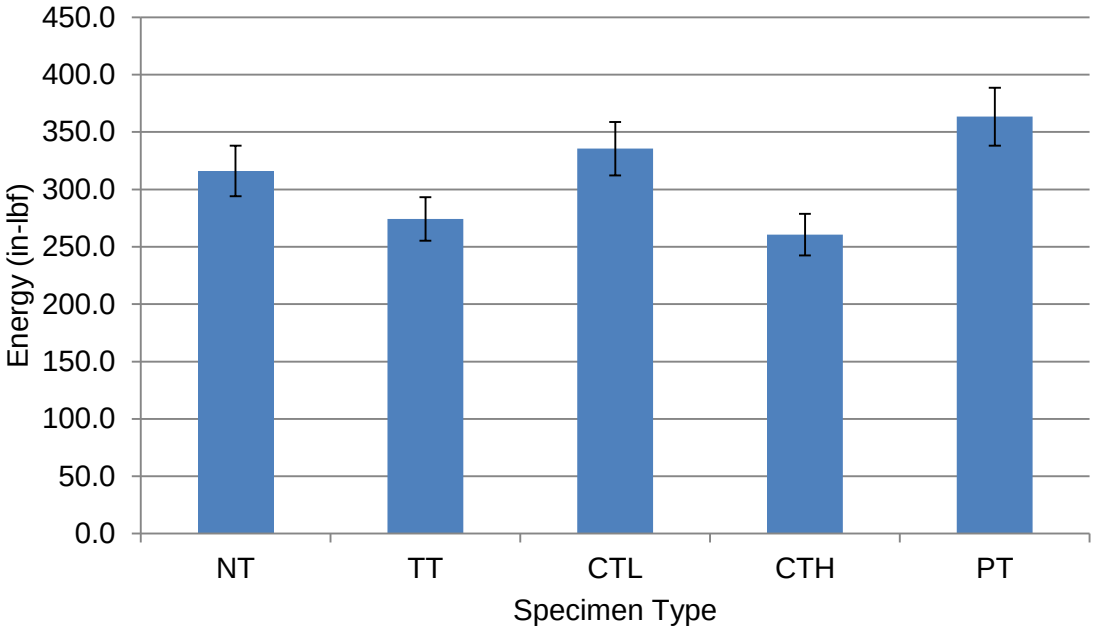

Figure H-1. Standard deviation of averaged LC-RST results.

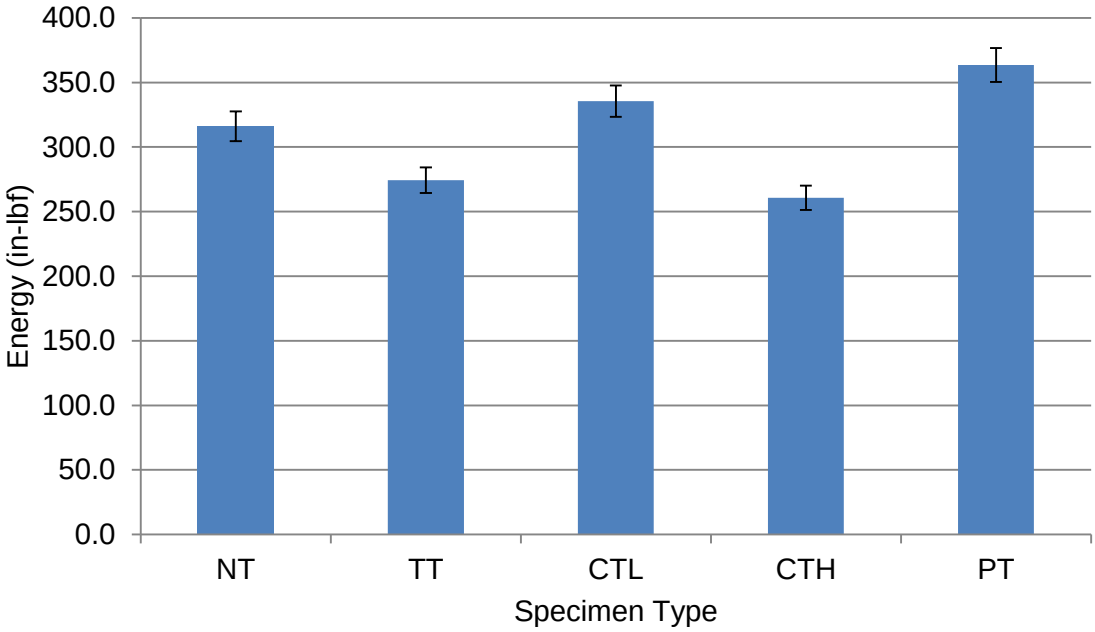

Figure H-2. 90 percent confidence interval of averaged LC-RST results.

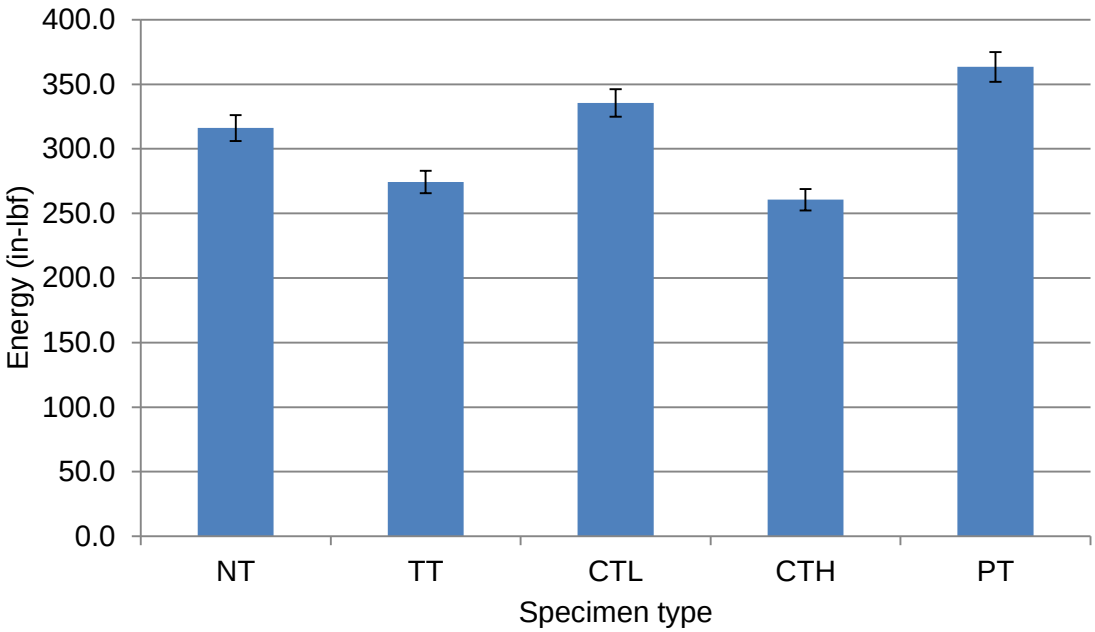

Figure H-3. 85 percent confidence interval of averaged LC-RST results.

Table H-1. LC-RST ANOVA summary.

Groups	Count	Sum	Average	Variance
NT	2.0	632.241	316.121	569.026
TT	2.0	548.576	274.288	199.976
CTL	2.0	671.034	335.517	3151.023
CTH	2.0	521.273	260.636	0.192
PT	2.0	726.884	363.442	1573.771

Table H-2. LC-RST ANOVA

Variation Source	SS	df	MS	F	P-value	F crit
Between Groups	14513.492	4	3628.373	3.302	0.111	5.192
Within Groups	5493.988	5	1098.798			
Total	20007.480	9				

Table H-3. F-Test two sample for variances: NT to TT.

	Variable 1	*Variable 2*
Mean	316.1207	274.2879
Variance	569.026	199.9759
Observations	2	2
df	1	1
F	2.845473	
P(F<=f) one-tail	0.34067	
F Critical one-tail	39.86346	

Table H-4. F-Test two sample for variances: NT to CL.

	Variable 1	*Variable 2*
Mean	316.1207	335.5171
Variance	569.026	3151.023
Observations	2	2
df	1	1
F	0.180585	
P(F<=f) one-tail	0.255813	
F Critical one-tail	0.025086	

Table H-5. F-Test two sample for variances: NT to CH.

	Variable 1	*Variable 2*
Mean	316.1207	260.6364
Variance	569.026	0.192309
Observations	2	2
df	1	1
F	2958.918	
P(F<=f) one-tail	0.011702	
F Critical one-tail	39.86346	

Table H-6. F-Test two sample for variances: NT to PT.

	Variable 1	*Variable 2*
Mean	316.1207	363.4419
Variance	569.026	1573.771
Observations	2	2
df	1	1
F	0.361569	
P(F<=f) one-tail	0.344653	
F Critical one-tail	0.025086	

Table H-7. F-Test two sample for variances: TT to CL.

	Variable 1	*Variable 2*
Mean	274.2879	335.5171
Variance	199.9759	3151.023
Observations	2	2
df	1	1
F	0.063464	
P(F<=f) one-tail	0.157108	
F Critical one-tail	0.025086	

Table H-8. F-Test two sample for variances: TT to CH.

	Variable 1	*Variable 2*
Mean	274.2879	260.6364
Variance	199.9759	0.192309
Observations	2	2
df	1	1
F	1039.869	
P(F<=f) one-tail	0.019736	
F Critical one-tail	39.86346	

Table H-9. F-Test two sample for variances: TT to PT.

	Variable 1	*Variable 2*
Mean	274.2879	363.4419
Variance	199.9759	1573.771
Observations	2	2
df	1	1
F	0.127068	
P(F<=f) one-tail	0.217994	
F Critical one-tail	0.025086	

Table H-10. F-Test two sample for variances: CL to CH.

	Variable 1	*Variable 2*
Mean	335.5171	260.6364
Variance	3151.023	0.192309
Observations	2	2
df	1	1
F	16385.22	
P(F<=f) one-tail	0.004973	
F Critical one-tail	39.86346	

Table H-11. F-Test two sample for variances: CL to PT.

	Variable 1	*Variable 2*
Mean	335.5171	363.4419
Variance	3151.023	1573.771
Observations	2	2
df	1	1
F	2.002212	
P(F<=f) one-tail	0.391661	
F Critical one-tail	39.86346	

Table H-12. F-Test two sample for variances: CH to PT.

	Variable 1	*Variable 2*
Mean	260.6364	363.4419
Variance	0.192309	1573.771
Observations	2	2
df	1	1
F	0.000122	
P(F<=f) one-tail	0.007037	
F Critical one-tail	0.025086	

Table H-13. T-Test two sample assuming equal variances: NT to TT.

	Variable 1	*Variable 2*
Mean	316.1207	274.2879
Variance	569.026	199.9759
Observations	2	2
Pooled Variance	384.501	
Hypothesized Mean Difference	0	
df	2	
t Stat	2.133377	
P(T<=t) one-tail	0.083252	
t Critical one-tail	1.885618	
P(T<=t) two-tail	0.166503	
t Critical two-tail	2.919986	

Table H-14. T-Test two sample assuming equal variances: NT to CL.

	Variable 1	*Variable 2*
Mean	316.1207	335.5171
Variance	569.026	3151.023
Observations	2	2
Pooled Variance	1860.024	
Hypothesized Mean Difference	0	
df	2	
t Stat	-0.44974	
P(T<=t) one-tail	0.348471	
t Critical one-tail	1.885618	
P(T<=t) two-tail	0.696941	
t Critical two-tail	2.919986	

Table H-15. T-Test two sample assuming unequal variances: NT to CH.

	Variable 1	*Variable 2*
Mean	316.1207	260.6364
Variance	569.026	0.192309
Observations	2	2
Hypothesized Mean Difference	0	
df	1	
t Stat	3.288864	
P(T<=t) one-tail	0.093957	
t Critical one-tail	3.077684	
P(T<=t) two-tail	0.187914	
t Critical two-tail	6.313752	

Table H-16. T-Test two sample assuming equal variances: NT to PT.

	Variable 1	*Variable 2*
Mean	316.1207	363.4419
Variance	569.026	1573.771
Observations	2	2
Pooled Variance	1071.398	
Hypothesized Mean Difference	0	
df	2	
t Stat	-1.44571	
P(T<=t) one-tail	0.142575	
t Critical one-tail	1.885618	
P(T<=t) two-tail	0.28515	
t Critical two-tail	2.919986	

Table H-17. T-Test two sample assuming equal variances: TT to CL.

t-Test: Two-Sample Assuming Equal Variances

	Variable 1	*Variable 2*
Mean	274.2879	335.5171
Variance	199.9759	3151.023
Observations	2	2
Pooled Variance	1675.499	
Hypothesized Mean Difference	0	
df	2	
t Stat	-1.49584	
P(T<=t) one-tail	0.136672	
t Critical one-tail	1.885618	
P(T<=t) two-tail	0.273344	
t Critical two-tail	2.919986	

Table H-18. T-Test two sample assuming unequal variances: TT to CH.

	Variable 1	*Variable 2*
Mean	274.2879	260.6364
Variance	199.9759	0.192309
Observations	2	2
Hypothesized Mean Difference	0	
df	1	
t Stat	1.364585	
P(T<=t) one-tail	0.201305	
t Critical one-tail	3.077684	
P(T<=t) two-tail	0.402609	
t Critical two-tail	6.313752	

Table H-19. T-Test two sample assuming equal variances: TT to PT.

	Variable 1	*Variable 2*
Mean	274.2879	363.4419
Variance	199.9759	1573.771
Observations	2	2
Pooled Variance	886.8733	
Hypothesized Mean Difference	0	
df	2	
t Stat	-2.99371	
P(T<=t) one-tail	0.047906	
t Critical one-tail	1.885618	
P(T<=t) two-tail	0.095812	
t Critical two-tail	2.919986	

Table H-20. T-Test two sample assuming unequal variances: CL to CH.

	Variable 1	*Variable 2*
Mean	335.5171	260.6364
Variance	3151.023	0.192309
Observations	2	2
Hypothesized Mean Difference	0	
df	1	
t Stat	1.886453	
P(T<=t) one-tail	0.155155	
t Critical one-tail	3.077684	
P(T<=t) two-tail	0.310309	
t Critical two-tail	6.313752	

Table H-21. T-Test two sample assuming equal variances: CL to PT.

	Variable 1	*Variable 2*
Mean	335.5171	363.4419
Variance	3151.023	1573.771
Observations	2	2
Pooled Variance	2362.397	
Hypothesized Mean Difference	0	
df	2	
t Stat	-0.57453	
P(T<=t) one-tail	0.311809	
t Critical one-tail	1.885618	
P(T<=t) two-tail	0.623619	
t Critical two-tail	2.919986	

Table H-22. T-Test two sample assuming unequal variances: CH to PT.

	Variable 1	*Variable 2*
Mean	260.6364	363.4419
Variance	0.192309	1573.771
Observations	2	2
Hypothesized Mean Difference	0	
df	1	
t Stat	-3.66467	
P(T<=t) one-tail	0.084795	
t Critical one-tail	3.077684	
P(T<=t) two-tail	0.16959	
t Critical two-tail	6.313752	

LIST OF REFERENCES

Al-Qadi, I. L., K. I. Hasiba, A. S. Cortina, H. Ozer, and Z. Leng. Best Practices for Implementation of Tack Coat: Part I - laboratory study. *Illinois Department of Transportation*, 2012, pp. 1-37.

Al-Qadi, I. L., S. H. Carpenter, Z. Leng, H. Ozer, and J. Trepanier. Tack Coat Optimization for HMA Overlays: Accelerated Pavement Test Report. *Illinois Center for Transportation (ICT)*, 2009.

Birgisson, B., J. Wang, and R. Roque. Implementation of the Florida Cracking Model into the Mechanistic-Empirical Pavement Design. *Florida Department of Transportation*, Final Report, 2006, pp. 1-36.

Canestrari, F., and E. Santagata. Temperature Effects on the Shear Behaviour of Tack Coat Emulsions used in Flexible Pavements. *International Journal of Pavement Engineering*, Vol. 6, No. 1, 2005, pp. 39-46.

Canestrari, F., G. Ferrotti, X. Lu, A. Millien, M. Partl, C. Petit, A. Phelipot-Mardele, H. Piber, and C. Raab. Mechanical Testing of Interlayer Bonding in Asphalt Pavement. *Advances in Interlaboratory Testing and Evaluation of Bituminous Materials*, Vol. 9, No. RILEM State-of-the-Art Reports, 2013, pp. 303-360.

Canestrari, F., G. Ferrotti, M. Partl, and E. Santagata. Advanced Testing and Characterization of Interlayer Shear Resistance. *Transportation Research Record: Journal of the Transportation Research Board*, No. 1929, 2005, pp. 69-78.

Caro, S., E. Masad, M. Sánchez-Silva, and D. Little. Stochastic Micromechanical Model of the Deterioration of Asphalt Mixtures Subject to Moisture Diffusion Processes. *International Journal for Numerical and Analytical Methods in Geomechanics*, Vol. 35, No. 10, 2011, pp. 1079-1097.

Chen, Y. Composite Specimen Testing to Evaluate the Effects of Pavement Layer Interface Characteristics on Cracking Performance. *University of Florida*, 2011.

Dauzats, M., and A. Rampal. Mechanism of Surface Cracking in Wearing Courses. *Proc,.Sixth International Conference, Structural Design of Asphalt Pavements*, Vol. 1, 1987, pp. 232-247.

Diakhaté, M., A. Millien, C. Petit, A. Phelipot-Mardelé, and B. Pouteau. Experimental Investigation of Tack Coat Fatigue Performance: Towards an Improved Lifetime Assessment of Pavement Structure Interfaces. *Construction and Building Materials*, Vol. 25, No. 2, 2011, pp. 1123-1133.

Diakhaté, M., C. Petit, A. Millien, A. Phelipot-Mardelé, B. Pouteau, and H. Goacolou. Interface Fatigue Cracking in Multilayered Pavements: Experimental

Analysis. *Proc. 6th RILEM International Conference on Cracking in Pavements*, Chicago, IL, 2008, pp. 649-659.

Diakhaté, M., A. Phelipot, A. Millien, and C. Petit. Shear Fatigue Behavior of Tack Coats in Pavements. *Road Materials and Pavement Design*, Vol. 7, No. 2, 2006, pp. 201-222.

Donovan, E. P., I. L. Al-Qadi, and A. Loulizi. Optimization of Tack Coat Application Rate for Geocomposite Membrane on Bridge Decks. *Transportation Research Record: Journal of the Transportation Research Board*, Vol. 1740, 2000, pp. 143-150.

Erlingsson, S., S. Said, and T. McGarvey. Influence of Heavy Traffic Lateral Wander on Pavement Deterioration. *Proc., 4th European Pavement and Asset Management Conference*, Malmö, Sweden, 2012.

Hachiya, Y., K. Sato. Effect of Tack Coat on Bonding Characteristics at Interface between Asphalt Concrete Layers. *Proc. Eighth International Conference on Asphalt Pavements*, Vol. 1, 1997, pp. 349-362.

Hakimzadeh, S., W. Buttlar, and R. Santarromana. Evaluation of Bonding between HMA Layers Produced with Different Tack Coat Application Rates Using Shear-type and Tension-type Tests. *Journal of the Transportation Research Board*, 2012.

Hakimzadeh, S., W. Buttlar, and R. Santarromana. Shear-and tension-type tests to evaluate bonding of Hot-Mix Asphalt layers with different tack coat application rates," *Transportation Research Record: Journal of the Transportation Research Board*, No. 2295, 2012, pp. 54-62.

Hakimzadeh, S., N. A. Kebede, and W. G. Buttlar. Comparison between Optimum Tack Coat Application Rates as Obtained from Tension-and Torsional Shear-type tests. *Proc., 7th RILEM International Conference on Cracking in Pavements*, Vol. 4, No.1, 2012, pp. 287-297.

Hakimzadeh, S., N. A. Kebede, W. G. Buttlar, S. Ahmed, and M. Exline. Development of Fracture-energy Based Interface Bond Test for Asphalt Concrete. *Road Materials and Pavement Design*, Vol. 13, No. 1, 2012, pp. 76-87.

Huang, Y.H., Pavement Analysis and Design, *Prentice Hall*, Vol. 2, 2003.

Jia, X., B. Huang, and L. Li. A Simplified Approach for Evaluating Interlayer Shear Resistance in Asphalt Pavement. *Proc., Transportation Research Board 92nd Annual Meeting*, No. 13-3943, 2013.

Kruntcheva, M. R., A. C. Collop, and N. H. Thom. Properties of Asphalt Concrete Layer Interfaces. *Journal of Materials in Civil Engineering*, Vol. 18, No. 3, 2006, pp. 467-471.

Masad, E., B. Muhunthan, N. Shashidhar, and T. Harman. Quantifying Laboratory Compaction Effects on the Internal Structure of Asphalt Concrete. *Transportation Research Record: Journal of the Transportation Research Board*, No. 1681, 1999, pp. 179-185.

Mehta, Y., and N. Siraj. Evaluation of Interlayer Bonding in HMA Pavements. *Wisconsin Department of Transportation*, 2007.

Mohammad, L. N., M. A. Elseifi, A. Bae, N. B. Patel, J. Button, and J. A. Scherocman. Optimization of Tack Coat for HMA Placement. *National Cooperative Highway Research Program*, Vol. 712, 2012.

Mohammad, L., M. Raqib, and B. Huang. Influence of Asphalt Tack Coat Materials on Interface Shear Strength. *Transportation Research Record: Journal of the Transportation Research Board*, No. 1789, 2002, pp. 56-65.

Mohammad, L., Z. Wu, and M. A. Raqib. Investigation of the Behavior of Asphalt Tack Interface Layer. *Federal Highway Administration*, 2005, pp. 1-107.

Muench, S.T., and T. Moomaw. De-bonding of Hot Mix Asphalt Pavements in Washington State. *Washington State Department of Transportation*, Report No. WA-RD 712.1, 2008.

Myers, L. Development and Propagation of Surface-Initiated Longitudinal Wheel Path Cracks in Flexible Highway Pavements. *University of Florida*, 2000.

Myers, L., and R. Roque. Top-Down Crack Propagation in Bituminous Pavements and Implications for Pavement Management. *Association of Asphalt Paving Technologists*, Vol. 71, 2002, pp. 651-670.

Patel, N. B. Factors affecting the Interface Shear Strength of Pavement Layers. *Louisiana State University*, 2010.

Petit, C., A. Millien, F. Canestrari, V. Pannunzio, and A. Virgili. Experimental Study on Shear Fatigue Behavior and Stiffness Performance of Warm Mix Asphalt by Adding Synthetic Wax. *Construction and Building Materials*, Vol. 34, 2012, pp. 537-544.

Piber, H., F. Canestrari, G. Ferrotti, X. Lu, A. Millien, M. Partl, C. Petit, A. Phelipot-Mardelle, and C. Raab. RILEM: Interlaboratory Test on Interlayer Bonding of Asphalt Pavements. *Proc., 7th International RILEM Symposium on Advanced Testing and Characterisation of Bituminous Materials*, 2009, pp. 1181-1189.

Raab, C. Development of a Framework for Standardisation of Interlayer Bond of Asphalt Pavements. *Technical University of Darmstadt*, 2010.

Raab, C., M. Partl, and A. O. Abd El Halim. Evaluation of Interlayer Shear Bond Devices for Asphalt Pavements. *The Baltic Journal of Road and Bridge Engineering*, Vol. 4, No. 4, 2009, pp. 186-195.

Raab, C., M. Partl, and A. O. Abd El Halim. Effect of Gap Width on Interlayer Shear Bond Results. *International Journal of Pavement Research and Technology*, Vol. 3, No. 2, 2010, pp. 79-85.

Romanoschi, S. A., and J. B. Metcalf. Characterization of Asphalt Concrete Layer Interfaces. *Transportation Research Record: Journal of the Transportation Research Board*, No. 1778, 2001, pp. 132-139.

Roque, R., S. Chun, J. Zou, G. Lopp, and C. Villiers. "Continuation of Superpave Projects Monitoring. *Florida Department of Transportation*, Tallahassee, FL, Final Report BDK-75-996-06, 2011.

Sholar, G. A., G. C. Page, J. A. Musselman, P. B. Upshaw, and H. L. Moseley. Preliminary Investigation of a Test Method to Evaluate Bond Strength of Bituminous Tack Coats. *Journal of the Association of Asphalt Paving Technologists*, Vol. 73, 2004.

Tashman, L., K. Nam, and T. Papagiannakis. Evaluation of the Influence of Tack Coat Construction Factors on the Bond Strength between Pavement Layers. *Washington State Department of Transportation*, 2006, pp. 1-83.

Tozzo, C., A. D'Andrea, D. Cozzani, and A. Meo. Fatigue Investigation of the Interface Shear Performance in Asphalt Pavement. *Modern Applied Science*, Vol. 8, No. 2, 2014, pp. 1-11.

Tozzo, C., N. Fiore, and A. D'Andrea. Dynamic Shear Tests for the Evaluation of the Effect of the Normal Load on the Interface Fatigue Resistance. *Construction and Building Materials*, Vol. 61, 2014, pp. 200-205.

Tran, N. H., J. R. Willis, and G. Julian. Refinement of the Bond Strength Procedure and Investigation of a Specification. *National Center for Asphalt Technology*, 2012, pp. 1-83.

Uhlmeyer, J., K. Willoughby, L. Pierce, and J. Mahoney. Top-Down Cracking in Washington State Asphalt Concrete Wearing Courses. *Transportation Research Record: Journal of the Transportation Research Board*, No. 1730, 2000, pp. 110-116.

Uzan, J., M. Livneh, and Y. Eshed. Investigation of Adhesion Properties between Asphaltic Concrete Layers. *Asphalt Paving Technology*, No. 47, 1978, pp. 495-521.

West, R. C., J. Zhang, and J. Moore. Evaluation of Bond Strength between Pavement Layers. *National Center for Asphalt Technology*, 2005, pp. 1-58.

Wheat, M. Evaluation of Bond Strength at Asphalt Interfaces. *Kansas State University*, 2007.

Willis, J. R., and D. H. Timm. Forensic Investigation of a Rich-Bottom Pavement. *National Center for Asphalt Technology*, 2006, pp. 1-62.

Willis, J. R., and D. H. Timm. Forensic Investigation of Debonding in Rich-Bottom Pavement. *Transportation Research Record: Journal of the Transportation Research Board,* No. 2040, 2007, pp. 107-114.

BIOGRAPHICAL SKETCH

Jeremy Alexis Magruder Waisome was born in Orlando, Florida in 1987. She became passionate about pursing her doctoral degree in middle school, while standing in a nuclear reactor at Oak Ridge National Laboratory. After graduating from Edgewater High School in 2005, she attended the University of Florida where she received a Bachelor of Science degree in civil engineering in May 2010 and was inducted into the Hall of Fame. Upon graduating, she immediately enrolled in the doctoral program at the University of Florida. She received her Master of Science degree in civil engineering in May 2012, in addition to a graduate certificate in sustainable engineering in May 2013. She has been co-advised throughout her graduate studies by Drs. Reynaldo Roque (chair) and Mang Tia (co-chair). Upon completing her Ph.D., she plans to pursue a career in the academy and work towards improving the diversity of the engineering pipeline.

T